Journal Pre-proofs

NMR studies of amyloid interactions

David A. Middleton

PII: S0079-6565(24)00014-1
DOI: https://doi.org/10.1016/j.pnmrs.2024.07.001
Reference: JPNMRS 1553

To appear in: *Progress in Nuclear Magnetic Resonance Spectroscopy*

Received Date: 26 March 2024
Accepted Date: 16 July 2024

Please cite this article as: D.A. Middleton, NMR studies of amyloid interactions, *Progress in Nuclear Magnetic Resonance Spectroscopy* (2024), doi: https://doi.org/10.1016/j.pnmrs.2024.07.001

NMR studies of amyloid interactions

David A. Middleton

Department of Chemistry, Lancaster University, Lancaster LA1 4YB, United Kingdom

E-mail: d.middleton@lancaster.ac.uk

Telephone: +44 1524 594328

Contents

Highlights

- Amyloid proteins associated with human diseases interact with various accessory molecules and metal ions, and with cell membranes
- NMR provides unique atomic insights into interactions of amyloid species with physiological interaction partners.
- Solution NMR is ideal for characterizing interactions involving small, soluble amyloid species
- Solid state NMR methods report interactions with insoluble amyloid fibrils
- Information is obtained from the perspective of the protein and/or interaction partner.
- Also provides information on amyloid diagnostic and therapeutic molecules

Keywords

Solid-state NMR; HSQC; amyloid fibril; oligomer; metal ions; glycosaminoglycan; heparin; EGCG; curcumin; flutemetamol; thioflavin T; Congo red; ligand orientation; STD NMR; waterLOGSY; paramagnetic relaxation enhancement.

Abstract

Amyloid fibrils are insoluble, fibrous nanostructures that accumulate extracellularly in biological tissue during the progression of several human disorders, including Alzheimer's disease (AD) and type 2 diabetes. Fibrils are assembled from protein monomers via the transient formation of soluble, cytotoxic oligomers, and have a common molecular architecture consisting of a spinal core of hydrogen-bonded protein β-strands. For the past 25 years, NMR spectroscopy has been at the forefront of research into the structure and assembly mechanisms of amyloid aggregates. Until the recent boom in fibril structure analysis by cryo-electron microscopy, solid-state NMR was unrivalled in its ability to provide atomic-level models of amyloid fibril architecture. Solution-state NMR has also provided complementary information on the early stages in the amyloid assembly mechanism. Now, both NMR modalities are proving to be valuable in unravelling the complex interactions between amyloid species and a diverse range of physiological metal ions, molecules and surfaces that influence the assembly pathway, kinetics, morphology and clearance *in vivo*. Here, an overview is presented of the main applications of solid-state and solution-state NMR for studying the interactions between amyloid proteins and biomembranes, glycosaminoglycan polysaccharides, metal ions, polyphenols, synthetic therapeutics and diagnostics. Key NMR methodology is reviewed along with examples of how to overcome the challenges of detecting interactions with aggregating proteins. The review heralds this new role for NMR in providing a comprehensive and pathologically-relevant view of the interactions between protein and non-protein components of amyloid. Coverage of both solid- and solution-state NMR methods and applications herein will be informative and valuable to the broad communities that are interested in amyloid proteins.

1. Introduction

A molecular snapshot of the cellular proteome would reveal a distribution of disordered and partially-unfolded proteins alongside structurally well-defined globular protein entities. Unstructured proteins can contain exposed sequence elements that assemble with identical protein copies to form fibrous supramolecular assemblies called amyloid fibrils [1]. The morphology of amyloid fibrils is remarkably independent of the primary amino acid sequence of the protein precursor, and structurally may be more thermodynamically stable than the native protein fold. Fibril formation is exothermic, and occurs via nucleation and growth processes that are akin to supersaturation-limited crystallization, culminating in the precipitation of insoluble material [2]. NMR spectroscopy has, for many years, been at the forefront of methods for (i) visualising

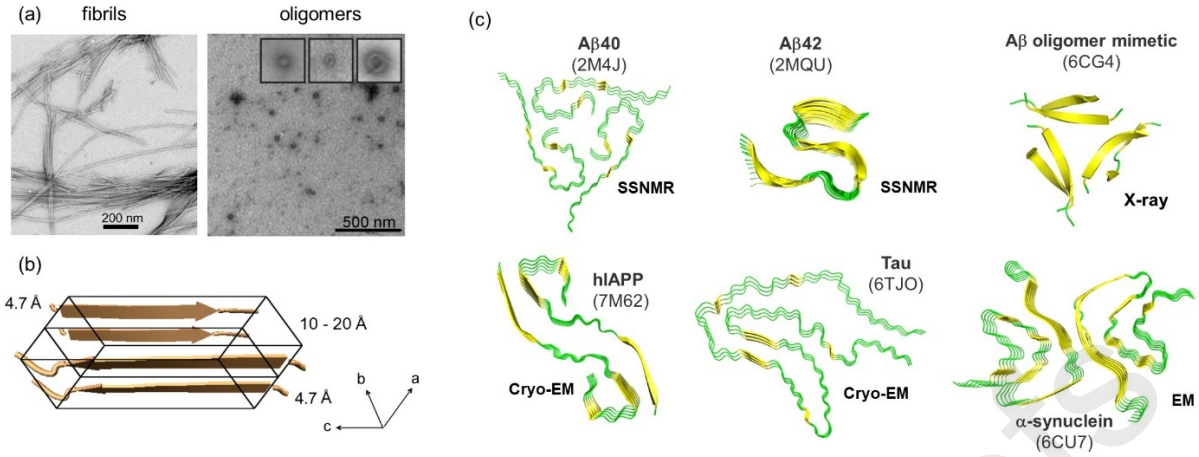

Fig. 1. Structure and morphology of amyloid species. (a) Transmission electron micrographs of amyloid fibrils (of Aβ40) and oligomers (of the aortic amyloid peptide medin). (b) Typical dimensions of an amyloid repeating unit. (c) Cross-sectional atomic structural models of amyloid fibrils formed by the proteins in Table 1. Models are viewed down the fibril long axis. Panel (a) adapted from [3] with permission. Panel (b) adapted with permission from [4]; copyright 2008 American Chemical Society.

Table 1. Summary of the key disease-associated amyloidogenic proteins studied by NMR spectroscopy.

Protein	Description
α-synuclein	A highly soluble unfolded protein that accumulates in Lewy bodies in Parkinson disease and other synucleinopathies.
Amyloid-β peptides Aβ40/Aβ42	40- and 42 residue peptides produced through the proteolytic processing of the transmembrane amyloid precursor protein (APP), by β- and γ-secretases. Accumulation of Aβ fibrillar plaques in the brain in the brain is an early event in the pathogenesis of Alzheimer's disease (AD).
Human islet amyloid polypeptide	A 37-residue polypeptide neuropancreatic hormone, also known as amylin. hIAPP fibril accumulation associated with type 2 diabetes may contribute to progressive loss of islet β-cells.
Microtubule-associated protein tau	A family of protein isoforms of varying amino acid lengths from 352 to 441. Hyperphosphorylated tau assembles into filaments associated with Alzheimer's and Pick's diseases.

the early mechanisms of amyloid formation in solution and (ii) determining the atomic architectures of fibrils in the solid state. More recently, cryo-electron microscopy (cryo-EM) has arguably emerged as the method of choice for delineating the three-

dimensional architectures of amyloid fibrils [5]. NMR is now fulfilling the new and important role of resolving the interactions and dynamics of amyloid species with the large array of accessory molecules and ions that act as accomplices in the aggregation pathway.

Amyloid is defined clinically as the insoluble fibrous deposits that accumulate extracellularly in tissue and contain proteins with a high content of β-sheet secondary structure. Up to 50 human diseases, including Alzheimer's disease, type 2 diabetes and Parkinson's disease (**Table 1**), are associated with amyloid that accumulates either systemically, or locally in specific organs. The pathological effects of amyloid may arise from the insoluble fibrillar plaque burden, which places stress on organs such as the heart, liver and kidneys, or from soluble cytotoxic oligomeric species that form transiently before fibril elongation. Additionally, but not covered here in depth, peptides and proteins may assemble into functional amyloids acting as fibrillar storage assemblies and playing beneficial roles in a variety of biological processes [6].

Transmission electron microscopy (TEM) of amyloid extracted from tissue or assembled *in vitro* under controlled conditions reveals unbranched filamentous structures typically 10 nm in diameter and micrometres long. The core structure of fibrils is the so-called cross-β morphology, consisting of repeated arrays of β-strands assembled via intermolecular hydrogen bonds into β-sheet layers stabilised by a steric zipper of side-chains [7, 8]. The cross-β structure gives rise to a characteristic X-ray fibre diffraction pattern with reflections at ~4.7 Å (the repeating distance along the hydrogen-bonding direction) and at >10 Å (the typical spacing between β-sheet laminae) [7, 8] (**Fig. 1**). Oligomers are critical intermediates formed on the pathway to the filamentous aggregates and take on a range of sizes and morphologies, including spherical structures [9]. They are considered to be the most pathologically important species formed during protein aggregation, and their cytotoxic properties may involve penetration into, and disruption of, cellular membranes.

NMR spectroscopy has been used widely to elucidate the structure and assembly mechanisms of amyloid fibrils and oligomers assembled from a variety of protein precursors. Solution-state NMR is best suited to analysing small, water-soluble species (monomers and oligomers) that dominate in the early pre-nucleation stages of aggregation pathway and have rapid tumbling rates [10-12]. Solid-state NMR – specifically, magic-angle spinning (MAS) NMR – is used to characterise the atomic details of the mature, insoluble fibrils isolated at the end of aggregation [13-20]. There is nevertheless some overlap of the capabilities of the two techniques (**Fig. 2**). The vast majority of NMR studies on amyloid have concentrated on the species that form from a single protein precursor alone, in buffered solution under well-defined conditions

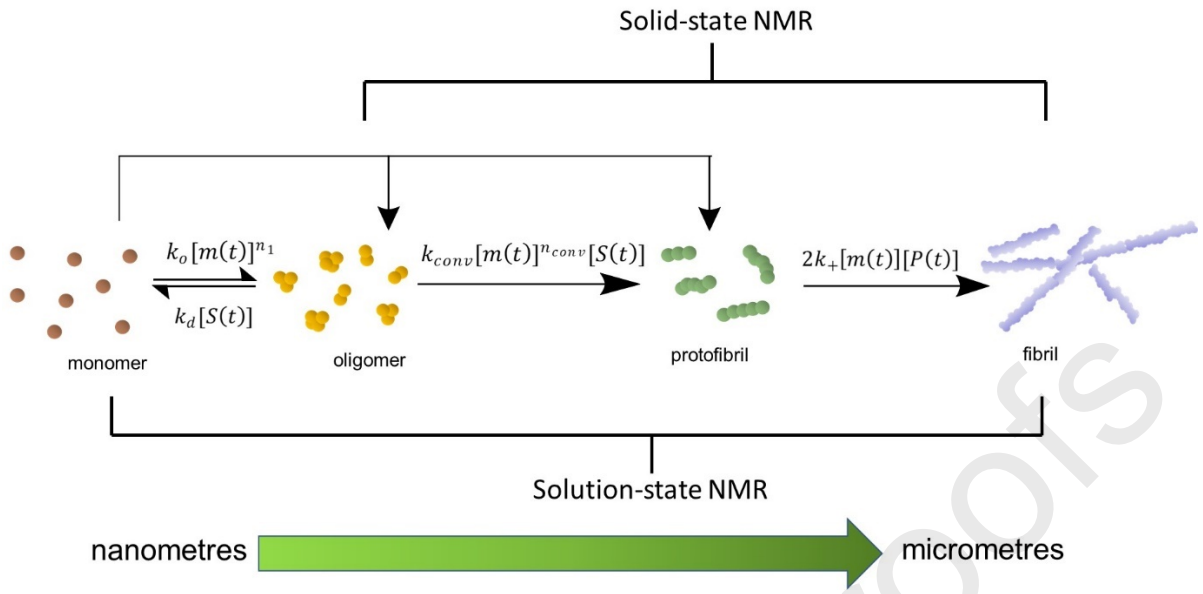

Fig. 2. Stages of the amyloid assembly pathway and their accessibility to NMR.

at a constant ionic strength. It is now clear, however, that amyloid plaque composition *in vivo* is highly diverse and heterogeneous, comprising protein fibrils, non-fibrillar proteins and auxiliary non-protein components including metal ions [21, 22], glycosaminoglycans (GAGs) and proteoglycans [23, 24], nucleic acid fragments [25-28], cholesterol and lipids [29]. Many of these *accessory molecules* and ions modulate amyloid aggregation kinetics, assembly pathway and fibrillar morphology, and some are considered culpable in the onset and progression of pathology [30]. Interactions of amyloid with exogeneous synthetic molecules, such as therapeutic amyloid inhibitors and diagnostic radioligands, are also of considerable interest for research and clinical applications *in vitro* and *in vivo*.

The mechanisms by which accessory molecules and ions influence protein aggregation depend on the nature of the interacting species, together with environmental factors such as pH, ionic strength and local protein concentration. Aggregation in general is usually initiated by the partial unfolding of proteins into transiently-populated intermediate states that expose aggregation-prone regions [31]. This process promotes the formation of stable oligomers that may undergo internal structural ordering into aggregation-competent species that rapidly catalyse fibril growth via a templating mechanism. The early assembly stages may be accelerated or impeded by interactions with accessory species, and further molecules and ions may be recruited into the growing fibrils. Hydrophobic effects likely play a central role in promoting aggregation [32]. Metal ions, for example, may partially or fully neutralize charged residues in the partially folded protein according to local pH, which can promote hydrophobic collapse that restricts the solvent exposed surface area of the protein. In such cases, formation of intermolecular backbone hydrogen bonds between proteins - a key feature of amyloid – may occur to offset the loss of the solvent-accessible area [32]. Polyanionic molecules, such as heparin, and charged surfaces of lipid bilayers may further act as concentration zones to promote collisions between proteins or templates to facilitate aggregation [33]. Other molecules, such as polyphenols, which tend to be planar entities, may inhibit protein aggregation by inserting between nascent β-sheet laminae of mature or growing fibrils [34].

NMR spectroscopy is ideal – and, arguably, the method of choice – for probing these interactions in detail in order to observe the effects from the perspectives of the aggregating protein and the interacting species. NMR can provide molecular and atomic-resolution details that are inaccessible to other techniques because of the heterogeneity of the systems. This article reviews the NMR methodology for studying amyloid interactions, in order to highlight the main applications and the associated challenges and considerations.

2. Applications of NMR to amyloid

2.1. Practical considerations

Amyloid formation may be described reductively as the conversion of metastable, soluble protein monomers into thermodynamically stable, insoluble fibrils. These two extreme states bookend the complex, stochastic and environmentally-dependent pathways of primary and secondary nucleation processes and the highly variable periods during which monomeric, oligomeric, protofibrillar and fibrillar species

Table 2. **Definitions of common terms for amyloid species**.

Terminology	Definition	Notable references
Monomer	The initial building block of amyloid. Usually, an intrinsically disordered protein with a propensity to form α-helices in the presence of micelles or membranes.	[35-37]
Oligomers	Soluble supramolecular clusters of amyloid proteins formed as critical kinetic intermediates in the formation of fibrillar aggregates. They exhibit a great diversity of structures and morphologies, including annular, spherical and globulomeric forms, with sizes ranging from < 10 kDa to hundreds of kDa. Oligomers are cytotoxic, and Aβ oligomers are widely believed to be the most pathogenic form of Aβ.	[38-41]
Protofibrils	Major cytotoxic Aβ species and candidate structures for the causative agent of AD. Protofibrils have been identified as the earliest fibrillar aggregates within the Aβ amyloidogenic pathway. They are large (>100 kDa; 60 – 220 nm long) soluble oligomeric species appearing as a peak in the void volume of size exclusion chromatography.	[42-45]
Protofilaments	Filamentous building blocks of amyloid fibrils, typically 20 - 25 Å in diameter. They are a substructure of the	[46, 47]

	amyloid fibril and consist of highly ordered peptide chains that form the fibrillar cross-β-structure.	
Fibrils	Fibrous protein polymers consisting of β-sheets of repeating arrays of identical monomer units, held together by backbone amide hydrogen bonds oriented approximately parallel with the fibril axis, and by a "steric zipper" of amino acid side chain interactions perpendicular to the fibril axis. This so-called cross-β structural motif is common to all amyloid fibrils regardless of the underlying protein sequence. Fibrils are typically 7 – 13 nm in diameter and several micrometres in length.	[48-50]
Filaments	A term normally applied to microtubule-associated protein tau (MAPT or tau) aggregates that are one of the pathological hallmarks of Alzheimer's and Pick's diseases. Pairs of individual filaments typically coil around each other (paired helical filaments) and have a combined width of 5 – 30 nm and a crossover distance of 65 – 100 nm. The filaments consist of a structured protein core, made mostly of the tau repeat domain, with less structured N- and C-terminal regions forming a fuzzy coat.	[15, 51, 52]

co-exist (**Table 2**). The complexity and lifetime of the intermediate stages are modulated by the presence of accessory species that can alter the assembly pathway and hasten the formation of fibrils. For example, polyanionic organic molecules (e.g. glycans) [53] and metal ions [54] can accelerate insoluble fibril formation, as described above, which may shorten the useful time window for conducting solution-state NMR measurements of early aggregating species before enhanced transverse relaxation broadens the lines beyond detection. NMR protocols must therefore be designed to account for the often-rapid kinetics in which monomeric proteins undergo changes in size and structure in the presence of accessory species. Conversely, molecules that inhibit amyloid formation and stabilise soluble species may be unsuitable to study using solid-state NMR.

NMR studies of amyloid interactions with accessory molecules are reported either by the amyloid protein resonances, for example to monitor structural changes and binding surfaces, or by resonances from the binding partner. NMR analyses are typically performed using multi-dimensional experiments that require selective, sparse or uniform isotopic labelling of the protein with combinations of ^{2}H, ^{15}N and ^{13}C nuclei [55]. Organic accessory molecules may also be labelled by chemical synthesis, or may already possess functional groups containing NMR active isotopes such as ^{31}P or ^{19}F. Smaller amyloid polypeptides of < 50 amino acids containing selective isotope labels, in contiguous blocks of amino acids, for example, can be prepared by solid-phase chemical synthesis [13]. This approach can be costly but is particularly useful for solid-state NMR of fibrils, because the simplification of the spectra allows for unambiguous

site-specific assignments and enables selective measurements of through-space dipolar couplings that restrain the supramolecular structure. Bacterial expression is the preferred option for the routine and economical isotope labelling of most proteins for NMR, and robust protocols have been developed for expression of many ^{13}C and ^{15}N amyloid proteins in *E. coli* [56]. Various isotope labelling patterns can be implemented by incorporating appropriate ^{13}C and ^{15}N enriched precursors in the bacterial expression medium to allow for an array of NMR assignment strategies, developed with the aid of small microcrystalline model proteins [57, 58].

Purification of amyloid-prone proteins can present challenges as compared to folded globular proteins, because it is necessary either to maintain the protein in a soluble monomeric state, or else to refold it from inclusion bodies [59, 60] for NMR analysis. During bacterial protein production, amyloid-forming proteins generally accumulate in inclusion bodies and need to be extracted (using, e.g., 8 M urea or 6 M guanidinium chloride), followed by purification using affinity- and size-exclusion chromatography. A further precautionary measure is to remove pre-existing fibril nucleating species by dissolution in hexafluoroisopropanol (HFIP), trifluoroethanol (TFE) or sodium hydroxide, followed by sonication and filtration [61, 62].

Whether solid-state or solution-state NMR methods are used is dictated by whether the subject of focus involves the early stages of protein aggregation or the mature, insoluble fibrils. The fibrils isolated at the end-point of aggregation are in many ways the easiest and least ambiguous amyloid species to study, by virtue of their relative structural homogeneity and their long-term stability in the condensed state. An abundance of MAS solid-state NMR methods have been designed to resolve the structures and interactions of fibrils, including in the presence of many accessory molecules. Soluble pre-fibrillar species, and interactions therewith, are more challenging to study because of their transitory and heterogeneous nature. Under NMR conditions, non-fibrillar proteins undergo assembly at rates that depend on a range of conditions under the control of the spectroscopist, including temperature, protein concentration, ionic strength and the chemical nature of any interacting species. Before commencing NMR analysis, it is useful to determine the amyloid assembly kinetics using Thioflavin T (ThT), a commonly-employed fluorescent dye that binds to the amyloid cross-β motif, or using circular dichroism spectroscopy to monitor the temporal changes in protein structure that accompany aggregation under different conditions. Both methods require relatively small amounts (<20 μM in < 200 μl) of unlabelled protein.

Protein aggregation is thermodynamically unfavourable below the crystalline solubility limit, and proteins remain stable in their monomeric states, potentially for an infinite time. Above the solubility limit, the solution becomes supersaturated and an equilibrium is established, with aggregated structures co-existing with the monomer. Closed sets of coupled rate equations have been devised for the conversion of free monomers, *m*, into fibrils, *P*, via on-pathway oligomers, *S* [63]. Simple forms are

$$\frac{d[S]}{dt} = k_o[m(t)]^{n_1} - k_{conv}[m(t)]^{'} - k_d[S(t)] \quad [1a]$$

$$\frac{d[P]}{dt} = k_{conv}[m(t)]^{n_{conv}}[S(t)] \quad [1b]$$

$$\frac{d[M]}{dt} = 2k_{+}[m(t)][P(t)] \quad [1c]$$

where *M* is the concentration of monomer in the fibrils ($m_{total} = m(t) + M(t)$), $k_o[m(t)]^{n_1}$ is the rate of formation of oligomers from monomers and $k_d[S(t)]$ is the reverse process, $k_c[S(t)]$ is the rate of conversion of oligomers into the species that undergo elongatation into fibrils and $2k_{+}[m(t)][P(t)]$ is the rate of monomer addition to either end of the growing fibrils. Further terms may be included for off-pathway assembly and secondary nucleation, whereby the surface of the growing fibrils catalyses the formation of further nucleating species. Monomeric protein may be lost immediately after dissolution, with rapid formation of a low population of short-lived oligomeric species co-existing with the larger, growing fibrils. The typical kinetic profile (e.g., as monitored by ThT fluorescence) is a sigmoidal curve (**Fig. 3**), representing an early lag regime that precedes the formation of a critical nucleating species, followed by rapid elongation of the protofibrils and fibrils until the curve plateaus as the monomer pool is depleted. Protein concentrations required for NMR are typically 0.1 – 1 mM and in the supersaturation regime, which is 10- to 100-fold higher than required for kinetic studies and several orders of magnitude higher than physiological concentrations.

One consequence of equations [1a] - [1c] is that aggregation rates measured for 20 μM protein using ThT fluorescence may be accelerated considerably at the 10-fold

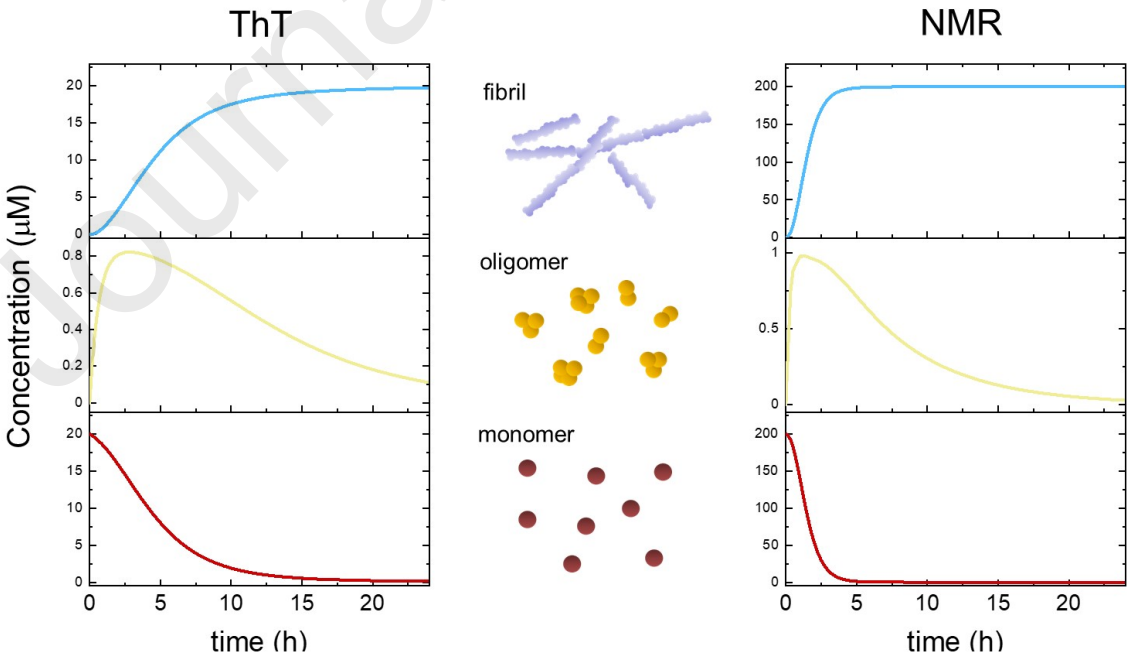

Fig. 3. Time dependence of amyloid oligomer and fibril formation described by rate constants (k_o, k_{conv}, k_+) at two different protein concentrations. ThT analysis typically requires a protein concentration of 20 μM, and solution-state NMR usually requires a protein concentration of at least 200 μM. Note the comparatively low transient concentration of oligomers during aggregation.

higher concentration required for solution NMR analysis (**Fig. 3**). Rapid growth of the aggregates may broaden the NMR signals in a matter of minutes or hours. For example, signal intensities in solution NMR spectra of the Alzheimer's Aβ40 peptide at concentrations of < 100 μM have been reported to remain stable for several weeks, but signals for protein concentrations above 150 μM decay uniformly to less than 70 % of their original intensity over a period of about 1 week until a pseudo-equilibrium is established [41].

2.2. Considerations for the solution NMR analysis of amyloid

In favourable cases, solution-state NMR methods may be used to study the full range of amyloid species, from monomers to fibrils, and their interactions. The challenges for NMR posed by the dynamics of transitory amyloid species in the early stages of aggregation may be heightened by the addition of accessory molecules and ions, which often enhance the rate of aggregation and the size of the assembling species. The widths and heights of NMR peaks are directly proportional to the nuclear transverse relaxation rate constant, R_2, which, in turn, depends on the molecular rotational correlation time, τ_C.

As the aggregating proteins increase in size, they tumble more slowly (i.e., τ_C becomes longer) and the NMR resonances become broader and decrease in height. The rotational diffusion constant D_r is described by the Stokes-Einstein equation for a spherical particle of hydrodynamic radius R in solvent of viscosity η,

$$D_R = \frac{k_B T}{8\pi\eta r^3} \quad [2]$$

The overall rotational correlation time, τ_C, of the molecule is given by $\tau_C = 1/(2 D_R)$. This form of Eq. [2] is relevant to spherical amyloid oligomers, for which diameters of 15 – 16 nm have been measured (for Aβ42 [64]). Transverse relaxation rates can be calculated according to (see, e.g., [65] and references therein),

$$R_2 = \frac{d^2}{2}[J(\omega_H - \omega_X) + 6J(\omega_H) + 6J(\omega_H + \quad [3]$$

where ω_H and ω_X are the Larmor frequencies of protons and the X nucleus (^{15}N or ^{13}C), respectively, c and d are constants representing the chemical shielding and dipolar contributions to relaxation, and $J(\omega)$ is the spectral density function. Various definitions of $J(\omega)$ have been proposed, including from the model-free approach described by Lipari and Szabo [66],

$$J(\omega) = \frac{2}{5}\left[\frac{S^2}{1+(\tau_c\omega)^2} + \frac{(1-S^2)(\tau_c+\tau_i)\tau_i}{(\tau_c+\tau_i)^2+(\tau_c\tau_i\omega)^2}\right] \quad [4]$$

where τ_i is the correlation time for local internal dynamics. *S* is an order parameter describing the amplitude of $^{13}C - {}^{1}H$ or $^{15}N - {}^{1}H$ bond motions ($0 \leq S \leq 1$, where $S = 0$ when motion is isotropic and $S = 1$ when no motion occurs). According to Eqs. [3] and [4], one would expect T_2 relaxation times of 3 – 5 μs for spherical oligomers of diameter 16 nm in the absence of local motion ($S = 1$) at 25°C in a solvent of typical viscosity (~0.7 mPa s for water at 310 K). Visualisation of larger aggregates formed in the later stages of protein self-assembly is therefore favoured if the protein contains regions of high local flexibility.

Larger protein aggregates such as protofilaments tend to have more elongated, rod-like morphologies. An equation for the rotational diffusion constant of a rod-like molecule of diameter *d*, perpendicular to a long axis of length *L*, has been formulated by Tirado *et al.* [67]:

$$D_{r\perp} = \frac{3k_BT(\ln p + \delta)}{\pi\eta L^3} \quad [5]$$

where $p = L/d$ and $\delta = -0.662 + 0.917/p - 0.05/p^2$. Appropriate to such a case, Tjandra proposed an approximate spectral density function, $J(\omega)$, for an axially symmetric diffusion tensor ($D_X = D_Y = D_\perp$, $D_Z = D_\parallel$) [68]

$$J(\omega) = S^2 \sum_{k=1,\ldots,3} A_k \left[\frac{\tau_k}{1+\omega^2\tau_j} + (1-S^2)\frac{\tau}{1+\omega^2\tau^2}\right] \quad [6]$$

with $A_1 = (1.5\cos^2\alpha - 0.5)^2$, $A_2 = 3\sin^2\alpha\cos^2\alpha$, $A_3 = 0.75\sin^2\alpha$, where α is the angle between the N-H bond vector and the cylinder axis (approximately 90° in the case of amyloid fibrils). The time constants are $\tau_1 = 1/(6D_\perp)$, $\tau_2 = 1/(D_\parallel + 5D_\perp)$, $\tau_3 = 1/(4D_\parallel + 2D_\perp)$. Calculated transverse relation times for the typical dimensions (hydrodynamic radius and length) of monomers, oligomers and (proto)fibrils are shown in **Fig 4a**.

NMR measurements of protein structural changes and interactions during the early stages of aggregation, in which the protein species are relatively small and soluble, rely upon two-dimensional (2D) $^{1}H - {}^{15}N$ HSQC experiments and variations thereof. With judicious choice of experimental conditions, amyloid-forming proteins may be observable in $^{1}H - {}^{15}N$ HSQC spectra recorded over days or weeks, whereas in other cases aggregation may occur over a matter of hours and the spectra become

broadened beyond detection. The size distribution of amyloid aggregates can change dynamically during a typical multidimensional NMR experiment. It may be desirable, therefore, to reduce NMR measurement times by using rapid methods such as ^{1}H – ^{15}N SOFAST-HMQC [69], which combines band-selectivity with optimized flip angles and short transients to obtain 2D spectra in a matter of seconds, or with non-uniform sampling to reduce the number of increments in the indirect dimension [70].

Peaks from larger aggregates, and even fibrils, may be visible in HSQC NMR spectra if the amino acid residues outside of the fibril core are mobile enough to scale down the contributions of dipolar interactions to transverse relaxation rates [71]. Locally flexible regions may occur naturally or can be engineered into the protein, and rapidly rotating side-chain methyl protons of valine, (iso)leucine, methionine and threonine residues may further preserve long-lifetime coherences of fibrillar species [72]. Local dynamics

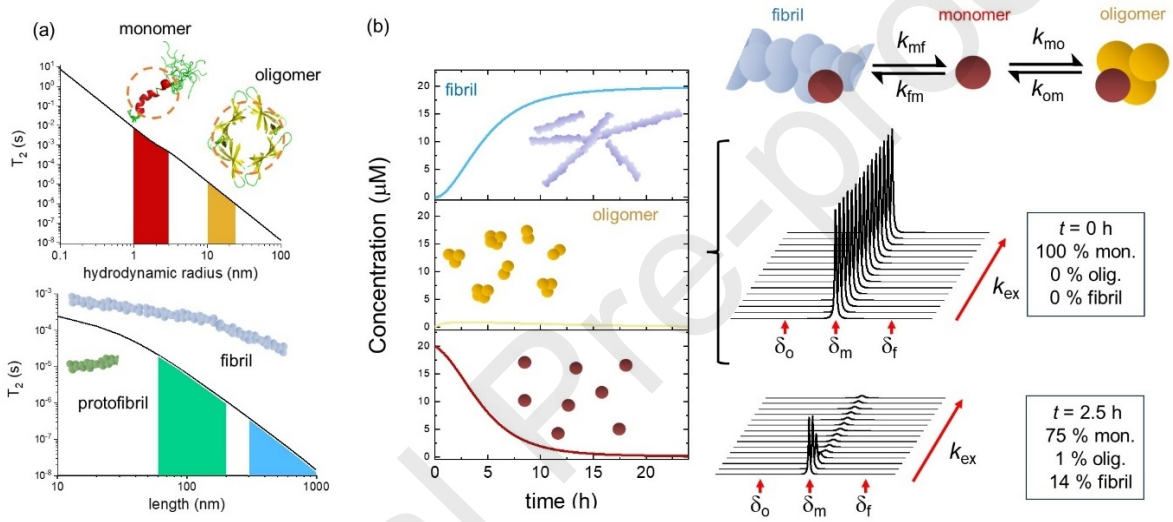

Fig. 4. Amyloid dynamics and NMR visibility. (a) Relationship between molecular dimensions of amyloid species and T_2 relaxation times. Monomer and oligomer relaxation times are calculated using the spherical approximation of molecular diffusion (Eq. [2]). Protofibrils and fibril relation times are calculated using the approximation for rod-like molecules (Eq. [5]). (b) Effects on NMR peak widths and intensities of the rates of monomer exchange between fibril and oligomers at different stages of the protein aggregation time course. The time course of amyloid aggregation is redrawn from Fig. 3 (left) to emphasise the low concentration of oligomers. The overall exchange rate constant $k_{ex} = k_{mo} + k_{om} + k_{mf} + k_{fm}$.

may therefore favour NMR linewidths comparable to those of monomeric peptides in solution, making possible the application of a wide range of NMR techniques for analysis of structure and determination of anisotropic diffusion coefficients and of sizes of molecular aggregates.

When amyloid fibrils do not contain flexible regions, additional measures can be used to observe resonances in the NMR spectrum. For example, solution NMR spectra of intact fibrils of β_2-microglobulin (β_2m) exhibit few signals because the fibrils have limited flexibility and are hundreds of nanometres long, which corresponds to a size of several tens of MDa [73]. Ultrasonic fragmentation of the fibrils enabled

recovery of solution NMR signals by reducing the fibrillar size and increasing their rate of reorientation. Pulsed field gradient (PFG) NMR of the fragmented fibrils obtained an effective translational diffusion coefficient (D_t) value corresponding to a molecular weight of 330 kDa, which equates to 30 – 40 monomer units on average per fibril fragment [73]. The fragmented fibrils are still large, but the presence of moderately flexible regions makes the direct observation of some residues possible. An alternative approach to observe broadened NMR peaks is to use indirect detection methods. For instance, incubation of the Aβ40 peptide for a week established an equilibrium between an NMR-visible monomeric species and NMR-invisible oligomeric "dark" state with enhanced R_2 relaxation rates [41]. By using saturation transfer NMR, the underlying broad resonances of the large oligomers were partially saturated and saturation transferred to the monomer, resulting in an overall decrease in intensity of the ^1H_N backbone amide envelope. The saturation profiles were fitted to yield values for the dissociation rate constant, k_{off}. Hence, it is possible to observe amyloid species up to fibrillar scale by combining appropriate sample preparation and solution NMR methods.

Chemical exchange is a further source of NMR line broadening, which may occur at any stage of protein aggregation independently of molecular size. Exchange phenomena include the association and dissociation of accessory molecules and ions with monomers and aggregates, as well as the exchange of monomeric proteins on and off the surfaces of fibrils and oligomers (**Fig. 4b**). The widths of observed NMR resonances depend on the chemical shifts of the species in the free and bound states, and the rate of exchange between the states. The free precession of transverse magnetization, *M*, in the presence of chemical exchange is described by a set of linear differential equations and can be represented by Bloch-McConnell exchange-coupled equations 7 of the form:

$$\frac{d}{dt}\begin{pmatrix} M_A \\ M_B \end{pmatrix} = \begin{pmatrix} i\omega_A - R_A - k_f & k_r \\ k_f & i\omega_B - R_B - k_r \end{pmatrix}\begin{pmatrix} M_A \\ M_B \end{pmatrix} \quad [7]$$

The given example is for a 2-site exchange model, where M_A and M_B represent the transverse magnetisation of species *A* and *B* and ω_A and ω_B are their frequencies, $k_f$and k_r are the forward and reverse rate constants for chemical exchange and R_A and R_B are the transverse relaxation rates in the absence of exchange. The solution to [7] is an equation of the form

$$M(t) = c_{11}e^{\Lambda_1 t} + c_{12}e^{\Lambda_1 t} + c_{21}e^{\Lambda_2 t} + c_{22}e^{\Lambda_2 t} \quad [8]$$

in which Λ_i are the eigenvalues of Eq. [6] and coefficients c_{ij} are derived from the eigenvalues and eigenvectors. **Fig 4b** shows that, even when the concentration of oligomers and fibrils is low compared to the monomer concentration, exchange can significantly broaden the resonances of the monomer.

Chemical exchange between two states is classified as slow, intermediate or fast according to the relative values of the exchange rate constant, k_{ex}, and the chemical shift difference between the two states, $\Delta\omega = |\Omega_A - \Omega_B|$. The broadening of NMR peaks is greatest when $k_{ex} \sim \Delta\omega$, where the two resonance lines coalesce and often apparently disappear from the spectrum (see below). To determine the contributions of aggregation and exchange mechanisms to line broadening, it is useful to acquire a series of NMR spectra (e.g., ^{1}H-^{15}N HSQC) during temperature cycling [74]. Increasing the temperature will generally accelerate line broadening originating from protein aggregation, but may either sharpen or broaden further the NMR lines if chemical exchange is the principal broadening mechanism. Protein aggregation is generally irreversible when the temperature is lowered and the line broadening involved at the higher temperature will persist, whereas exchange broadening is reversible, and the spectrum should revert to its original appearance.

When the resolution of the NMR spectrum is too poor to allow structural analysis, a limited number of NMR signature peaks may be used to measure the effects of interactions on amyloid diffusion constants, using PFG experiments. With sophisticated multilinear analysis methods, it is possible to deconvolute NMR diffusion curves into individual groups of differently sized species and monitor their kinetic rates of formation or disappearance. This approach was used to identify oligomeric species that form transiently during aggregation of human superoxide dismutase 1 (SOD1) associated with ALS [75]. The translational diffusion coefficient, $D = (1.40 \pm 0.02) \times 10^{-10}$ m^2 s^{-1}, for this species corresponds to a Stokes' radius $r_s = 23$ Å. However, for micrometre-sized objects, such as amyloid fibrils, diffusion curves must take into account the rotational diffusion of the molecular assembly in addition to translational diffusion [76]. Modifying a protein with non-proteinogenic nuclei, such as ^{19}F in trifluoromethyl groups, may be beneficial because the NMR spectra do not suffer from overlapping signals that can hinder the interpretation of proton-detected spectra. Moreover, the large range and sensitivity to environment of the ^{19}F chemical shift is ideal for detecting multiple soluble species formed during protein aggregation. For example, ^{19}F solution NMR of Aβ40, modified by solid-phase synthesis to replace the methyl group of Met35 with a -CF_3 group, resolved peaks from 35.5 – 36.0 ppm from multiple low molecular weight oligomers that formed over the course of several days [77]. An alternative approach was employed to attach ^{19}F labels to monomers of the 127-resiue transthyretin (TTR), the protein precursor of familial TTR amyloidosis (ATTR) associated with early-onset amyloid polyneuropathy and cardiomyopathy. The size of the protein is not suitable for solid-phase synthesis and so recombinantly-expressed TTRs containing individual cysteine mutations at different positions were reacted with 3-bromo-1,1,1-trifluoroacetone (BTFA). The ^{19}F chemical shifts were sensitive to the location of the -CF_3 groups and to the aggregation status of the protein, chemical shifts distinguishing the native tetrameric, aggregation-prone monomeric and oligomeric forms [78]. Chemical shifts, peak intensity and relaxation measurements reported on the aggregation rate and monomer-oligomer exchange rate of the protein.

2.3. Considerations for the solid-state NMR analysis of amyloid fibrils

Solid-state NMR has been used chiefly to examine the structures of insoluble amyloid fibrils and their sites of interaction with accessory molecules. One of the flagship achievements of biomolecular solid-state NMR has been to provide structural constraints underpinning atomic-level models of amyloid fibrils, including models of Aβ

peptides and tau. At the time of writing, the Protein Data Bank (PDB) contains the atomic coordinates of 45 models of amyloid fibril architectures that are based partly or wholly on structural restraints measured by solid-state NMR. Solid-state NMR is now proving to be an exceptional tool for mapping the sites of interactions of amyloid fibrils with accessory ions and molecules that influence the formation and degradation of amyloid *in vivo* [79].

Amyloid fibrils prepared for NMR analysis are hydrated, gel-like substances that behave similarly to solid materials, in that their restricted overall and local mobility averages the chemical shift anisotropy (CSA) of nuclear spins and spin-spin dipolar couplings incompletely. Insoluble fibrils are isolated by centrifugation and transferred to a MAS rotor as a hydrated pellet or after freeze-drying. Accessory molecules or ions can be titrated into fibrillar suspensions for solid-state NMR mapping of binding affinities and interaction sites, or else can be present from the onset of aggregation to observe how interactions modulate the fibril growth pathway and morphology. MAS solid-state NMR coherently averages the anisotropic nuclear spin interactions of fibrils and their binding partners to yield high-resolution spectra from which structural restraints can be obtained. An advantage of MAS solid-state NMR over X-ray diffraction is that structural studies of large molecules and complexes lacking long-range order are possible. Nevertheless, some degree of local order is required to obtain a sufficient level of resolution to enable resonance assignments and measurements of chemical shifts and dipolar couplings that define structures and interaction sites. Without optimisation of sample preparation protocols, the line widths and resolution of resultant spectra can be disappointingly broad owing to the structural heterogeneity of the fibrils. Many amyloid proteins assemble into coexisting structurally-distinct fibrillar morphologies with different underlying molecular structures, which are difficult to separate once formed. Structural polymorphism is brought about by intermolecular interactions that compete with the intramolecular interactions that drive metastable folding intermediates towards native low energy folded states [80]. In some cases, a limited number of fibrillar polymorphs may form, which manifest as the duplication of NMR resonances with distinct chemical shifts [4] (**Fig. 5**). Multiple resonances may originate from co-existing species with different arrangements of protofilaments or individual peptide β-strands [4]. More commonly, NMR resonances are broadened indistinctly by the formation of a broad distribution of polymorphs. Solid-state NMR experiments to map the interactions of amyloid fibrils with accessory molecules and ions rely upon being able to observe selective chemical shift perturbations for residues around the interaction site. It is essential, therefore, that resonance lines be as narrow as possible if chemical shift perturbations that may be a fraction of a ppm are to be detected.

Fortunately, unique fibrillar morphologies and structures with favorable NMR linewidths can be isolated by carefully optimizing the conditions of sample preparation. Studies on Aβ peptides have shown that the observed fibril architectures, and hence the quality of NMR spectra, can be controlled by subtle variations in fibril growth conditions, such as pH, temperature, and whether the fibrils grow whilst the sample is

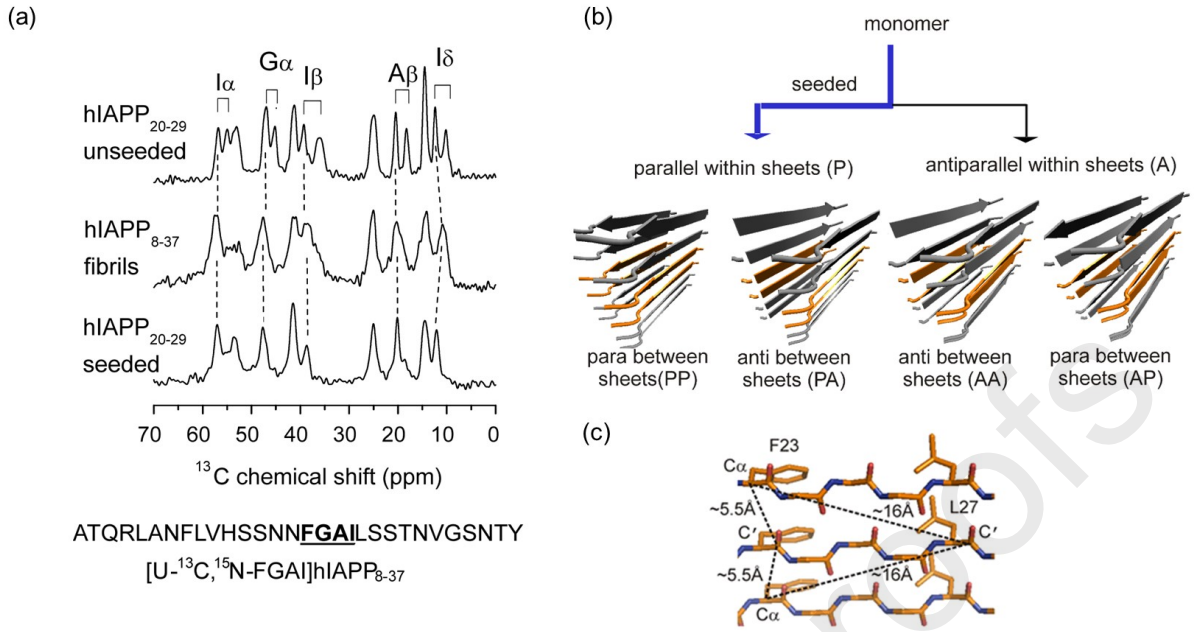

Fig. 5. Detection of fibril polymorphism by solid-state NMR. (a) ^{13}C CP-MAS solid-state NMR spectrum (at 9.39 T) of fibrils formed by a decapeptide, hIAPP$_{20-29}$, exhibit peak doubling consistent with two or more distinct fibrillar structures (top). Seeding fibril growth with preformed fibrils of the larger hIAPP$_{8-37}$ peptide (middle) eliminates peak doubling, consistent with morphologically pure fibrils (bottom) (b) Further dipolar-recoupling solid-state NMR experiments are consistent with the distinct fibril structures of hIAPP$_{20-29}$ having parallel and antiparallel β-strand arrangements. Adapted with permission from [4]. Copyright 2008 American Chemical Society.

agitated or quiescent [81, 82]. Fibrillar morphology and molecular structure are self-propagating when fibril growth is nucleated by preformed seeds of homogenous fibrils isolated from previous generations formed under specific conditions [82]. Repeated seeding (over tens of generations) can yield a homogeneous fibril structure with a unique set of sharp NMR resonances [83]. Pathological amyloid morphologies may be propagated through cross-seeding with *ex vivo* fibrils isolated from human tissue, as demonstrated for Aβ fibrils derived from post-mortem Alzheimer's brains [84, 85]. Solid-state NMR-derived ^{13}C chemical shifts, combined with cryo-EM images and supplemented by mass-per-length (MPL) measurements, indicate that the predominant molecular structure in brain-seeded fibrils differs from the structures of purely synthetic Aβ40 fibrils [84] [86]. One of the key messages from this work is that amyloid structure must be considered in the context of the growth environment, including the presence of accessory molecules.

A wide repertoire of experiments is available for NMR resonance assignments and to obtain structural constraints; many of these are implemented in the standard pulse sequence libraries supplied with modern spectrometers. Pulse sequences include 3D CANCO [87], NCACX and NCOCX [88] experiments, enabled by SPECIFIC-CP cross-polarisation from ^{13}Cα-^{15}N or ^{13}C'-^{15}N (where C' is the backbone amide carbon) [89]. Proton-assisted insensitive nuclei (PAIN) cross-polarisation enhances magnetisation transfer at high MAS rates and magnetic fields [90]. The development of superconducting magnets with persistent homogeneous fields greater

than 23 Tesla (^{1}H frequencies $\geq$ 1 gigahertz) has gone hand-in-hand with advances in ultrafast probe technology achieving MAS frequencies of > 110 kHz to extend the coherence lifetimes of protons in solids [91], including amyloid fibrils [92]. The longer coherence lifetimes enable the use of pulse sequences where polarisation transfer is mediated by scalar couplings. ^{1}H – ^{15}N HSQC-like spectra can be obtained with proton-detected experiments on fully protonated proteins [93]. At lower MAS frequencies (e.g., 40 kHz), perdeuteration of a protein yields efficient dilution of the proton spin system and subsequent back-exchange of amide protons reintroduces only weak ^{1}H – ^{1}H dipolar couplings which are efficiently suppressed by MAS [94, 95]. Once the resonances have been assigned, secondary structure across the sequence of the fibrillar protein may be determined using secondary chemical shifts and TALOS predictive methods [96]. Longer-range constraints on tertiary and quaternary structure are obtained using dipolar recoupling methods, including rotational-echo double resonance (REDOR) NMR (e.g., ^{13}C – ^{15}N) and 2D dipolar-assisted rotational resonance (DARR) experiments (^{13}C – ^{13}C) recorded at various mixing times [97] to measure through-space interactions between spins up to 6 Å apart.

A recent development in solid-state NMR applied to studies of the amyloid assembly process has been the development of time-resolved methods to monitor the transient nature and heterogeneity of intermediates formed in the early stages of Aβ self-assembly [98]. These methods are based on a combination of rapid mixing to initiate aggregation, rapid freezing to trap intermediate states, and sensitivity enhancements enabled by dynamic nuclear polarization (DNP) [99]. The ability of solid-state NMR to detect freeze-trapped unstable intermediate species is a unique feature of the technique that could be exploited further in the future to observe the effects of accessory molecules on aggregation pathways. The low temperatures (< 20°C) required to maintain frozen samples usually limits the MAS rates that can be used, however, and so sample spinning may be insufficient to eliminate ^{1}H dipolar couplings for proton observation. Broadening of the NMR signals may also arise from chemical disorder in the trapped species.

3. NMR studies of interactions during and after amyloid assembly

3.1. Interactions with glycosaminoglycans and proteoglycans

Glycosaminoglycan polysaccharides are negatively-charged, branched biopolymers that occur in every mammalian tissue type, and play extracellular roles in maintaining cell hydration, structural scaffolding and cell signalling [100]. The four main GAG types are heparan sulfate, chondroitin/dermatan sulfate, keratan sulfate and the unsulfated hyaluronic acid. GAGs accumulate with amyloid plaques ubiquitously *in vivo*, and enhance the rate of formation *in vitro* of amyloid and amyloid-like fibrils of α-synuclein [101], prion proteins [102] and the Alzheimer's Aβ40 and Aβ42 polypeptides [103] They can also have a marked effect on the resulting fibril morphology and neurotoxicity. GAG mimetics, which either accelerate fibril deposition and eliminate cytotoxic amyloid species, or inhibit amyloid deposition, are being evaluated clinically as Alzheimer's disease therapies [104].

NMR studies of amyloid protein-GAG interactions routinely employ low-molecular-weight heparin (LMWH; ~5 kDa) and high-molecular weight heparin (HMWH; ~16 kDa) as readily-available close analogues of the less abundant heparan sulfate. Certain amyloid-forming proteins, including the microtubule-associated

protein tau and the apolipoprotein A-I scaffold protein of high-density lipoprotein, require the presence of heparin or other polyanions to rapidly assemble into fibres for NMR analysis [105, 106]. The structure of heparin is heterogenous, and largely represented by the *N*-, 2-*O*- and 6-*O*-sulfated disaccharide sequence IdoA(2*S*)-(1→4)-GlcNS(6*S*) (**Fig. 6a**), as compared to HS, which consists of domains of highly sulfated disaccharides, minimally-sulfated blocks and partially N-sulfated, partially N-acetylated domains.

Amyloid-heparin interactions in the early aggregation stages, when the dominant protein species are monomers and small oligomers, can be probed by solution-state NMR (**Fig. 6**). However, GAGs typically enhance the rate of protein

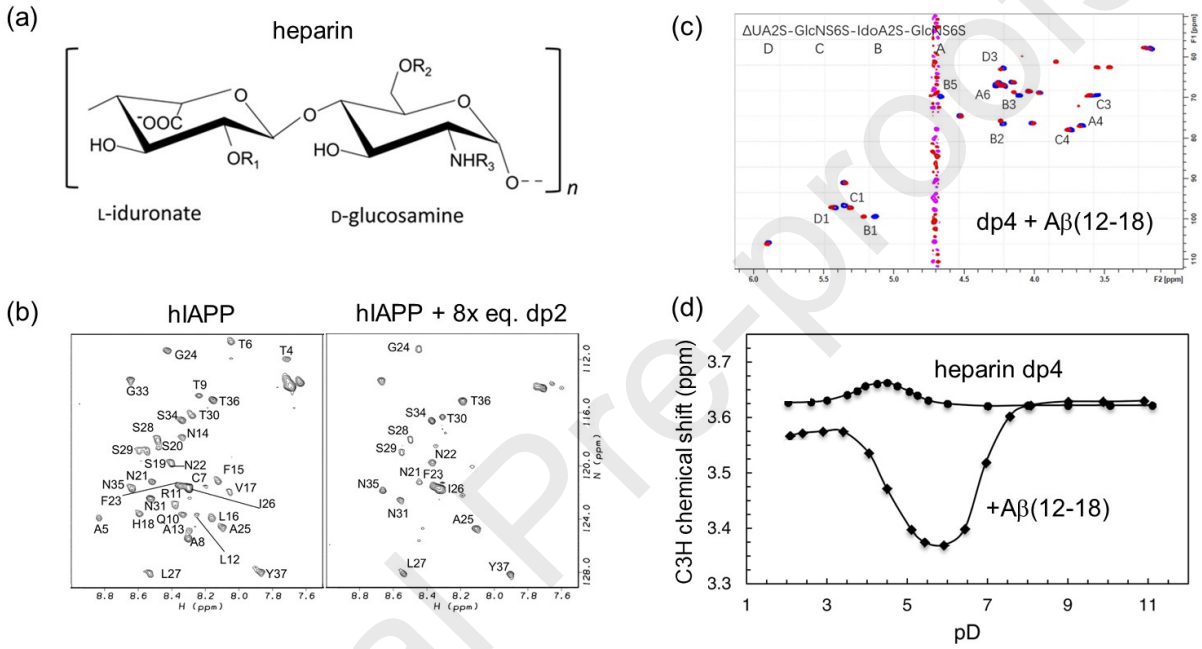

Fig. 6. Solution-state NMR analysis of heparin interactions with monomeric amyloid-forming peptides, from the perspectives of the two interacting partners. (a) The principal repeating unit of heparin (b) ^{1}H-^{15}N HSQC NMR spectrum (at 14.10 T) of hIAPP in the absence and presence of heparin-derived saccharides. Selective peak broadening, consistent with peptide aggregation, is similarly induced by equimolar heparin dp16 and by an 8-fold molar excess of dp2. (c) Spectra of a shorter peptide, Aβ(12-18), alone and in the presence of a heparin tetrasaccharide (at 14.10 T). Resonances remain narrow enough to enable binding to be mapped from chemical shift perturbations. (d) Observation of the C3H chemical shift of heparin dp4 (measured at 11.75 T) reveals different pD behaviour in the absence and presence of Aβ(12-18). Panel (b) adapted from [107] with permission. Panel (c) adapted from [108] with permission. Panel (d) adapted with permission from [109]; copyright 2016 American Chemical Society.

aggregation several-fold, and so the time window open to solution NMR analyses of GAG interactions may be limited before the complexes become too large and therefore NMR-invisible. Over short measurement times, 2D ^{1}H – ^{15}N HSQC NMR is a useful tool for mapping interaction sites for GAGs on the protein, by exploiting selective

backbone amide chemical shift perturbations [108, 110] or line broadening [110, 111] induced by titrating the protein monomer with polysaccharide, or by varying pH in the presence of the GAG at constant concentration. The underpinning 2D and 3D NMR experiments that are required to sequentially assign the backbone resonances in the HSQC spectrum can often be optimised first in the absence of GAGs under favourable conditions of pH, temperature and protein concentration, in which the protein remains stable for hours or days. For example, the ^{1}H – ^{15}N HSQC spectrum of 37 amino acid hIAPP, recorded from a fresh solution at pH 6 over 30 minutes, detects a single set of narrow resonances for all but the 3 N-terminal residues, and is consistent with the peptide remaining monomeric over this period. Addition of an equimolar concentration of a dp16 heparin fragment (dp = degree of polymerisation, followed by the number of monosaccharides) to monomeric hIAPP broadens resonances from residues 1–20 beyond detection, whereas resonances from residues 21–37 remain visible [107]. The selective NMR line broadening suggests a selective interaction between heparin and the amylin N-terminus that undergoes intermediate exchange on the chemical shift timescale. The effect of heparin dp16 is reproduced by an 8-fold higher concentration of the disaccharide, dp2, and hence the overall concentration of monosaccharide units and not the overall chain length appears to be important in this case (**Fig. 6b**). The range of concentrations over which the broadening effects are observed points to a K_d of 200 M for the binding of disaccharides to monomeric hIAPP.

Chemical shift perturbations and resonance line broadening have also been exploited to detect binding of heparin to monomeric tau protein [111]. Tau aggregates into filaments with a rigid and NMR-invisible core, flanked by flexible regions that remain visible to NMR. After tau aggregation in the presence of heparin, no chemical shift perturbations were observed from the remaining visible resonances flanking the core region. This observation suggests that all the available heparin is sequestered within the rigid core, losing its capacity to reversibly associate with parts of tau outside of the core.

An advantage of solution-state NMR when applied to GAG-protein interactions is that resonances from the protein and from the GAG occur in different regions of the ^{1}H and ^{13}C spectra. Solution NMR spectra of GAGs alone exhibit signature resonances from the anomeric and C3H protons at 5.0 – 5.5 ppm and carbons at 90 – 100 ppm [112], which lie outside the typical chemical shift ranges of protein backbone and side-chain resonances (**Fig. 6c**). Observations of these resonances can provide information on the interactions from the GAG perspective, provided appropriate water suppression techniques are used to avoid saturation transfer and bleaching of GAG signals. The negatively charged sulfate moieties of GAGs are critical for enhancing fibril formation [113] and may associate with clusters of basic residues of the amyloid protein, such as the predicted heparin binding motif $H_{13}HQK$ of Aβ peptides. Proton NMR measurements of the interaction between heparin tetrasaccharide (*dp*4) and the Aβ(12−18) model peptide showed a large upfield shift of the resonance for the C3H proton of the GlcNS(6S) residue in the presence of the peptide in 100 % D_2O, consistent with binding of the tetrasaccharide to the peptide [109] (**Fig. 6d**). The extent of the chemical shift perturbation was greatest around the pKa of histidine, suggesting a role for His-6, His-12 or His-13 in the binding. Titration of the heparin fragment with the amino acid histidine reproduced the ^{1}H chemical shift perturbation for the C3H proton of the GlcNS(6S) residue. It was inferred that the

deprotonated imidazolium ring of histidine interacts site-specifically with a cleft formed by an IdoA(2S)−GlcNS(6S)−IdoA(2S) triad sequence.

A suite of solid-state NMR experiments, combined with novel isotope labelling approaches, have provided unique and comprehensive atomic insights into the interaction sites of heparin with amyloid fibrils of Aβ40 and Aβ42, from both the perspective of the polypeptide and that of the GAG molecule [30, 114-116]. A ^{13}C-labelled chemically-modified heparin derivative was prepared as a reporter molecule for NMR observation. This was achieved by N-desulfating the GlcNS moiety of native heparin and adding an N-^{13}C-acetyl group. The labelled heparin derivative bound tightly to the Aβ40 fibrils and dipolar recoupling measurements detected close contact (< 5 Å) between the heparin acetyl $^{13}CH_3$ and an arginine side chain $^{13}C\zeta$, possibly Arg5 at the N-terminus [117] (**Fig. 7a**). Further solid-state NMR measurements were guided by a bespoke biochemical binding assay to detect heparin binding to the fibrils, in which unbound heparin is detected enzymatically in the supernatant after sedimentation of the bound heparin with the insoluble fibrils. Heparin binding to Aβ40 fibrils depends on the fibrillar morphology, and binds with higher affinity to fibrils of the three-fold-symmetric (3Q) seeded morphology than to the two-fold symmetry (2A) seeded fibril morphology. Titration of unlabelled heparin into uniformly ^{13}C-labelled fibrils resulted in selective ^{13}C chemical shift perturbations that were detected in 2D ^{13}C – ^{13}C dipolar correlation (DARR) experiments (**Fig. 7b**). The perturbations were greater for the 3Q fibril morphology than for the 2A morphology.

Chemical shift perturbations of <1 ppm could be observed because of the favourably narrow resonances, achieved by seeding the homogeneous 3Q fibril morphology. A 2D ^{1}H – ^{1}H spin diffusion experiment was then used to identify the residues situated closest to bound heparin (**Fig. 7c**). In this experiment, proton magnetization from the uniformly ^{13}C-labelled fibrils, but not from heparin, is dephased by an initial ^{1}H – ^{13}C REDOR step. A mixing period allows proton magnetization to be transferred by ^{1}H spin diffusion from heparin to the contact sites in the fibrils. After a short ^{1}H – ^{13}C Hartmann-Hahn cross-polarization time, the fibril ^{13}C magnetization is detected in a 2D ^{13}C – ^{13}C resolved double-quantum spectrum. Resonances are observed only for ^{13}C sites that are close to heparin and as a result of the ^{1}H – ^{1}H spin diffusion. With the combined chemical shift and spin diffusion data, the heparin binding site could be localized to the corner regions that are unique to the triangular cross-sectional 3Q fibril structure [114] (**Fig. 7d**). The binding specificity of heparin for this region was probed further by creating 14 seeded 3Q fibril variants of Aβ40 containing point substitutions in the amino acid sequence of Aβ40, followed by binding analysis of heparin to the variant fibrillar forms [116]. Solid-state NMR spectra confirmed that the mutations did not disrupt the 3Q morphology, inferred from the similarity of the backbone amide, Cα and Cβ ^{13}C chemical shifts of the different variants and, importantly, by detecting a cross-peak signifying a long-range interaction between H30 and V40 side chains, which is a signature of the hairpin structure of the protofilaments. Binding analysis of the variants confirmed that disruption of binding by non-conservative substitutions occurs at the corners of the triangles, where the spin diffusion and chemical shift perturbations also placed the interaction site (**Fig. 7e**). Charged residues at the fibril three-fold apices provide most of the binding free energy, while charged residues elsewhere are less critical for binding. The results suggest that LMWH binding to 3Q fibrils requires a precise molecular complementarity of the sulfate moieties on the GAG and charged residues displayed on the fibril surface.

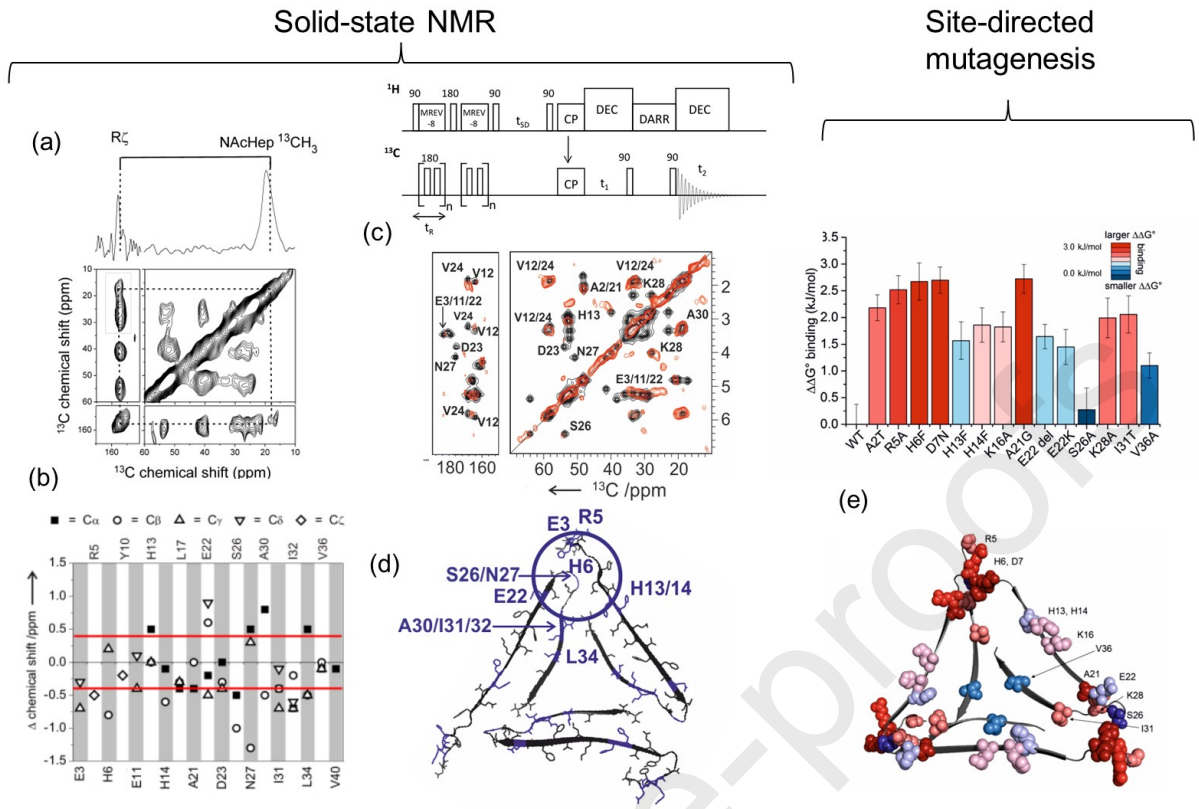

Fig. 7. Mapping the heparin recognition site within Aβ40 fibrils prepared with a threefold (3Q) structural symmetry. (a) A ^{13}C - ^{13}C DARR solid-state NMR spectrum (9.39 T) of fibrils bound to an N-[$^{13}CH_3$]acetyl heparin derivative is consistent with close proximity of the CH_3 group and arginine guanidinium group. (b) ^{13}C chemical shift perturbations (Δ chemical shift) for [U-^{13}C]Aβ40 after addition of heparin, determined from a 2D ^{13}C – ^{13}C dipolar correlation (DARR) CP-MAS solid-state NMR spectrum at 19.97 T). (c) A ^{13}C-detected ^{1}H – ^{1}H spin-diffusion experiment (9.3 T) detects residues in close contact with heparin (see text). (d) Fibril structure of Aβ40 (from PDB 2LMQ and [118]) showing the cluster of residues involved in heparin binding according to the NMR data. (e) Replacement by mutagenesis of the binding residues predicted by NMR results in lower affinity of heparin for the fibrils (coloured in red). Panel (a) reproduced from [117] with permission from The Royal Society of Chemistry. Panels (b)-(d) adapted from [114] with permission. Panel (e) reproduced from [116] with permission.

As was stated in the previous section, the morphology of fibrils is highly sensitive to growth conditions, and the presence of heparin and other GAGs may influence the rate and pathway of protein aggregation. The chemical shift signatures of fibrils can be exploited to understand how GAGs alter the fibrillar molecular architecture when they are included as an integral factor in the growth environment, as shown for the peptide hormones salmon calcitonin [119] and β-endorphin [120]. Fibrils of the bioactive C-36 peptide from the α_1-antitrypsin serine protease inhibitor gave different spectral ^{13}C – ^{13}C correlation signatures depending on whether they were assembled in the presence or absence of heparin [121]. The spectral resolution was greater for heparin-derived fibrils than for fibrils grown alone, likely due to the more homogeneous structural arrangement, suggesting that GAGs act as a template to direct the protein monomers into highly-ordered fibrils.

Solid-state NMR has also offered insights into how the sulfation pattern of heparin affects the growth rates and mechanism of tau filaments (**Fig. 8a**). The proportions of *N*-sulfate, 6-*O*-sulfate and 2-*O*-sulfate groups in GAGs are known to change during the lifetime of humans, which may contribute to the increased risk of developing amyloid disease in older age. A library of short heparin polysaccharides was prepared, in which the sulfate groups were removed from specific sites. Biochemical binding studies indicated that the *N*-sulfate or 6-*O*-sulfate of GlcNS(6S) residues is required for strong binding to Aβ40 fibrils, but that removal of the 2-*O*-sulfate of IdoA(2S) has minimal impact upon binding [105] (**Fig. 8b**). The results point to a selectivity in the interactions of GAG-fibril interactions that extends beyond general electrostatic complementarity. Solid-state NMR measurements of filaments formed by a truncated variant of ^{15}N,^{13}C-labelled tau were then performed to identify the rigid and mobile regions of the filaments formed in the presence of different de-sulfated HMWH analogues. Dipolar mediated ^{1}H – ^{13}C Hartmann-Hahn cross-polarization magic-angle spinning (CP-MAS) experiments are used to detect less mobile regions of fibrils in which molecular motions do not average dipolar interactions [15] (**Fig. 8c**). *J*-coupling mediated coherence transfer in experiments such as ^{1}H – ^{13}C INEPT (also with MAS) visualise mobile regions from the β-sheet cores of fibrils and filaments if the coherence lifetimes are long enough [119, 122]. Filaments formed in the presence of 2-*O*-desulfated heparin (HMW-2OH) were found to give CP-MAS NMR spectra with reduced intensity, consistent with a higher degree of overall flexibility, whereas ^{1}H – ^{13}C INEPT spectra exhibited many more peaks than are seen than in the spectrum of HMWH-induced filaments. Taken together, the combination of experiments confirmed that filaments formed in the presence of HMW-2OH-induced fibrils contain a greater number of flexible residues than do fibrils induced by HMWH.

Solid-state NMR detection of heparin and other GAGs bound to amyloid fibrils is challenging, since the direct observation of GAG ^{1}H signals is not straightforward. Although rapid MAS techniques are now facilitating ^{1}H-observed experiments for

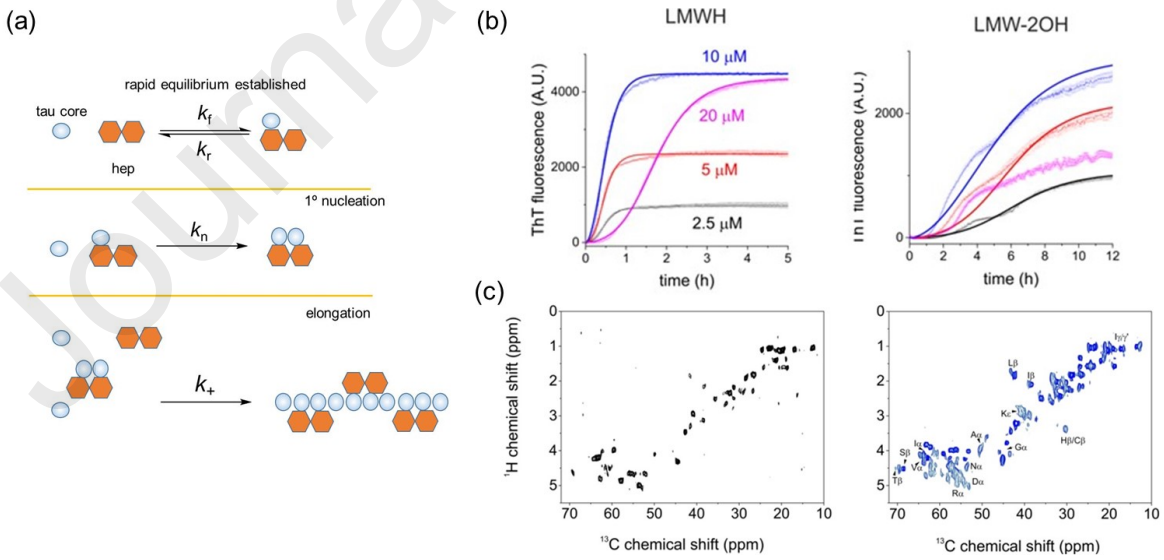

Fig. 8. Effects of heparin sulfation patterns on tau aggregates, determined by solid-state NMR. (a) Proposed role of heparin in tau filament assembly. Heparin acts as a template that nucleates aggregation-competent tau species and is also incorporated into the growing fibrils. (b) ThT analysis indicates that the heparin 2-OH group is

important for tau aggregation. (c) $^{1}H - {}^{13}C$ refocused INEPT solid-state NMR (at 16.44 T) indicates that the tau filaments are considerably more mobile in the presence of the 2-OH depleted heparin than with intact heparin. Adapted from [105] with permission. Copyright 2020 American Chemical Society.

protein analysis in the solid state by pushing the MAS rotation rate to >150 kHz [123], direct detection of GAG protons in the presence of fibrils is hampered by crowding and poor resolution. Observation of ^{13}C is therefore preferable, but requires isotope labelling to enhance sensitivity. As shown in **Fig. 7a**, limited ^{13}C labelling can be achieved by chemical derivatization of naturally sourced heparin, but it is necessary to confirm that derivatization does not hinder binding to the fibrils, such as happens when sulfate groups are removed (**Fig. 8b**). Chemoenzymatic methods developed over 15 years ago are available for isotope labelling of authentic GAGs [124], but control and isolation of the products is difficult and requires careful optimisation. Synthetic chemical methods offer more control and flexibility, but are costly.

A more labour-intensive approach was used, which required total synthesis of a uniformly ^{13}C-labeled heparin-derived octasaccharide, terminating with a closed, 1,6-anhydro iduronate residue at the former reducing end to prevent mutarotation [115]. The uniform ^{13}C labelling scheme was exploited using ^{13}C CP-MAS NMR to first confirm that heparin binds to hydrated and sedimented Aβ40 fibrils and then to observe the dynamics of heparin exchange between the free and bound environments. Dynamics were monitored from ^{13}C signal build-up curves for the ligand measured in a variable contact time $^{1}H - {}^{13}C$ Hartmann-Hahn cross-polarization experiment. The effect of the ligand dissociation rate constant, k_{off}, on the cross-polarization profile was simulated approximately by expressing the evolution of ^{13}C magnetisation, M_c, for heparin exchanging between free and bound environments as:

$$M_C(t_C) = \sum_N \left[\int_0^{t_1} \frac{dm_1}{dt} + \int_{t_1}^{t_2} \frac{dm_2}{dt} + \int_{t_2}^{t_3} \frac{dm_1}{dt} + \ldots \right] \quad [9]$$

Here, N is the total number of heparin molecules in the simulation and m_1 and m_2 represent the magnetisation for a particular chemical site of heparin in free or bound environments during the contact time t_c. The ligand is allowed to exchange stochastically between environments according to a probability density function that is dependent on k_{off}. The contact time is divided into steps $0 - t_1$, $t_1 - t_2$, etc, where the start point of each step is the time at which the ligand switches between free and bound states. The association rate constant, k_{on}, was assumed to be diffusion controlled and invariant. The build-up of magnetization in the two environments can be estimated according to

$$m_n(t) = m_n(0)\left(1 - \frac{R_n^{1\rho H}}{R_n^{HC}}\right)^{-1} \left[\exp\left(-R_n^{1\rho H} t\right) - \mathrm{e}\right. \quad [10]$$

where the subscript *n* (*n* = 1, 2) represents either the free or bound environments, $m_n(0)$ is the magnetization at the start of each switching point, R_n^{HC} is the proton rotating frame relaxation rate constant and $R_n^{1\rho H}$ is the ^{1}H – ^{13}C Hartmann-Hahn cross-polarization rate constant. Experimentally, it was found that the intensity profiles reached a maximum at 1 – 2 ms and then decayed to 30 – 50 % of the maximum value at a contact time of 8 ms and temperature of 4°C. Comparison with simulations indicated that the dynamics were consistent with a tight heparin-fibril complex in which all saccharide residues are restrained without undergoing substantial conformational changes. Further measurements of the Aβ40 fibril-octasaccharide complex (in which Aβ40 was ^{15}N-labelled) using frequency-selective REDOR NMR revealed intramolecular ^{13}C – ^{15}N dipolar dephasing that was consistent with close (< 5 Å) contact between the GAG anomeric position(s) and one or more histidine residues (His-6, His 12 and/or His-13) in the fibrils [115].

Many questions remain unanswered about the specificity of different GAG types for amyloid proteins and their effect on fibril structure. NMR in solution and in the solid state will continue to advance research endeavours in this field, aided by developments in GAG isotope labelling methods coupled with fast-MAS technology to overcome the issues associated with direct proton observation of fibril-bound GAGs.

3.2. Interactions with biological membranes

Many amyloidogenic peptides and proteins are amphipathic, and have a high propensity to associate with the lipid bilayer components of cellular, subcellular and vesicular membranes. Such interactions are considered to be pathologically important because amyloid proteins (principally Aβ, but also tau, hIAPP, α-synuclein and others) can destabilise cell membranes, compromise cellular ionic homeostasis, and exert cytotoxicity [125]. Amyloid-membrane interactions are driven initially by electrostatic and ionic associations between protein amino acid side-chains and the zwitterionic or anionic headgroups of phospholipids and gangliosides. The electrostatic biomembrane surface can stabilize protein secondary structures - often inducing α-helical intermediates [126] - and facilitate further cooperative conformational changes to amyloid-competent β-sheet species. High local concentrations and reduced translational degrees of freedom of amyloid proteins at membrane surfaces favour productive molecular encounters to form oligomers and fibrillar species [127, 128].

Mechanistically, amyloid-lipid membrane interactions are complex and may involve the assembly of protein oligomers that form membrane-spanning pores and nucleate the elongation of fibrils that extend away from the membrane surface (**Fig. 9**). Some protein aggregates may also sequester lipid molecules from cellular membranes: for example, tau filaments extracted from diseased brain tissue assemble with a hydrophobic pocket containing non-polar molecules such as sterols or fatty acids [129]. Amyloid proteins generally have highest affinity for membranes containing phospholipids bearing an overall negative charge (e.g., phosphatidylserine, phosphatidylglycerol), but the affinity of amyloid for specific lipid chemistries has also been demonstrated. For example, amyloid interactions with brain sphingolipids containing branched carboxylated polysaccharides, called gangliosides, appear to be pathologically relevant [130]. NMR has helped to unravel the complex interplay between protein-lipid and protein-protein interactions when proteins assemble into amyloid species in the presence of heterogenous membrane environments [128, 131,

132]. Specific questions that have been addressed by NMR are (i) the structural changes induced in the monomeric protein that precede aggregation, (ii) the

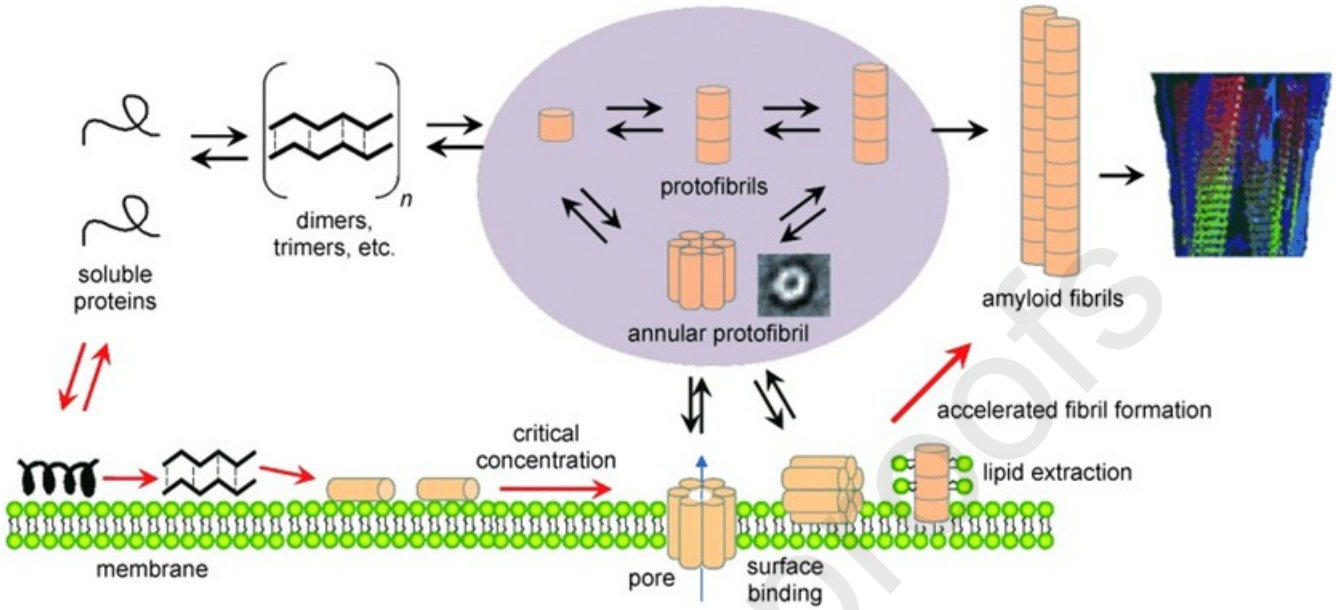

Fig. 9. Modes of interaction of amyloid with phospholipid bilayers. Reproduced from [133] with permission.

recognition sites for lipid-protein interactions, including the role of specific lipid headgroups, (iii) the mechanism of membrane pore-formation by amyloid oligomers and (iv) the influence of membrane-induced nucleation on the pathway of aggregation into fibrils.

Suitable model systems replicating the bilayer structures and compositions of cell membranes must be used for NMR analysis. A key consideration is the size and type of model membrane system [133], typical choices being detergent micelles (diameter d = 10 – 20 nm), discoidal bicelles (d = 20 – 50 nm) and liposomes. The latter may take the form of small unilamellar vesicles (SUVs; d = 20 – 100 nm), large unilamellar vesicles (LUVs; d = 100 – 250 nm) or large multilamellar vesicles (MLVs; d > 250 nm). Oriented lipid nanodiscs (d = 8 – 16 nm) have also been used [134]. Importantly, the model membrane system employed must be compatible with the NMR methodology; micelles, SUVs and some LUVs [126] tumble rapidly enough to permit high-resolution studies in solution, whereas the incomplete averaging of anisotropic spin interactions by slowly tumbling MLVs requires solid-state NMR using MAS for high-resolution spectra, or static samples to extract anisotropic spin information from line shapes. The size and surface curvature of model membranes may also influence protein interactions, and consequently the kinetics and pathway of amyloid aggregation [135].

Solving the high-resolution structures of monomeric amyloid proteins in lipid environments by NMR can be a major challenge due to molecular heterogeneity and rapid protein aggregation. Low temperatures may be employed to decrease the rate of aggregation during the measurement times. Detergent micelles may help to stabilize proteins in their monomeric states for solution-state NMR analysis; if this is the objective, optimisation of the detergent is required. Commonly-used detergents

[136] include sodium dodecylsulfate (SDS) [137], octyl glucoside (OG) [138], dodecylmaltoside [139], 1,2-dihexanoyl-sn-glycero-3-phosphocholine (DHPC) [140] and dodecylphosphocholine (DPC) [141]. For example, SDS micelles were found to stabilise hIAPP in its monomeric state at a detergent-to-peptide molar ratio of 80:1, by surrounding the hydrophobic detergent chains to minimise protein-protein contacts [142]. At 900 MHz, a combination of standard ^{1}H-^{1}H 2D TOCSY and NOESY spectra, combined with Mn^{2+} paramagnetic broadening experiments to identify exposed and buried residues, revealed an amphipathic helix-turn-polar helix structure of hIAPP that recurs as a common structural motif in monomeric amyloid proteins in detergent environments. The locations of the kinks largely correlate with the locations of the turns in the structure of the amyloid fibre. Further ^{15}N relaxation analyses of labelled hIAPP in SDS indicated that mobility increases from the N to the C terminus, and correlates with the accessibility of the polypeptide to extramicellar (Mn^{2+}) and intramicellar (16-doxyl-stearate) spin probes [143].

Aβ peptide interactions with ganglioside lipids have been the focus of several solution-state NMR studies, motivated by the prevalence of gangliosides in cells of the central nervous system and their ability to facilitate and promote the assembly of Aβ into fibrils *in vitro*. Micellar systems consisting of the single chain lyso-GM1 ganglioside are a useful model membrane system to identify how the lipid carbohydrate moiety interacts with Aβ in the prefibrillar stages of assembly. One approach is to exploit the ganglioside resonances to report the sites of Aβ interaction on the micelle surface. NOE and saturation transfer measurements on lyso-GM1 ganglioside micelles (approximately 60 kDa) enabled the structure and solvent exposure of the GM1 carbohydrate moiety to be determined [144] (**Fig. 10a**). By titrating the micelles with Aβ40 linked to a paramagnetic nitroxide via a C-terminally engineered cysteine, lipid-protein contact sites could then be determined from the extent of paramagnetic broadening of the carbohydrate resonances [144]. Resonances of Aβ have also been exploited to report where the ganglioside carbohydrates interact with the peptide (**Fig. 10b**). Titration of ^{15}N-labeled Aβ40 with GM1 induced chemical shift perturbations that were localized to the N-terminal half of the peptide, and implicated His13 and Leu17 in particular as residues involved in binding [145]. It was suggested that His13 of Aβ40 interacts specifically with the sialic acid (NeuAc) branch of GM1, as the chemical shift changes for this residue were less pronounced upon addition of asialo-GM1. An overall broadening of the resonances for Aβ40 was observed during the titration, as expected for binding to the large micellar assembly. Interestingly, the most dramatic broadening was seen around residues 27 and 37, even though these residues show only small chemical shift changes.

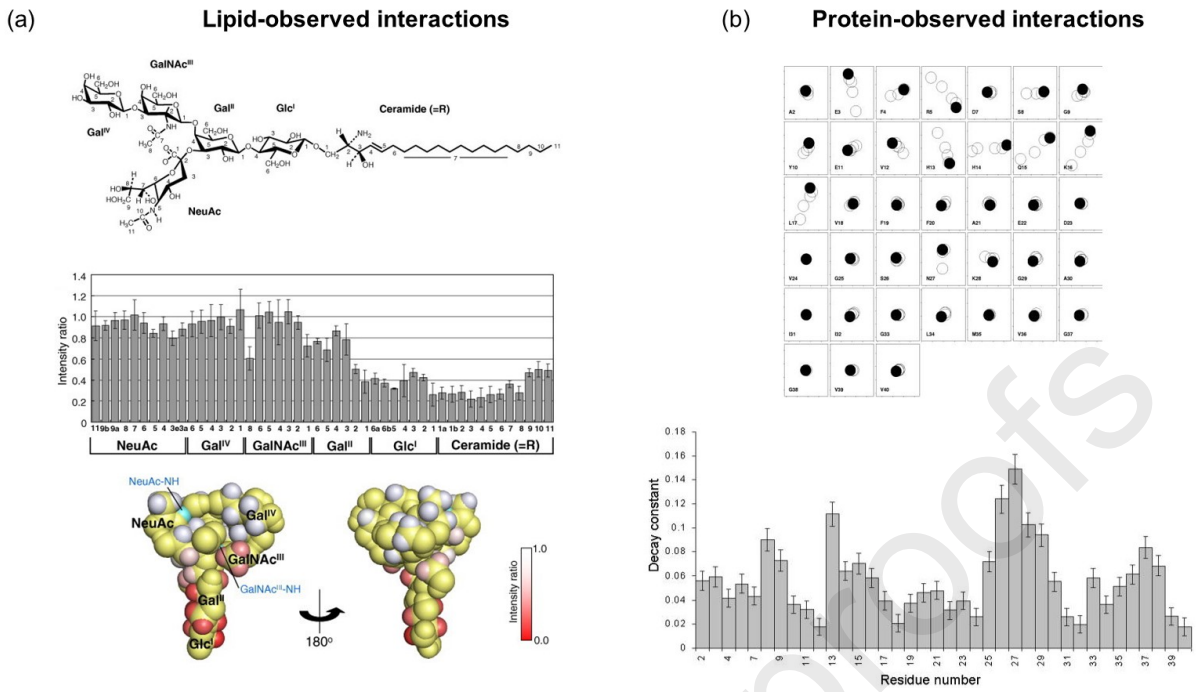

Fig. 10. Interactions between Aβ40 and GM1 ganglioside lipids, reported by solution NMR spectra of the lipid (a) and protein (b). (a) Structure of lyso-GM1 ganglioside (top); broadening of resonances (reported as an intensity ratio) for the different lipid moieties, induced by titration of nitroxide-labelled Aβ40 (middle); and intensity ratios mapped onto the structure of the GM1 headgroup determined from NOE constraints (bottom). (b) Summary of ^{15}N (vertical axis) and ^{1}H (horizontal axis) chemical shift perturbations (measured in an HSQC spectrum at 11.75 T) for Aβ40 titrated with GM1 (top); and summary of resonance broadening (reported as a decay constant) observed in the titration (bottom). Panel (a) adapted from [144] with permission. Panel (b) adapted from [145] with permission.

Solid-state NMR can be used to monitor structure and dynamics of amyloid proteins bound to larger model membrane systems like MLVs. Time-dependent structural changes in membrane-bound proteins may be observed that precede, or trigger, their assembly into amyloid species. For example, anionic phospholipids have been shown to promote α-synuclein aggregation into β-sheet fibrils via a partial α-helical intermediate state. The segmental transition from α-helical to β-sheet structures over a period of several days was evidenced by time-dependent chemical shift changes in 2D ^{13}C – ^{13}C NMR spectra, obtained at regular intervals from α-synuclein incubated with phospholipid vesicles [146-148]. During the structural transformation, distinct lipid binding domains of α-synuclein in close contact with the lipid bilayer can be probed in 2D experiments that monitor ^{1}H – ^{13}C spin diffusion rates from lipid to protein [146, 147]. The general form of the spin-diffusion experiment involves non-selective excitation of ^{1}H magnetization, which undergoes chemical shift evolution (with appropriate homonuclear decoupling) and then is stored longitudinally or under a spin-locking field to allow spin diffusion, before transfer to observed ^{13}C nuclei. Certain lipid and protein ^{1}H chemical shifts are distinct from each other and so correlations between ^{13}C resonances of the protein and ^{1}H resonances of the lipid chains, glyceryl backbone and headgroups can be detected. The observed intensities are dependent on ^{1}H – ^{13}C distances (**Fig. 11a**). This approach is similar in concept to

the method described in **Fig. 6c**, but relies on the mobility of the lipids to prepare selective magnetization before the spin diffusion step.

The formation of Aβ pores spanning the bilayers of cell membranes is a possible progenitor of the neurotoxicity observed in Alzheimer's, because the pores disrupt ionic homeostasis of the cells. Ion-conducting pores of Aβ oligomers have been successfully reconstituted into model membranes for NMR analysis. The relatively small sizes of detergent micelles provide a suitable membrane-like environment for solution NMR structural studies of pore-forming Aβ amyloid oligomers, but, as with studies of monomeric proteins, sample optimisation is vital to avoid adverse effects on the structure and oligomerization propensity of the protein [140]. A large excess of free micelles could act as a hydrophobic sink, causing unfavourable dissociation of Aβ oligomers into monomers and, conversely, low detergent concentrations may be insufficient to prevent further assembly of Aβ into amyloid fibrils. It is important therefore to vary the molar ratios of the Aβ and micelles and to screen a range of detergents, each having a characteristic critical micellar concentration (CMC), to optimise the conditions. Samples must be prepared to achieve monodispersity of the oligomer complex, which can be confirmed by size-exclusion chromatography [125]. NMR analysis of pore-forming Aβ40 oligomers in DPC micelles required TROSY-hyphenated methods combined with selective ^{13}C labelling and deuteration to improve signal resolution, because of the large combined size of the detergent-oligomer complex (τ_c = 22 ns at 37 °C). The observed chemical shifts were consistent with a β-barrel arrangement of the oligomers. Spectra of oligomers incorporated from the detergent into DPC/DMPC bicelles retained the same number and dispersity of peaks as observed for the detergent complex, consistent with a similar oligomeric structure in a bilayer environment. It should be noted that the transition from micelles to bicelles may cause broader signals because of increased correlation times of the latter system (τ_c > 30 ns at 37 °C).

Studies of membrane interactions of amyloid-forming protein oligomers with larger liposomal lipid bilayer environments usually require MAS solid-state NMR methods to obtain high-resolution spectra. For example, MAS NMR has been used to examine the membrane-bound structures of two distinct and stable α-synuclein oligomer species that have different characteristic membrane-disrupting properties and cytotoxicity [39]. The two species, which are prepared under different conditions, can be sedimented by ultracentrifugation at 300,000 *g* for MAS NMR analysis. The two functionally-distinct oligomers were distinguished structurally on the basis of their ^{13}C chemical shift signatures corresponding to the immobile and dynamic regions. Dynamically-distinct regions of the oligomers were visualised using ^{13}C – ^{13}C dipolar transfer (e.g., with dipolar-assisted rotational resonance mixing), to detect the most rigid regions in the core of the oligomers, and ^{1}H – ^{13}C with INEPT transfer to observe only the dynamic regions. Further, paramagnetic relaxation-enhanced ^{13}C – ^{13}C spectra of the two oligomer species added to phospholipid SUVs, by lipids labelled with a paramagnetic probe in either the acyl chains or lipid headgroups, confirmed that the more disruptive oligomer penetrated deeper into the hydrophobic core of the bilayer (**Fig. 11b**). In this work, the NMR resolution and sensitivity were insufficient to

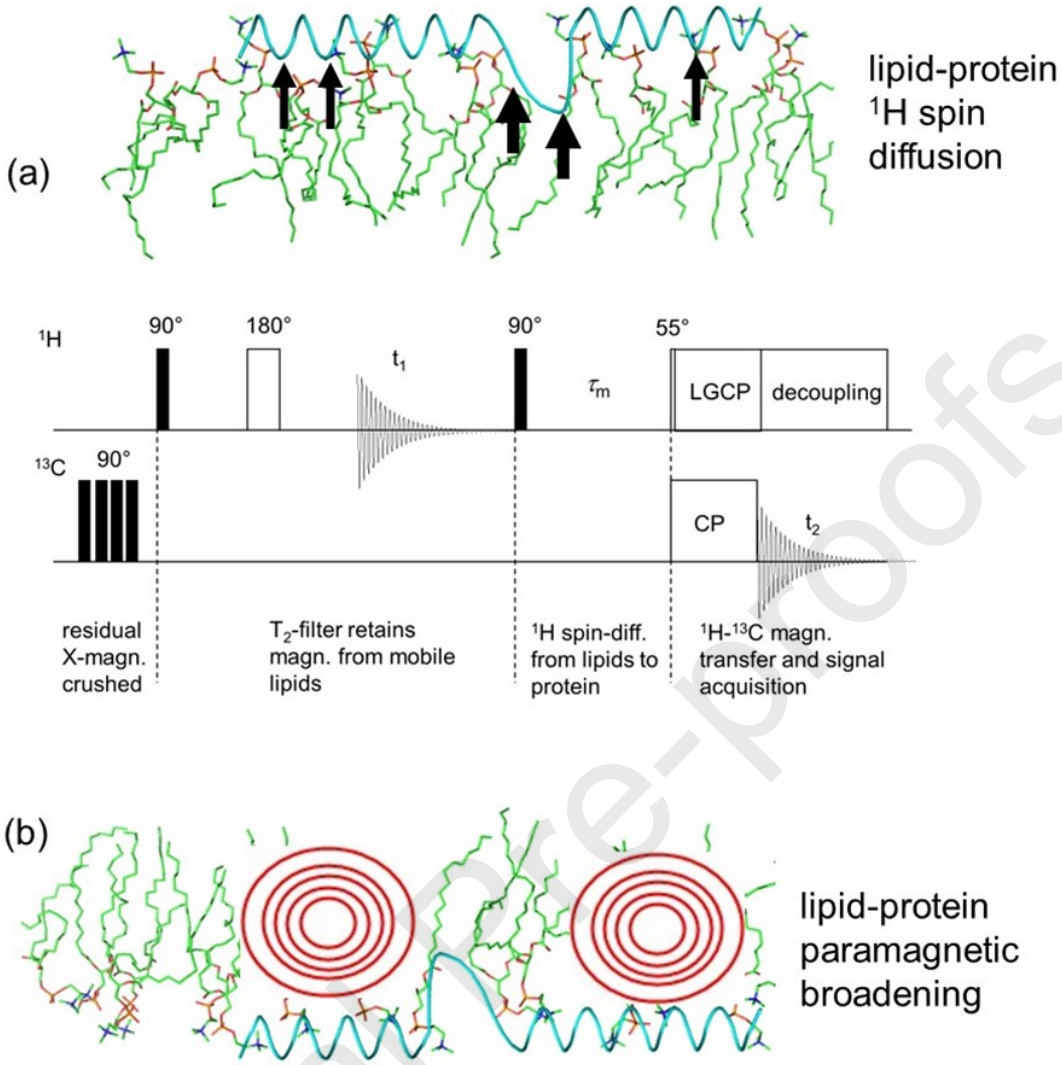

Fig. 11. Two solid-state NMR approaches to determine the topology (i.e., the exposed and buried regions) of amyloid proteins bound to lipid bilayers. (a) An experiment for detecting lipid-protein contacts from ^{13}C detection of rates of ^{1}H – ^{1}H spin diffusion from the lipid chains to the bound protein. (b) Depth of protein insertion into lipid bilayers, probed by protein resonance broadening by paramagnetic labels placed at a specific position in the lipid chains.

permit full sequential assignments of ^{13}C chemical shifts for α-synuclein when bound to membranes. Instead, ^{13}C – ^{13}C correlation spectra of membrane-bound protein were assigned by transferring known solution NMR chemical shifts for the fibrillar and monomeric protein in the absence of membranes [39].

A major challenge of solid-state NMR applied to amyloid protein-biomembrane complexes is the low signal-to-noise that is obtainable, particularly when ^{13}C and/or ^{15}N detection is required and measurement times are short. Sedimented liposomes occupy a large proportion of MAS rotors, which need to have small volumes (e.g., ~100 μl for a 4 mm diameter rotor, ~35 μl for a 3.2 mm rotor) to achieve the desired spinning rates. If proteins undergo different competing fibrillation pathways on and off

the membrane surface, it is desirable to maximise the lipid to protein ratio (LPR) to force aggregation along the membrane-facilitated pathway [149]. The drawback of doing this is that the protein concentration is low, which compromises the quality of the observed spectra. The signal from the protein can be increased by reducing the LPR, but the low lipid concentrations may be insufficient to direct aggregation toward the membrane pathway. A compromise is to use a LPR that enables acquisition of reasonable quality 2D solid-state NMR spectra that can be mapped on to higher-quality solution state spectra obtained at higher protein concentrations to facilitate chemical shift assignments.

The sensitivity issue can to some extent be overcome by observing protons under fast MAS conditions [150], but excessive crowding of the spectrum by the lipid and protein signals requires filtering through ^{13}C or ^{15}N to observe the protein. Alternatively, solid-state NMR combined with dynamic nuclear polarization (DNP) has been applied to obtain informative 2D ^{13}C – ^{13}C spectra, including double quantum-single quantum spectra that are inherently low in sensitivity, in a matter of hours. With DNP-enhancement, informative NMR spectra were obtained with a 14.1 T magnet (^{1}H Larmor frequency of 600 MHz) and 3.2 mm MAS probe from just 0.25 mg Aβ40 peptide with a molar LPR of 200:1, enabling the observation of changes in Aβ40 conformation upon peptide insertion into liposomes [151]. If the objective of an experiment is to simply observe how nucleation at the surface of liposomes modulates the fibril assembly pathway, the lipid: protein ratio can be less critical [152]. For example,^{13}C-^{13}C DARR spectra of Aβ40 fibrils formed in the presence of liposomes revealed different chemical shift patterns compared to fibrils grown alone in aqueous solution, consistent with a morphologically and structurally distinct form of fibrils nucleated by the liposomes. The low volume occupied by the liposomes did not compromise sensitivity and the spectra of the fibrils could be assigned using a range of 3D NCACX, NCONCA and NCOCX methods.

The effects of amyloid species on the order and stability of lipid bilayers can also be observed using static solid-state NMR methods, with slowly tumbling MLVs as the model membrane system. Aqueous suspensions of lipids and protein are vortexed and freeze−thawed to ensure an even distribution of proteins across the interlamellar space, and centrifuged to form a hydrated pellet for NMR. The intrinsic ^{31}P spins of the phospholipid headgroups have a chemical shift anisotropy (CSA) that is highly sensitive to changes in the bilayer structure, such as when an amyloid-forming protein destabilises the membrane [153]. Static wide-line ^{31}P NMR spectra can provide a useful confirmation of the effects of amyloid on bilayer integrity before conducting more advanced NMR measurements described earlier in this section. Static ^{31}P NMR spectra of fluid model membranes above the lipid chain melting temperature, T_m, exhibit characteristic lineshapes that can detect protein-induced transitions from lamellar (bilayer) to non-lamellar (e.g., micellar and hexagonal) phases. The dynamically-averaged ^{31}P CSA is also sensitive to changes in the average lipid headgroup orientation, relative to the bilayer normal [154]. For example, wide-line ^{31}P NMR spectra of mixed phosphatidylcholine/phosphatidylglycerol MLVs in the presence of Aβ40 have an axially symmetric line shape with CSA of ~46 ppm at lipid-to-protein ratios of 400:1 to 55:1, indicating that the peptide does not disrupt the multilamellar phospholipid dispersion [155]. Deuterated lipids also report on amyloid-membrane interactions. The quadrupolar anisotropy of ^{2}H (I = 1) incorporated into lipid headgroups and/or hydrocarbon chains is also highly sensitive to perturbations of

bilayer structure and dynamics. Wide-line ^{2}H NMR spectra revealed no change in the headgroup conformation of the choline moiety or in the flexibility and ordering of the hydrocarbon chains [155]. By contrast, ^{31}P NMR spectra of mechanically-oriented phosphatidylcholine bilayers in the presence of Aβ40 indicated that the peptide strongly perturbed the bilayer structure to form non-lamellar phases, possibly micelles [156]. These apparently contrasting results highlight how the type of lipid samples - unoriented liposome suspensions or supported oriented lipid bilayers, for example - can affect the extent to which amyloid proteins disrupt the lipid bilayer. The higher resolution of ^{31}P MAS NMR spectra obtained upon the binding of $A\beta_{1-40}$ peptide to bilayers allow the detection of chemical shift perturbations for the individual lipid components, reflecting a partial charge screening between negative lipid head groups and positive amino acids of the peptide, as shown previously for various systems [157].

3.3. Interactions with metal ions

Imbalances of metal ions - primarily iron, copper and zinc – in the brain have been linked to the onset and progression of AD and other neurodegenerative diseases for which protein aggregation is a pathological hallmark. The interactions of di- and trivalent metal ions with the key aggregating proteins in the brain, Aβ, tau and α-synuclein, have been shown to influence amyloid fibrillization kinetics, oligomer stability and toxicity. Cu^{2+}, Zn^{2+} and Fe^{2+}/Fe^{3+} occur in close to millimolar concentrations in amyloid plaques and in neurofibrillar tangles; zinc and copper ions are directly coordinated by the amyloid protein markers and iron also associates with plaques in a ferritin bound form. The rate of fibril growth and the size and morphology of aggregates formed *in vitro* are modulated by metal binding to specific coordination sites. Further, the redox activity of iron and copper ions can lead to the production of reactive oxygen species (ROS) through Fenton and Fenton-like reactions, which can generate aggregation-inducing protein modifications and cause more widespread cellular oxidative damage.

Understanding the mechanisms underpinning protein aggregation in the presence of metal ions is clearly important from a pathophysiological perspective. NMR investigations have played an important role in identifying metal coordination sites and probing the interaction dynamics of paramagnetic and diamagnetic metal ions within amyloid fibrils and their soluble amyloid precursors. This section highlights some of the principles, considerations, methodology and outcomes of NMR studies of metal ion interactions with Aβ, tau, hIAPP and α-synuclein. NMR has also enhanced our understanding of metal binding to transmissible prion proteins that accumulate in the brain and are associated with Creutzfeldt-Jakob disease (CJD) in humans, scrapie in sheep and bovine spongiform encephalitis (BSE) in cattle. These studies have been reviewed comprehensively elsewhere [158] and will not be covered here.

3.3.1. Paramagnetic ions

This section is limited to NMR studies of physiologically-relevant interactions of copper and iron ions with amyloid proteins. It does not cover engineered paramagnetic ion binding sites as a tool for exploring the structural topology of protein fibrils [159, 160]. Cu^{2+} (d^9), high-spin Fe^{2+} (d^6, $S = 2$) and Fe^{3+} (d^5) ions possess unpaired electrons and are paramagnetic. When paramagnetic ions coordinate with appropriate protein functionalities, the unpaired electrons couple with neighbouring nuclear spins

and shorten their nuclear spin relaxation rates and perturb the observed chemical shifts. Paramagnetic shifts arise from contributions from Fermi contact, the effects of which may be very large within the metal ion coordination sphere but are generally neglected for practical reasons, and smaller, but potentially significant, pseudocontact shifts when the metal ion has an anisotropic magnetic susceptibility tensor. Through-bond or through-space paramagnetic relaxation enhancement (PRE), Γ_i, corresponds to an increase in longitudinal (R_1), transverse (R_2) relaxation rates and rotating frame ($R_{1\rho}$) relaxation rates, as compared to a diamagnetic sample, according to

$$\Gamma_i = R_i^p - R_i^d \qquad [11]$$

where i = 1, 2 or 1ρ and the superscripts p and d signify spin relaxation of paramagnetic and diamagnetic samples, respectively. Longitudinal PRE may be expressed as [161, 162]

$$\Gamma_1 \approx \frac{2C}{r^6}\left(\frac{3T_{1e}}{1+\omega_I^2 T_{1e}^2} + \frac{7T_{1e}}{1+\omega_e^2 T_{1e}^2}\right) \qquad [12a]$$

and transverse and rotating frame PREs as

$$\Gamma_2 \approx \Gamma_{1\rho} \approx \frac{C}{r^6}\left(4T_{1e} + \frac{3T_{1e}}{1+\omega_I^2 T_e^2} + \frac{13T_{1e}}{1+\omega_I^2 T_e^2}\right) \qquad [12b]$$

where ω_I and ω_e are the nuclear and electron Larmor frequencies, T_{1e} is the electron longitudinal relaxation time constant and r is the distance of the nucleus I from the paramagnetic centre. The pre-factor $C = \frac{1}{15}\left(\frac{\mu_0}{4\pi}\right)^2 \gamma_I^2 g_e^2 \beta_e^2 S(S+1)$, where all the fundamental constants have their usual values, γ_I is the nuclear gyromagnetic ratio and S is the nuclear spin quantum number. The correlation time for electron-nucleus dipolar coupling, τ_c, is defined as

$$\frac{1}{\tau_c} = \frac{1}{T_{1e}} + \frac{1}{\tau_r} + \frac{1}{\tau_{ex}} \qquad [13]$$

where τ_r is the molecular rotational correlation time and τ_{ex} is the correlation time for chemical exchange of the paramagnetic species. The electron-nuclear distance dependence of pseudocontact shifts and PREs, and their relationship with molecular dynamics, have been exploited as a valuable structural aid in biomolecular NMR studies of metalloproteins for many years. Studies of paramagnetic ion interactions with amyloid-forming proteins and peptides follow essentially the same principles as for stable soluble metalloproteins, but additional considerations are warranted, not least in regard of the effects of ions on aggregation kinetics.

For studies of monomeric amyloid precursor peptides or small amyloid intermediates in solution, the most rapid and straightforward way to measure PREs is to observe the effects of a titrated paramagnetic metal ion on 1D ^{1}H NMR peak widths or on 2D $^{1}H-^{15}N$ HSQC amide signal intensities. According to equations [11] and [12], the extent of PRE depends entirely on the distance *r* between the paramagnetic centre and the observed nuclear spin, when all other terms remain constant. If the coordination geometry is known (e.g., from metalloprotein crystal structures), one may estimate the exchange rate, $1/\tau_{ex}$, between the *apo*- and *holo*- proteins, provided robust assumptions about the protein dynamics and electron relaxation are made [163]. PREs can be observed in 1D NMR spectra as the progressive, and often selective, broadening of peaks during titration of the metal ion. In ^{1}H – ^{15}N HSQC spectra, PREs are measured by comparing diminished signal intensities (I) with those of the same cross-peaks (I_0) in the data set of samples lacking metal ions or with diamagnetic ion replacement. The I/I_0 ratios are typically plotted as a function of the protein sequence to obtain the intensity profiles. PREs induced by localised metal ion binding to amyloid polypeptides may result in a "blind sphere" of amino acid residues that are invisible to NMR because their resonances are broadened beyond detection. Such information may be useful for pinpointing the metal binding site(s) qualitatively, but the lack of measurable linewidths makes it difficult to extract information on nuclear distances from the metal centre. More widespread broadening of protein resonances may be observed when the paramagnetic ion undergoes fast exchange between multiple sites, even when the ion is in sub-stoichiometric concentrations relative to the peptide [164]. In such cases it may be useful to observe directly a lower-gamma nucleus (e.g., ^{13}C) for which the PRE may not broaden the signal completely beyond detection [164]. Alternatively, invisible resonances can be recovered using modified HSQC experiments designed with a pre-INEPT inversion recovery filter and shortened INEPT transfer period to compensate for the short relaxation times [165, 166]. In 2D experiments such as ^{13}C – ^{13}C DARR or PDSD experiments with long mixing times, nuclear T_1 relaxation enhancement during longitudinal mixing periods may also further diminish cross-peak intensities. In NMR studies of insoluble fibrillar proteins, for which solid-state CP-MAS NMR methods are favoured, enhanced $T_{1\rho}$ relaxation during Hartmann-Hahn cross-polarization results in lower efficiency of magnetization transfer from ^{1}H to the observed nucleus (e.g., ^{13}C) and consequent reduction in peak intensity.

From NMR studies of metalloproteins in general, it is known that the geometries of copper centres influence the extent of PREs observed, and hence the scope of the blind sphere of broadened resonances. In Type I centres the copper ion is strongly coordinated to two His imidazole groups and one Cys thiol group in a distorted trigonal or tetrahedral geometry, and the small energy separation between the electronic ground and excited states provide a relatively efficient mechanism for rapid electronic relaxation ($T_{1e} \approx 10^{-10}$ s). Type II copper centres have a tetragonal or square planar geometry and lack low-energy excited states, which renders electronic relaxation mechanisms inefficient and causes a long correlation time for the electron-nucleus interaction (τ_C in the range 10^{-8}–10^{-9} s) [167] **(Fig. 12a**). Iron is typically coordinated by acidic or histidine residues. In the case of monomeric amyloid proteins, which tend to be unfolded, the conformational flexibility of the protein determines whether its residues can sample the geometry required for copper or iron coordination. For assembled amyloid fibrils the coordination geometry is dictated by the spatial arrangement of the fixed side-chain functionalities in the supramolecular architecture

(**Fig. 12b**). In both cases, the paramagnetic centre of the metal has a near isotropic magnetic susceptibility and so pseudocontact shift effects on neighbouring nuclear spins are negligible, and PRE is the dominant NMR process.

Cu(I) and Cu(II) ions bind to Aβ peptides with sub-nanomolar dissociation constants, K_D; high copper concentrations induce the rapid formation of amorphous Aβ aggregates and low concentrations of copper ions favour slow fibril growth [168]. $^{1}H - {}^{15}N$ HSQC experiments of Cu(II) titrations with monomeric Aβ40 have led to a consensus that protein monomers bind Cu(II) at the hydrophilic N-terminus, where coordinating imidazole groups of residues His6/13/14, Asp1 and other acidic groups

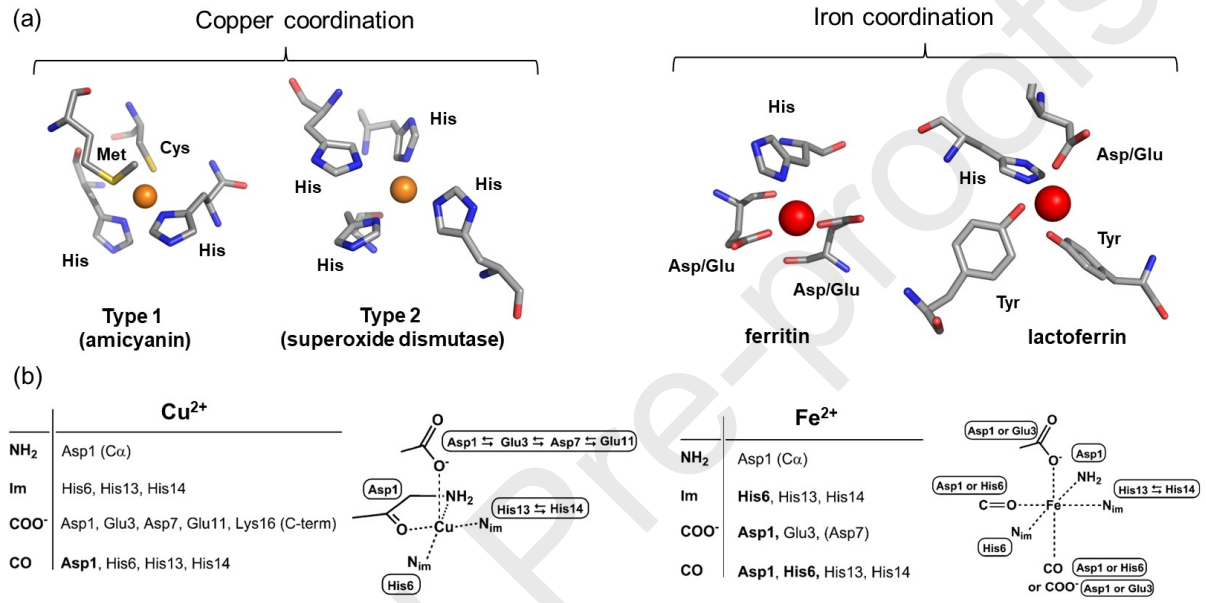

Fig. 12. (a) Common ion-coordinating residues and geometries in copper and iron binding proteins. (b) Proposed key Cu^{2+} and Fe^{2+} coordinating residues of monomeric Aβ (bottom). Panel (b) adapted from [169] with permission. Copyright 2011 American Chemical Society.

coordinate the ion in dynamic exchange [165, 170-172]. Modified HSQC and other 2D experiments were used to recover paramagnetically-broadened amide signals sufficiently to measure metal-nuclear distances, enabling the N-terminal residues of Aβ40 to be constrained to 6.5 – 9.0 Å from the copper centre [173]. In the same study, NMR measurements of Aβ40 translational diffusion were consistent with a decrease of the apparent hydrodynamic radius from 16.8 to 15.8 Å in the presence of Cu(II), suggesting a more compact structure as the N-terminal residues fold around the metal coordination site.

An important consideration when examining amyloid-Cu(II) interactions by NMR is to disentangle PRE from other potential sources of line broadening, namely chemical exchange phenomena and protein aggregation. One of the earliest reported NMR studies of Aβ40 -Cu(II) interactions noted that broadening of the N-terminal resonances by copper ions did not originate from the paramagnetic effect, because identical effects could be induced by diamagnetic Zn^{2+} [171]. Broadening was instead attributed to chemical exchange of the metal ions. Varying the temperature induced

strong modification in the broadening observed on His H_ε and H_δ and Asp1 H_α and H_β protons, as expected for dynamic exchange. However, subsequent CPMG relaxation dispersion experiments on Aβ40 at low Cu(II) concentrations, at which about 60 % of the initial N-terminal signal intensity remains, showed a flat transverse relaxation profile across all residues [165]. This result argued against chemical exchange and in favour of PRE as the principal source of broadening [165]. However, other studies of Aβ40 -Cu(II) interactions have found that fast amide proton exchange can be a significant source of line broadening in $^{1}H - ^{15}N$ HSQC spectra. Exchange effects can be minimised by replacing $^{1}H/^{15}N$ observation with the use of proton-decoupled, ^{13}C-detected NMR spectroscopy [164, 174]. The lower-γ ^{13}C spins are influenced less by PRE than are protons, resulting in narrower peaks and thereby allowing direct inspection of the effect of Cu^{2+} PRE on Aβ40 peptide signals (**Fig. 13**). Using this approach, it was shown that increasing the pH from 6.6 to 8.7 leads to a more pronounced Cu-induced PRE of the carbonyl peak of Asp1, the peaks of the His carbonyl are no longer affected [164]. The pH-dependence of peak broadening is consistent with a rearrangement of the Cu(II) coordinating residues after deprotonation of the Asp1-Ala2 peptide bond. Understanding the sources of broadening can be complicated further if the metal ions enhance the rate of protein aggregation. To circumvent this problem, some studies have utilized truncated N-terminal fragments of Aβ (16-aa Aβ16 and 28-aa Aβ28), which are more soluble and less prone to rapid aggregation but contain the key copper coordinating residues [175, 176]. Slower aggregation of millimolar concentrations of the Aβ fragments still occurs in aqueous solution, and so the peptide was dissolved in 0.1 M sodium dodecyl sulfate solution to stabilize it in a helical monomeric state [176].

NMR has also been used to study Cu(II) interactions with other fibril-forming proteins in their monomeric states, including tau [177, 178], hIAPP [163] and α-synuclein [179-182]. This last is an unfolded protein with an amphipathic N-terminus that can adopt a partial α-helical structure when interacting with lipid membranes. NMR PRE studies have identified the primary binding site for Cu(II) as residues 3−9 (K_D = 0.1 μM), 48−52 (k_D = 35.0 μM), including His50, and the D(119)PDNEA sequence motif (K_D ≈ 1 mM), in which Asp121 acts as the main anchoring residue [179-182]. A screen of divalent paramagnetic metal ion binding to monomeric α-synuclein found considerably higher affinity of the protein for Cu(II) (k_D < 1 μM) than for Mn(II), Fe(II), Co(II), and Ni(II) (k_D in the 1−2 mM range), and hence Cu(II) has the

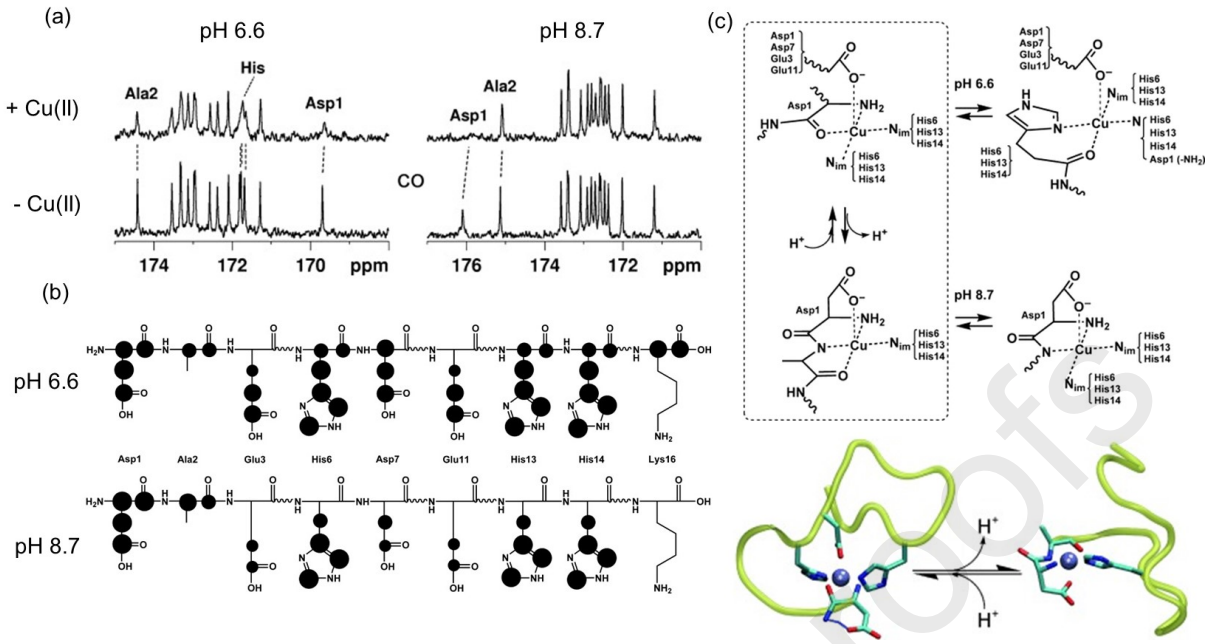

Fig. 13. Observation of PREs induced by Cu(II) binding (0.1 equiv.) to monomeric peptide Aβ18, using solution-state ^{13}C-detected, ^{1}H-decoupled NMR. (a) CO region of the spectrum of Aβ18, showing selective broadening of resonances at acidic and basic pH. (b) The size of the black circles increases according to the extent of broadening of the NMR signal. (c) Proposed mechanism of Cu(II) binding, based on the NMR data, involves a reshuffling of the binding site after deprotonation of the Asp1-Ala2 peptide bond. NMR measurements performed at 11.75 T and 14.10 T. Adapted from [164] with permission.

highest degree of occupancy and lifetime in the metal binding sites [179]. The shorter lifetimes of the α-synuclein complexes with ions other than Cu(II) affects the resonances of neighbouring nuclei more dramatically than the more tightly-bound Cu(II), owing to exchange broadening, and so it was important to use sub-stoichiometric concentrations of ion to avoid excessive broadening and to minimise exchange effects. Ranjan *et al.* [181] demonstrated that Cu(II) binding to α-synuclein resulted in localised PRE for residues 48-53, and that the effect was abolished by replacement of His50 with arginine (a known familial mutation). The histidine imidazole ring is a common copper-coordinating moiety of amyloid proteins and once identified by PRE or chemical shift perturbation it is possible to observe the interaction in higher focus. For example, proton spin–lattice relaxation rates of the imidazole protons Hε and Hδ for hIAPP(18–22) clearly differentiate Cu(II) binding to N1 from N3 of the imidazole ring [163].

Aβ peptides and α-synuclein are susceptible to oxidative modifications when the reduction of Cu(II) by a suitable electron donor converts molecular oxygen into reactive oxygen species (ROS). This process can, in turn, modify the proteins irreversibly and expedite their aggregation and precipitation. Chemical modifications are readily observed in the NMR spectrum. Methionine residues are one of the preferred targets of metal-catalysed oxidation and are present in the high-affinity Cu(II) coordination site in α-synuclein (M(1)DVFMK) and in Aβ peptides at position 35, a known oxidation substrate in plaques isolated from brain tissue. Solution-state NMR experiments on

monomeric α-synuclein have confirmed that the conversion of Cu(II) to Cu(I) can occur whilst the metal ion binds to the protein. ^{1}H – ^{15}N HSQC NMR spectra indicated that treatment of Cu(II)-bound α-synuclein with the extrinsically-supplied reducing agent ascorbate completely recovered the intensities of the Cu(II)-broadened resonances from the 3 copper binding regions [183]. This observation is consistent with paramagnetic Cu(II) being reduced to diamagnetic Cu(I); concomitant localised chemical shift perturbations of the recovered signals (as compared to shifts for the *apo*- protein) were consistent with α-synuclein retaining coordination of electron-rich Cu(I) at the same sites. NMR and MALDI-TOF mass spectrometry analyses of the NH_2-MDVFMK-$CONH_2$ peptide complex with Cu(II), treated with an excess of ascorbate, confirmed that 5 h of air exposure to re-oxidise Cu(I) resulted in oxidative conversion of Met1 and Met5 to methionine sulfoxides [183].

Solid-state NMR provides insights into the Cu(II) interaction sites within insoluble amyloid fibrils. A solid-state ^{13}C CP-MAS NMR study of Cu(II) binding to insoluble fibrillar Aβ40 reported selective broadening of resonances for N_ε in His13 and His14, the carboxylic acid groups in Val40 and in the side chains of the glutamic acid residues (Glu3, Glu11, and/or Glu22) [184]. Spectra were obtained from fibrils assembled from several chemically identical peptides, each containing different blocks of residue-specific ^{13}C, ^{15}N-labelling patterns. The reduced crowding of the spectra enabled the inherently broad peaks of the ^{13}C NMR spectra to be assigned and the atomic sites of selectively broadened resonances identified from 1D CP-MAS spectra. With reference to the 2-fold symmetry model of Aβ40 fibrils based on numerous solid-state NMR restraints [118], the residues most affected by Cu(II) are seen to cluster around the open ends of the hairpin-like structure of Aβ40 monomers in the fibril architecture. This region encompasses the N-terminal residues that constitute the Cu(II) binding site in soluble monomeric Aβ peptides [165, 170, 171]. Solid-state MAS NMR has also been used to investigate the role of Met35 in Aβ40 fibrils for binding Cu(II) and generating ROS through redox cycling [185]. The ^{13}C signal of $^{13}C^{\varepsilon}H_3$-S in Met35 showed little change after Cu(II) binding to the fibrils, indicating that copper binding alone does not induce Met35 oxidation. Proton longitudinal (spin-lattice T_1) relaxation measurements on Cu(II)-bound Aβ40 fibrils in the presence of ascorbate demonstrated a 5-fold increase in T_1 relaxation times over 1.5 h, consistent with the conversion of Cu(II) into diamagnetic Cu(I) while the reactive ions remain bound to the amyloid fibrils [185]. Both ^{13}C and ^{15}N chemical shifts indicate that the reduced copper ion coordinates to the fibrils primarily through the sidechain N_δs of His13 and His14 (as does Cu(II) to Aβ monomers). Biochemical analysis confirmed that this process generated H_2O_2 and was reversible, with the bound ion reverting to the more stable Cu(II) when ascorbate was depleted.

Similar NMR experiments exploiting the paramagnetism of Fe(II) and Fe(III) ions have been used to examine binding of these ions to amyloid in the solid and solution states [186]. Unlike for copper, NMR studies of iron binding must consider the anisotropic magnetic susceptibility of the ions, which potentially generates measurable pseudocontact shifts unless there is motion within the paramagnetic centre. Addition of sub-stoichiometric concentrations of Fe(II) to soluble monomeric Aβ40 and its shorter fragment Aβ16 under anaerobic conditions results in broadening of N-terminal resonances for His H_δ and H_ε imidazole protons and the two diastereotopic H_β protons of Asp1, as well as the H_α of Asp1 and H_α of Glu3, with no strong broadening of C-terminal residues from 17-40 [169]. However, at higher Fe:Aβ

molar ratios rapid exchange between binding sites loses the specificity of broadening, making it difficult to correctly discriminate which residues are mainly affected by Fe(II) addition [169]. In the case of Fe(III), binding to α-synuclein enhances the protein aggregation rate by shortening the lag period preceding nucleation and fibril elongation. Excessive Fe(III) concentrations promote the formation of spherical α-synuclein oligomers [187]. Selective chemical shift perturbations and PREs induced by Fe(III) are much smaller than observed for Cu(II) binding to α-synuclein, consistent with weak interactions with residues His50, Asp121 and Asn122 [187].

To summarise this section, the paramagnetism of Cu(II), Fe(II) and Fe(III) ions can be exploited by NMR to pinpoint the ion coordination centres within the monomeric protein precursors of amyloid, as well as within insoluble fibrils using solid-state NMR. Careful consideration must be given to the concentrations of the paramagnetic ions and the competing processes (PRE, chemical exchange and protein aggregation) that can induce NMR line broadening.

3.3.2. Diamagnetic ions

Amyloid species interact with several diamagnetic ions, including Cu(I), Zn(II) and Ca(II), and NMR spectra of the protein-metal complexes often exhibit selective chemical shift perturbations corresponding to the coordination site. For example, solution-state NMR spectra of monomeric Aβ16 titrated with Cu(I) display selective chemical shift perturbations consistent with metal coordination of His13 and His14 in a linear dyad [188]. Unlike their paramagnetic counterparts, diamagnetic ions do not induce PREs and so any observed peak broadening accompanying ion binding is usually caused by chemical exchange phenomena and/or enhanced protein aggregation.

Zinc is an essential trace element for humans and has been shown to modulate amyloid aggregation *in vitro*. Its electron-rich $4d^{10}$ configuration induces pronounced chemical shift perturbations for known zinc-binding sidechains (such as histidine imidazole groups), and its weak interactions with amyloid proteins can also give rise to substantial exchange broadening. 1D ^{1}H solution NMR spectra of a peptide comprising residues 1–28 of Aβ revealed a number of NMR resonances to be perturbed upon titration with Zn(II), including broadening of the His Hδ and Hε proton resonances for all three His residues (His6, 13 and 14) [189]. ^{1}H–^{15}N and ^{1}H–^{13}C HSQC spectra of monomeric Aβ40 titrated with Zn(II) reported small ^{1}H chemical shift perturbations for His13 and His14 and broadened out all peaks across the spectra [190]. Hence, peak broadening is a common feature observed when titrating Aβ peptides with Zn(II); in the absence of PREs, a challenge is to determine the source of this phenomenon. NMR measurements using a fragment of rat Aβ40, which is less susceptible to Zn^{2+}-induced aggregation than the human peptide, also reported similar peak broadening, which argued in favour of an intermediate exchange regime rather than aggregation [191]. Further, raising the temperature reduced line broadening, whereas aggregation would be expected to be enhanced [191]. By eliminating aggregation effects in this way, Zn(II)-induced line broadening was attributed to conformational exchange of the peptide at a rate in the intermediate regime with respect to the chemical shift time scale.

Zinc binding may also perturb the molecular conformation around the metal coordination site of the amyloid protein, which can have implications for the aggregation pathway and kinetics and also alter the structures of the fibrillar product. For example, high-resolution structures of monomeric hIAPP determined by NMR confirmed that zinc binding involves His18 and is accompanied by localized disruption of the peptide secondary structure around the binding site [192]. The peptide was dissolved in a solvent mixture containing HFIP and TFE, which promotes an α-helical structure resembling that of an aggregation-competent hIAPP intermediate but avoids the otherwise rapid aggregation that occurs in aqueous solution.

Zn(II) is found in senile plaques in the Alzheimer's brain and binds to Aβ amyloid fibrils *in vitro*. Solid-state NMR investigations of Zn(II) binding to Aβ42 fibrils utilised 2D dipole-dipole correlation spectra with block-wise isotope labelling of peptides to reduce crowding of the spectra, avoid ambiguities and and assist with chemical shift assignments. In the absence of Zn(II), 1D ^{13}C and ^{15}N spectra exhibited two sets of resonances each for Cγ of Asp23 and Nζ of Lys28, which are residues known to participate in a stabilising salt bridge across the loop region connecting two β-strands. After addition of Zn(II), single peaks for each site were observed at chemical shifts that were consistent with a change in ionization states that would be unfavourable for salt bridge formation. A ^{15}N-observed, ^{13}C-dephased REDOR experiment showed frequency-selective dephasing of the Lys28 ^{15}N signal in the absence of Zn(II), which was consistent with the Lys Nζ and Asp Cγ sites being close in space, as would be expected for a salt bridge between these two residues. No dephasing was seen after the addition of Zn(II), which implies that zinc binding causes the two sites to move further apart and disrupts the salt bridge [193].

3.4. Amyloid-modifying therapies

Molecules that interact non-covalently with aggregation-prone proteins and/or recognise and bind to the cross-β motif of amyloid fibrils are both useful biophysical research tools and potential diagnostic and therapeutic agents. Such molecules have consequently attracted interest as probes to visualise amyloid deposition *in vitro* and *in vivo*, and for their ability to manipulate the rate and pathway of protein assembly from monomers into cytotoxic oligomers and fibrils. NMR spectroscopy has been a valuable method to characterise small molecule binding to protein aggregates [194], and this section describes some of the key developments and findings.

3.4.1. NMR methodology

Agents that block or interfere with protein self-assembly into toxic oligomers and amyloid fibrils *in vivo* have been investigated widely for the treatment and prevention of Alzheimer's and other protein misfolding disorders. Their mode of action may be to disrupt existing amyloid species or to prevent protein aggregation by destabilising the non-covalent interactions that stabilize the cross-β structure. The most promising molecules identified to date are monoclonal antibodies that recognise, bind to and sequester amyloid in the brain, and several of these have shown recent clinical success in slowing the progression of Alzheimer's symptoms in human patients [195]. Small molecules having similar functions to antibodies are attractive by virtue of their lower production costs and relative ease of administration (i.e., orally versus intravenous infusion) [196], although none has yet demonstrated clinically significant

effects. Small molecules can also more easily cross the blood-brain barrier, avoid immunological responses, and are more stable in biological fluids and tissues. Health-promoting dietary polyphenols from abundant food-stocks are appealing owing to their advantageous safety profiles and because they can be consumed long before Alzheimer's symptoms have presented [197].

In this context, NMR spectroscopy is capable of identifying molecular binding hits from screens, characterising the sites of interaction with target proteins, and can also aid the design of inhibitor molecules. One important NMR method is saturation transfer difference (STD) NMR, which is used widely to screen for molecules that interact with macromolecular targets with K_D in the micromolar to millimolar range [198, 199]. The method is suitable for detecting molecules that interact weakly with amyloid oligomers and fibrils [199, 200]. A weak radiofrequency pulse is applied to selectively saturate the methyl protons of the amyloid assembly (e.g., Aβ oligomers) in the presence of a potential small molecule inhibitor or ligand. The methyl saturation diffuses across the amyloid assembly and is transferred to the protons of bound ligands to an extent that depends on the proximity of the ligand to the target protein, and on the ligand binding affinity. Signals from the bulk free ligand are observed and a loss in signal intensity indicates that transient binding to the oligomers or fibrils has occurred.

After binding of a compound has been confirmed by STD NMR, follow-up ^{1}H – ^{15}N HSQC titration experiments with ^{15}N-labelled proteins may help to pinpoint where the molecule binds to the protein from selective chemical shift perturbations and broadening of resonances. For example, upon titration of ^{15}N-enriched α-synuclein with increasing concentrations of a cyclic tetrapyrrole inhibitor, PcTS, ^{1}H – ^{15}N HSQC spectra demonstrated significant broadening and chemical shift changes for selective N-terminal aromatic residues of the protein [201]. Resonances from free and bound states of α-synuclein cannot be resolved but are averaged in a manner that leads to resonance line broadening. Specifically, assuming two-site fast chemical exchange, a contribution to the relaxation rate of transverse magnetization arises that is proportional to the square of the chemical shift difference between the free and bound states and the lifetime of the small molecule-protein complex. Complete loss of PcTS binding to the 35–41 region was observed when the Tyr residue in position 39 was replaced by Ala, as evidenced by the recovery of the resonances for the *N*-terminal residues. Plotting the ratio of resonance intensity in the presence of drug to intensity for the protein alone (I/I_0) as a function of residue number is convenient way of depicting the selective line broadening, and can be useful to compare the binding of different drugs [202].

WaterLOGSY NMR is an alternative to STD NMR for detecting molecular interactions with soluble amyloid species in solution [203]. Like STD NMR, waterLOGSY was originally developed to screen for weak binding of drug-like molecules with general protein targets and was later adapted for amyloid inhibitor screening [204]. Both waterLOGSY and STD NMR detect ligands in the free state after dissociation from the target protein [203]. In the waterLOGSY pulse sequence, selective excitation of the bulk water signal is followed by a mixing period that results in magnetization transfer via NOEs from water molecules trapped in the protein aggregates to the protons of the protein. The transferred magnetization is then relayed to transiently-bound ligands and detected at the chemical shift of the free molecule

after dissociation from the aggregates (**Fig. 14a**). The original design of the waterLOGSY experiment detects interactions between the drug and the amyloid-forming protein but does not report on whether the drug modifies protein aggregation. A useful adaption of waterLOGSY identifies whether the molecule inhibits amyloid formation by using a known binder of the amyloid protein as a reporter molecule [205] (**Fig. 14b**). In this approach, a series of spectra is acquired during incubation of the initially monomeric protein with the reporter molecule that binds to the protein but does not affect its aggregation. The NMR peaks for the reporter molecule are initially negative and become positive as the LOGSY effect changes sign and continue to increase to reach a plateau at longer incubation times. The change in sign of the peaks from negative to positive occurs because the monomer assembles into aggregates of increasing size, which changes the intermolecular NOEs from positive to negative. When the experiment is repeated in the presence of an inhibitory compound, the time-dependent peak intensities for the reporter signal are altered if the aggregation kinetics are modified by the inhibitor (**Fig. 14c**). Care must be taken to ensure that the reporter molecule does not itself inhibit or modulate amyloid formation, or compete with the screened compounds for binding to the amyloid protein. Whether this approach will find wider utility will depend on whether it can be demonstrated to offer advantages over other, conventional and more sensitive screening modalities, for example, by providing additional mechanistic information that is otherwise unobtainable.

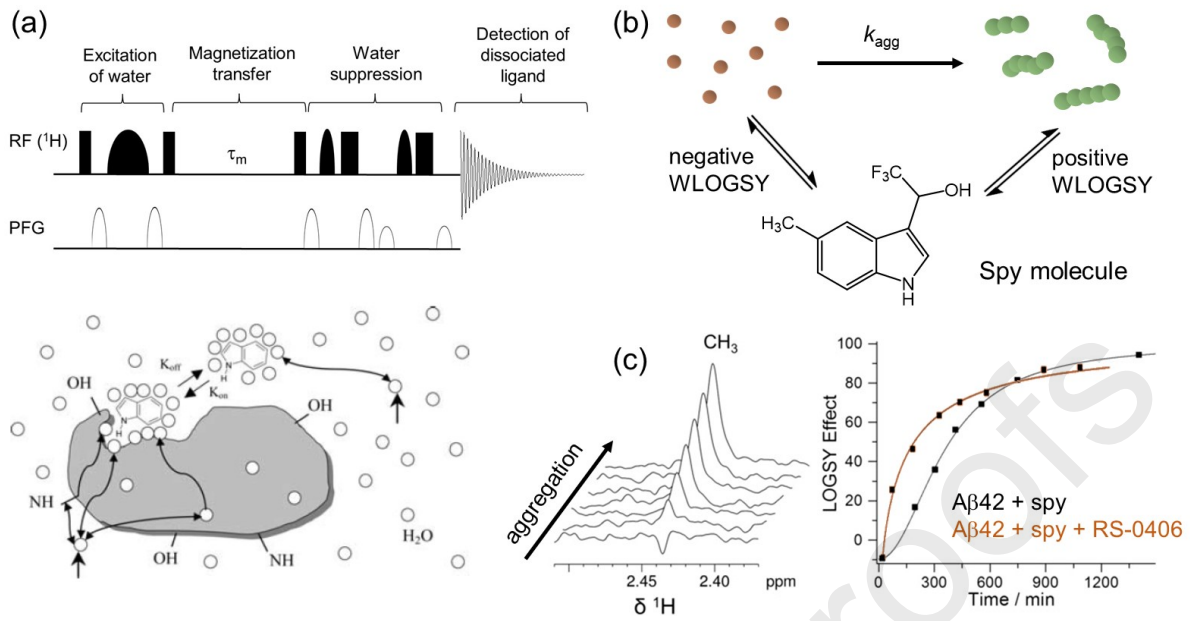

Fig. 14. Detection of amyloid-modifying agents using waterLOGSY with a spy ligand. (a) A typical pulse sequence (top). After selective excitation of the water magnetization, transfer to the protein and bound ligands occurs during mixing period of duration τ_m. The water signal is suppressed and the signal from the ligand after dissociation from the protein is detected. Exchange mechanisms of water resulting in magnetization transfer to the protein and to the transiently-bound ligand (bottom). (b) The spy molecule gives negative waterLOGSY effects when bound predominantly to protein monomers or small oligomers and positive effects when bound to larger aggregates. (c) The CH_3 proton signal monitored over time (at 9.39 T) in the presence and absence of amyloid-modifying agents (left). Example of a time course measured in the absence and presence of amyloid-modifying compound RS-0406 (right). Panel (a) taken from [203] with permission. Panel (c) adapted from [205] with permission.

3.4.2. Repurposed pharmaceuticals

The development of new drug entities incurs considerable costs, suffers high attrition rates and can take many years before clinical approval is granted. Repurposing old drugs to treat disease indications other than those for which they were developed is an attractive therapeutic proposition that can potentially expedite clinical development [206]. Several established drugs have been investigated for their efficacy in preventing the accumulation of amyloid in Alzheimer's and other amyloid diseases. NMR is now being used to investigate the binding mechanisms of these known drugs with amyloid proteins.

Models of fibrils derived from solid-state NMR have assisted docking analysis of known drugs with amyloid assemblies. For example, the selective serotonin reuptake inhibitors fluoxetine and paroxetine reduce Aβ42 fibrillogenesis, and computational molecular docking of the drugs with the NMR-derived S-shaped assembly suggested an interaction with a region close to the N-terminal (Lys16-Glu22 [207]. Similarly, the Aβ40 fibril model with 2-fold symmetry, based on solid-state NMR constraints by Tycko and co-workers, informed molecular dynamics simulations of naproxen and ibuprofen with fibrils [208]. In other cases, NMR has

played a more direct role in characterising repurposed drug-amyloid interactions. A simple 1D solution-state ^{1}H NMR method was used to investigate the effect of the cholesterol-lowering drug atorvastatin on monomeric Aβ42 aggregation in solution [209]. The signal intensities in the backbone amide and aromatic regions of the spectrum gradually diminished over time in a sigmoidal fashion as Aβ assembled into larger aggregates. The rate of signal loss was not initially affected by the addition of atorvastatin, but after removal of calcium from the drug formulation it was found that aggregation was inhibited in a drug concentration-dependent fashion. STD NMR and chemical shift perturbations in ^{1}H – ^{15}N HSQC spectra were consistent with a weak interaction of atorvastatin with monomeric Aβ42. It should be noted that although NMR is a relatively insensitive technique for screening amyloid inhibitors, this approach is less prone to ambiguities than are the more commonly used ThT fluorescence and circular dichroism spectroscopy methods.

Approximately 30 % of clinically approved pharmaceuticals contain one or more fluorine atoms, and there is great potential to exploit ^{19}F NMR for characterising amyloid interactions with fluorinated drugs. The non-steroidal anti-inflammatory drug sulindac sulfide is a fluoroaromatic compound that was investigated for binding to Ab40 fibrils by solid-state NMR. Small chemical shift perturbations of labelled Aβ40 fibrils in the presence of the drug indicate that sulindac sulfide does not induce drastic architectural changes in the fibrillar structure. ^{13}C – ^{19}F REDOR NMR spectra were recorded to observe dephasing of Aβ ^{13}C nuclei in close proximity to the ^{19}F atom of sulindac sulfide. The dephasing profile suggested that the drug intercalates between the two strands of the amyloid fibril and binds to hydrophobic cavities [210].

3.4.3. Peptide inhibitors

The vast chemical diversity and ease of synthesis of peptide molecules has been exploited to design peptidic amyloid inhibitors that are tailored to recognise specific sequences of amyloid-forming proteins. The peptides are designed to bind to amyloidogenic regions of a target amyloid protein, and block self-assembly by disrupting its ability to form the cross-β motif [211]. They may be derivatives of specific sequences, or “self-recognition elements” (SREs), of the target protein containing chemical adaptations to improve biological activity.

NMR spectroscopy can play a useful role in screening for inhibitory peptides and in guiding their design. For example, STD NMR screening was used to confirm that hydrophobic Ala-Val and Val-Leu dipeptides linked to a D-glucopyranosyl scaffold interact with Aβ40 aggregated species mediated by hydrophobic amino acid residues [212]. Similarly, STD NMR epitope mapping was used to study three different peptide that affect lysozyme fibril formation, each derived from fragments of the parent lysozyme protein sequence. Saturation transfer from the target protein to bound ligand is greatest for those ligand sites in close contact with the target. By observing the strength of the STD effects across all resonances for the peptide, it could be concluded that the ring protons of peptide tryptophan residues are in close proximity to lysozyme [213].

A flexible approach to inhibitor design is to synthesize short peptides mimicking the SREs of target amyloid proteins, but incorporating N-methyl groups into the backbone amide linkages to favour *cis*-peptide bonds [214]. The peptides recognise

and bind to the target protein and can destabilise the intermolecular hydrogen-bonding networks that are required for elongation of the fibrils, thereby inhibiting fibrillar growth. It is important to ensure that the peptide does not itself undergo aggregation, which would render it unavailable for interaction with the target protein. For example, *N*-methylated and sequence-modified peptides derived from hIAPP were shown to be highly potent inhibitors of Aβ amyloid self-assembly [215]. STD NMR was used to observe the propensity of the modified peptides to self-associate in the absence of Aβ. The very intense signals in the STD experiment suggest that the peptide undergoes chemical exchange between a monomeric random-coil-like conformation and an aggregated state that is too large to be observable by solution-state NMR analysis [215].

Solid-state NMR has been valuable for guiding the design and optimization of N-methylated peptide inhibitors of α-synuclein [216] (**Fig. 15**). The hydrophobic,

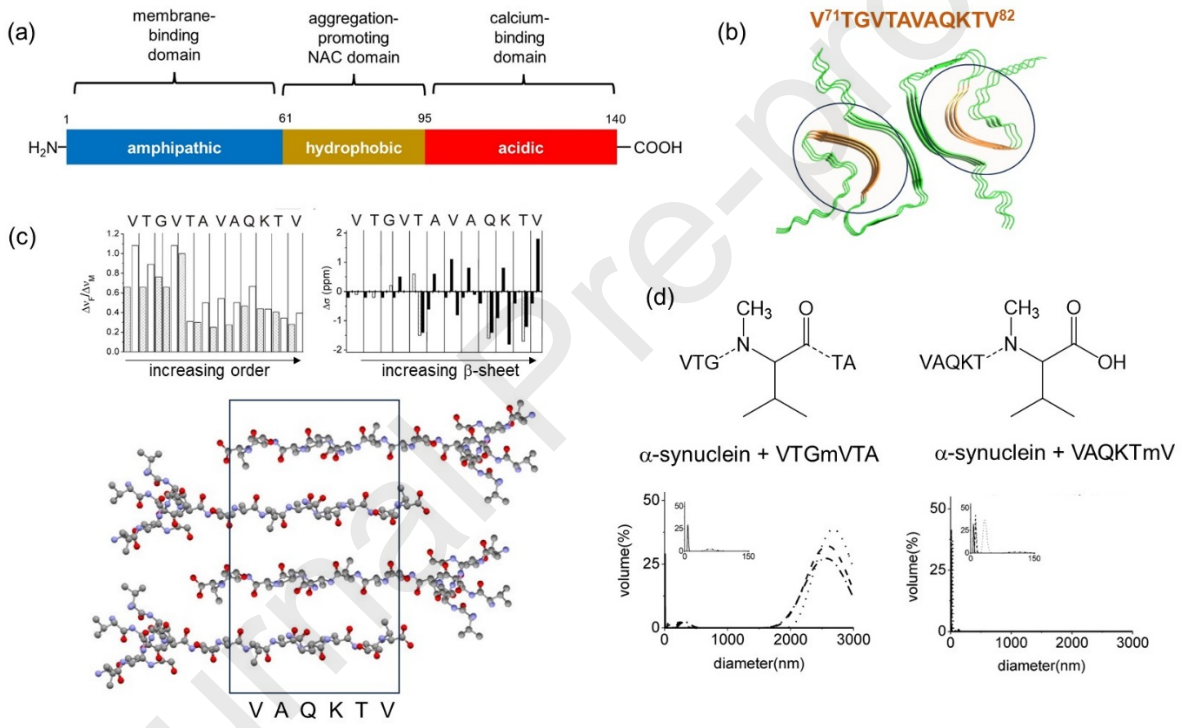

Fig. 15. Design of an N-methylated peptide inhibitor of α-synuclein, guided by solid-state NMR. (a) Domain structure of α-synuclein, including the aggregation-prone NAC domain that forms the core β-sheet region of fibrils and containing the self-recognition element from residues 71-82. Example structures taken from PDB 7YK2 and [217]. (b) 2D ^{13}C DARR spectra (at 9.4 T) of block-labelled fibrils of asyn(71-82) reveal chemical shifts and line widths consistent with ordered C-terminal residues that form the critical self-recognition element, and disordered N-terminal residues that are unnecessary for amyloid formation. An N-methylated hexapeptide asyn(77-82), containing the critical residues, successfully inhibits full-length α-synuclein aggregation whereas the peptide asyn(71-76) does not. Adapted with permission from [216]. Copyright 2008 American Chemical Society.

aggregation-prone (NAC) region of α-synuclein contains the sequence V^{71}TGVTAVAQKTV, which was identified as a critical SRE in aggregation. The peptide asyn(71-82), corresponding to this sequence, was used as the starting point for the design of N-methylated peptides that recognise and bind to the SRE in full-length α-synuclein and inhibit protein aggregation. Solid-state NMR analysis of asyn(71-82) fibrils was used to identify the most aggregation-critical residues in the peptide and guide a refinement process to generate shorter and more efficient N-methylated variants. Asyn(71-82) alone readily aggregates into amyloid-like fibrils, and ^{13}C CP-MAS NMR spectra of block-^{13}C-labelled fibrils indicated changes in line widths at half-height for Cα and Cβ sites that were consistent with increasing structural order of residues from the N-terminus to the C-terminus. PREs observed from the spectra after titrating paramagnetic Mn^{2+} ions into the fibrils suggested that the disordered N-terminal residues are more exposed than are the ordered C-terminal residues, and outside the fibrillar core. From the results of the NMR experiments, a hexapeptide (VAQKTmV) containing the critical C-terminal residues with an N-methylated valine successfully inhibited full-length α-synuclein aggregation. By contrast, N-methylated peptides derived from the redundant N-terminus of the parent asyn(71-82) peptide were ineffective at inhibiting α-synuclein [216].

3.4.4. Natural product inhibitors: EGCG and curcumin

Molecules derived from natural products, including dietary substances, are attractive modulators and inhibitors of amyloid formation by virtue of their low cytotoxicity and immunogenicity. Flavonoid polyphenols form the largest group of the natural compounds that have been tested for amyloid therapeutic applications [218]. They have been demonstrated to target amyloid peptides at various stages of assembly, by stabilizing monomers, inhibiting nucleation, redirecting toxic oligomers into off-pathway aggregation, and disrupting amyloid fibrils, all of which are accessible to NMR analysis. One of the most well-known amyloidophilic flavonols, (-)-epigallocatechin-3-gallate (EGCG) in its aglycone form from green tea, consists of two phenolic rings linked with a fused heterocyclic ring (**Fig. 16a**). Studies of EGCG-Aβ40 interactions are given here as principal examples, but NMR has also illuminated EGCG interactions with α-synuclein [219], hIAPP [220, 221], apoA-I [222], calcitonin [223] and tau [224].

Soluble Aβ40 forms non-toxic oligomers in the presence of EGCG that are well structured, stable and amenable to both solution- and solid-state NMR investigations [225]. A 5-fold excess of EGCG triggers the aggregation of Aβ40 oligomers and precipitation from solution, which rapidly renders the aggregates invisible in HSQC spectra. With the aid of SOFAST ^{1}H,^{15}N-HSQC experiments [69] to reduce

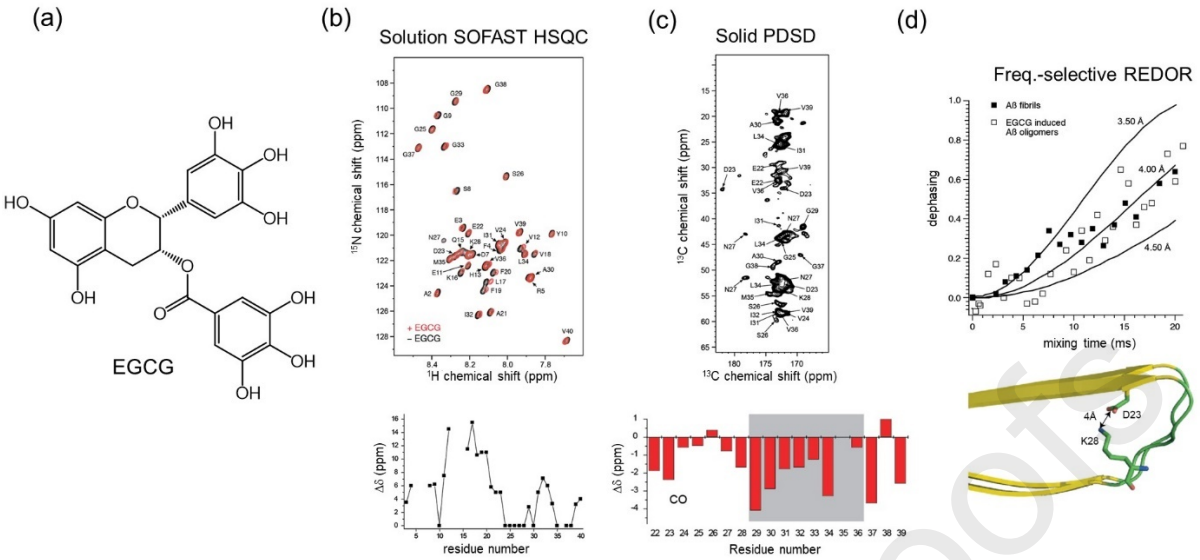

Fig. 16. Combined NMR approach to monitor the rapid formation of Aβ40 oligomers, induced by EGCG. (a) Chemical structure of EGCG. (b) Chemical shift perturbations for monomeric Aβ40 determined by SOFAST HSQC NMR at 14.12 T are consistent with EGCG interacting with the hydrophobic core. (c) Chemical shift analysis of precipitated oligomers determined from an assigned ^{13}C – ^{13}C proton-driven spin diffusion solid-state NMR spectrum at 16.47 T. (d) REDOR NMR dephasing at 16.47 T is consistent with a common D23 – K28 salt bridge in Aβ40 oligomers and fibrils. Adapted from [225] with permission.

measurement times to 16 min at 14.1 T, well-defined chemical shift changes of the soluble peptide can be observed before the signals are lost [225] (**Fig. 16b**). Selected resonances undergoing shift changes could then be detected for the soluble Aβ component (for residues 17–20) indicating specific interactions of EGCG with hydrophobic aromatic core region of Aβ. By contrast, an earlier study reported only small chemical shift changes, consistent with a weak, poorly-defined interaction, observed with a 4-fold excess of EGCG [226]. The insoluble oligomer fraction (formed by uniformly ^{13}C,^{15}N-enriched Aβ40) is amenable to solid-state analysis, and ^{13}C CP-MAS NMR spectra show narrow defined correlation signals consistent with homogeneously-structured peptide across the C-terminal region (**Fig. 16c**). Unlike for fibrillar Aβ40, resonances from the ~20 N-terminal residues of the oligomers were missing, owing to unfavourable dynamics or broadening by structural heterogeneity. However, an ^{15}N-detected frequency-selective ^{15}N,^{13}C-REDOR experiment, measuring dipolar coupling between the D23 carboxyl group and the amine of K28, yielded a ^{15}N$^{\zeta}$,^{13}C$^{\gamma}$ distance of ~ 4 Å, which is consistent with the salt bridge across the interstitial hairpin structure also observed for Aβ40 fibrils (**Fig. 16d**).

Information pertaining to EGCG-Aβ40 oligomer interactions may also be reported from the perspective of the flavonoid ligand. STD NMR measurements of EGCG at different concentrations in the presence of Aβ40 oligomers have been used to estimate the binding affinity of the flavonoid [199]. The proton-detected STD NMR experiments are most effective when the concentration of ligand is high and in large excess with respect to the protein, under which conditions the resonances from EGCG remain narrow and signals from the oligomers are broadened beyond detection by

slow molecular tumbling. The oligomer resonances can be irradiated at NMR frequencies well away from where the ligand resonates, which allows for effective saturation of the entire protein through $^{1}H - {}^{1}H$ dipolar-mediated spin diffusion. If ligand binding is weak (K_D ~$10^{-3} - 10^{-6}$ M), saturation is transferred to the binding parts of the dissociated ligand by intermolecular saturation transfer. A binding isotherm measured at different ligand concentrations can be constructed from STD amplification factors, which represent the fractional saturation of a given proton multiplied by the excess of the ligand over the Aβ oligomers. For EGCG binding to Aβ40 oligomers, an effective K_D of ~150 μM per EGCG binding site was calculated by this method [199]. Further, the STD NMR method can identify the parts of the ligand having the strongest contact with the protein from protons having the most intense NMR signals, enabling the mapping of the ligand's binding epitope [227]. Group epitope mapping of the EGCG ligand found the greatest saturation for protons in rings A and D, consistent with these rings being in closest contact with Aβ40 oligomers. The close contact with ring D is not surprising, given that other flavones lacking this moiety are less active against Aβ. To complete the picture of ligand binding, $^{1}H - {}^{1}H$ ROESY and NOESY spectra were consistent with a conformational change in EGCG in the presence of Aβ monomers, involving rotation of the planes of rings B and D [199]. Care must be taken with EGCG, however, because the flavonoid is prone to covalent dimerization at higher concentrations [219].

EGCG is known to remodel amyloid fibrils into non-fibrillar supramolecular structures, and solid-state NMR can offer unique insight into the atomic basis for remodelling. One example is apolipoprotein A-I (apoA-I), the main protein component of high-density lipoprotein, which accumulates as fibrils in atherosclerotic plaques and may contribute to coronary artery disease by increasing plaque burden and instability. Signature ^{13}C chemical shifts of apoA-I fibrils formed in the presence of heparin, measured from a solid-state 2D $^{13}C - {}^{13}C$ dipolar correlation spectrum, are consistent with the fibrils comprising a mixture of native α-helical elements and newly-formed β-sheet regions [106]. After adding EGCG to apoA-I fibrils, cross-peaks corresponding to the α-helical residues disappear from the spectrum when Hartmann-Hahn cross-polarization is used for excitation of the observed nucleus [222]. The missing peaks were shown to correspond to regions of increased mobility according to a 2D $^{1}H - {}^{13}C$ INEPT NMR spectrum, which detects signals only from mobile regions [115]. The increased mobility occurred within specific amino acid sidechains and there was much less signal intensity in the Cα/Hα region of the INEPT spectrum, which implies that most of the protein backbone remains relatively constrained. Together with transmission electron microscopy, the NMR data revealed that EGCG remodels of apoA-I fibrils into soluble 20 nm diameter oligomers with a largely α-helical structure [222].

Curcumin is a yellow phenolic diaryl heptanoid pigment from the rhizome of the common spice turmeric. Studies *in vitro* have shown that curcumin inhibits the formation of, and/or disaggregates, fibrils of Aβ and other amyloidogenic polypeptides. Further evaluations in transgenic mice have shown that curcumin crosses the blood-brain barrier, binds to Aβ amyloid plaques, and lowers Aβ deposition in the brain. Although the pharmacological efficacy of curcumin against amyloid disorders in humans has been debated extensively, its inhibitory properties remain of great interest for mechanistic studies and as a basis for drug design.

Solution-state NMR studies of curcumin interactions with monomeric amyloid proteins or small oligomeric species have faced several challenges. Many amyloid proteins are intrinsically disordered in their monomeric states and by definition sample many random conformations. Consequently, chemical shift pertur ations induced b by curcumin binding may be very small as compared to ligand interactions with folded, globular proteins. Indeed, a specific recognition site may not exist until the protein assumes an ordered amyloid state. In the case of α-synuclein, ^{1}H – ^{15}N HSQC NMR spectra of the monomeric protein alone in solution showed narrow resonances and low chemical shift dispersion, consistent with unstructured protein. Addition of a 2-fold lower concentration of curcumin had little effect on the chemical shifts and line widths, suggesting that any interaction of curcumin with the protein was very weak [228]. Larger changes in chemical shifts and linewidths were observed when curcumin was added to low molecular weight α-synuclein aggregates having more defined structures. Nevertheless, no pattern was observed across the protein sequence and no preferential binding site could be identified. In the case of Aβ42, HSQC spectra of the monomeric peptide exhibited chemical shift perturbations after addition of curcumin, but these were observed along all of the residues and it was not possible to identify critical binding residues [229]. Furthermore, detection of binding using STD NMR, as demonstrated for hIAPP, may not be possible for small peptides [230]. A further drawback is the poor solubility of curcumin, which limits the concentration of the compound that can be used in NMR analyses in aqueous solution without the use of potentially interfering organic solvents. Pithadia *et al*. [230] addressed this issue by designing a diacetate derivative of curcumin with improved aqueous solubility.

Solid-state NMR experiments to characterise curcumin binding to amyloid fibrils do not suffer from the same drawbacks as experienced in solution NMR studies. The fibrils have a defined three-dimensional architecture, within which specific binding sites for accessory molecules are likely to exist. Further, the poor solubility of curcumin can be overcome by titrating low concentrations of drug into the fibrils, followed by centrifuging to isolate the fibril-curcumin complex, and repeating the process until sufficient amounts of the drug have accumulated in the fibrils. The effect of curcumin on the assembly pathway of Aβ40 and fibril structure was analysed with the aid of 2D ^{13}C – ^{13}C dipolar correlation solid-state NMR spectra of the uniformly ^{13}C labelled peptide in the presence of unlabelled ligand [231].

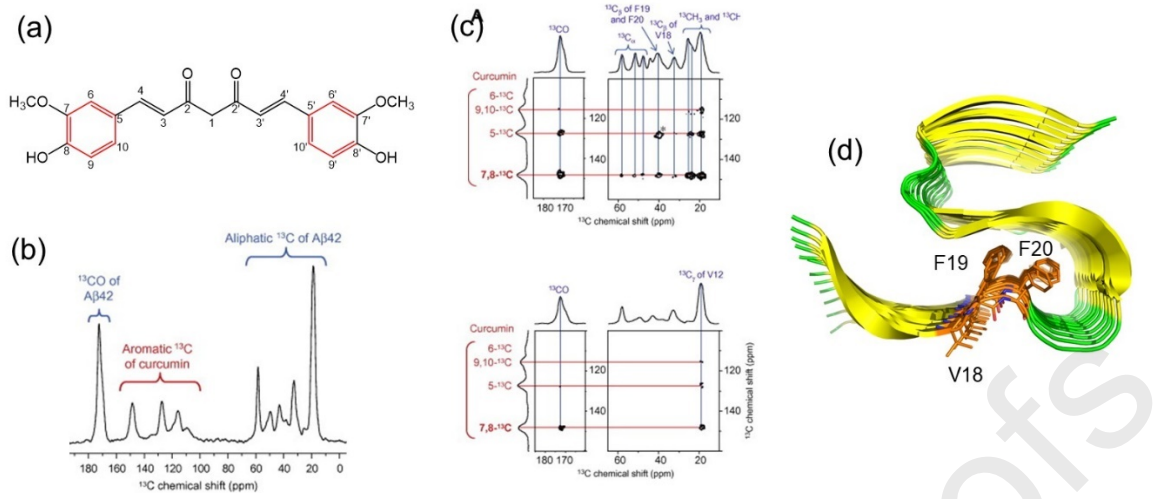

Fig. 17. Solid-state NMR analysis of curcumin binding to Aβ42 fibrils. (a) Structure of curcumin. For NMR, ^{13}C was incorporated into the aromatic rings (red). (b) A 1D ^{13}C CP-MAS NMR spectrum shows signals from curcumin distinct from labelled residues in Aβ42 fibrils. (c) 2D ^{13}C – ^{13}C DARR NMR spectra at 14.10 T, obtained with covariance NMR processing, exhibits cross-peaks correlating aromatic sites in curcumin and specific amino acid side-chain resonances. Location of the specific valine and phenylalanine side chains in Aβ42 fibrils. Structure obtained from PDB 2MXU and [232]. Panels (b) and (c) adapted from [233] with permission.

The spectra of fibrils formed alone and with curcumin exhibit chemical shift differences that are consistent with major structural changes in the region encompassing the Asp23–Lys28 salt bridge region. A sophisticated isotope labelling strategy, combined with CP-MAS methods, was performed to focus on the sites of curcumin binding to pre-formed Aβ42 fibrils [233]. The ^{13}C labels were incorporated into selective sites of both Aβ and curcumin by chemical synthesis. Non-aromatic carbons of Aβ42 residues A2, F4, G9, V12 and 17-21 were labelled and only the aromatic carbons of curcumin were labelled (**Fig. 17, a,b**), so as to avoid overlap of resonances that could cause ambiguities in peak assignments to the peptide and the ligand. 2D dipolar-assisted rotational resonance (DARR) NMR spectra of the fibril-curcumin complex revealed weak cross-peaks correlating the aromatic carbons of curcumin with the CH_3, CH_2, CH and carbonyl carbons of residues V12 and 17-21 of Aβ42. The cross-peaks were consistent with detectable intermolecular dipolar couplings arising from interactions of curcumin with the central region of Aβ42 that constitutes the exposed β-sheet of the fibrils (**Fig. 17, c,d**). An interesting feature of this work was the application of covariance processing to the 2D spectra [234] to enhance weak intermolecular cross-peaks between peptide and ligand. Strong dipolar couplings between bonded ^{13}C nuclei (~3.5 kHz for a ^{13}C-^{13}C distance of 1.5 Å) in extensively labelled molecules may give rise to dipolar truncation effects, whereby weaker couplings between nuclei separated by 4 – 6 Å are suppressed or diminished in intensity. The relative intensities of weak cross-peaks with respect to diagonal peaks can be enhanced by obtaining a symmetrical covariance matrix $\boldsymbol{C}$ by first multiplying the processed 2D NMR n x n data matrix $\boldsymbol{A}$ by its transpose, i.e., $\boldsymbol{B} = \boldsymbol{A} \cdot \boldsymbol{A}^T$, followed by calculation of $\boldsymbol{C} = \boldsymbol{P}\, \boldsymbol{D}^{\frac{1}{2}} \boldsymbol{P}^{-1}$, where $\boldsymbol{P}$ contains the eigenvectors of $\boldsymbol{B}$ and $\boldsymbol{D}$ is the diagonal matrix of the eigenvalues of $\boldsymbol{B}$. Several distinct intermolecular cross-peaks could be observed with this additional processing. However, the limited

number of labelled residues in the peptide, whilst being advantageous for the analysis of the spectra, meant that any additional binding sites for curcumin in other, unlabelled regions of the peptide could not be detected. Furthermore, dipolar couplings measured under MAS conditions carry no information on the orientation of curcumin relative to the fibril geometry. This issue will be addressed in more detail later.

3.5. Antibodies and small molecule agents for sequestering amyloid

Monoclonal antibodies are of interest in amyloid research because of their ability to recognise, and hence enable identification of, specific aggregation states of amyloid proteins. Antibodies are also clinically important in amyloid-related diseases because they can bind to oligomeric or fibrillar species and dissolve or sequester them. Anti-amyloid immunotherapy has recently attracted attention owing to its effectiveness in reducing plaque burden and disease progression in clinical trials for Alzheimer's and in systemic light chain amyloidosis.

Solution-state NMR has been used to elucidate the origins of compatibility of amyloid-antibody interactions, from observations of selective chemical shift perturbations and relaxation enhancements to identify contact sites on the two interacting partners. For example, a conformation-specific antibody fragment, KW1, binds selectively to Aβ40 oligomers but not to amyloid fibrils [235]. ^{1}H – ^{15}N HSQC spectra of ^{15}N-labeled Aβ40 oligomers in the presence or absence of the oligomer-specific antibody fragment KW1 revealed a selective loss of cross-peak intensity at two structural sites of Aβ (residues 15–24 and 31–37) (**Fig. 18, a,b**). The loss of intensity is attributed to enhanced transverse relaxation arising from the loss of local mobility of Aβ around the interaction regions, combined with the increased size of the Aβ-antibody complex. The results indicated that the epitope site of Aβ consisted mainly of hydrophobic and aromatic residues, which implies a different presentation in the oligomeric and fibrillar state that underlies the antibody selectivity [235].

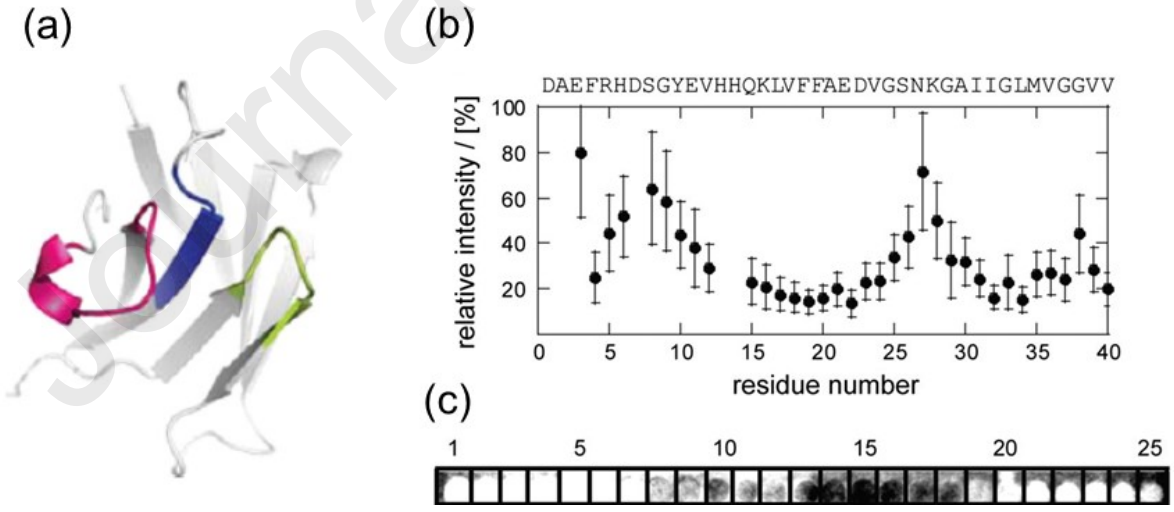

Fig. 18. NMR analysis of antibody fragment KW1 with Aβ40 oligomers. (a) Structure of KW1. (b) Residue-specific broadening of resonances from Aβ40 oligomers after the addition of KW1, measured as the relative intensities of ^{1}H – ^{15}N cross-peaks in a HSQC spectrum at 14.1 T. (c) KW1AP binding to an array of Aβ-derived peptide

fragments immobilized on a cellulose membrane. Black spots indicate positive binding. Adapted from [235] with permission. Copyright 2012 National Academy of Sciences.

Molecules like KW1 are useful research tools that can enable detailed analysis of otherwise transient amyloid species by trapping and stabilising them. Recombinant human prion protein (huPrP) constructs have been shown to function similarly to antibodies by binding to Aβ42 oligomers and sequestering them into large heterogenous precipitates. MAS solid-state NMR was used to investigate the conformations of Aβ42 oligomers and huPrP in the complex, by isotopically-labelling one or other of the interaction partners [236]. By labelling the huPrP component, INEPT NMR spectra, which detect mobile residues, and cross-polarization NMR spectra, which detect motionally-restrained regions, indicated that the disordered N-terminal region of huPrP becomes immobilized in the complex. ^{13}C chemical shifts of huPrP in the complex measured from a dipolar correlation spectrum were similar to those in a TOCSY spectrum of the monomeric protein in solution, indicating that the two species had similar secondary structure. Repeating the approach but with labelled Aβ42 oligomers indicated that the oligomers take on a predominantly β-sheet structure across virtually all residues. It should be noted that NMR spectra of these complexes in the solid-state typically have broad resonance lines, consistent with high structural heterogeneity of the system, and so it is useful to have access to sequentially-assigned spectra in the solid or solution state for comparison.

Affibodies are rationally-designed proteins that mimic monoclonal antibodies and can bind tightly (with nanomolar affinity) to and sequester specific amyloid protein sequences. A cysteine-linked dimer of the affibody protein $Z_{Aβ3}$ has been shown to bind to monomeric Aβ40 with nanomolar affinity [237, 238]. ^{1}H – ^{15}N HSQC spectra of the Aβ40-affibody complex indicated that both proteins undergo folding upon complex formation, as signified by the improved resonance dispersion. Further structural analysis of the complex utilized intra- and inter-molecular NOEs and backbone dihedral angle constraints derived from chemical shifts using TALOS. The data revealed that $Z_{Aβ3}$ dimers form a 4-helix bundle that encapsulates monomeric Aβ40 in a hydrophobic tunnel-like cavity. Aβ40 adopts a similar β-strand-turn-β-strand hairpin motif to that seen in fibrillar aggregates. Protein-specific NMR assignments were enabled by using mixtures of ^{13}C,^{15}N-labelled and unlabelled proteins, and intermolecular NOEs detected using 3D F1(^{13}C,^{15}N)-filtered, F2(^{13}C or ^{15}N)-edited NOESY experiments.

Nanobodies are single (heavy) chain antibodies that are uniquely produced in camels and llamas and have the desirable features of small sizes (Mw < 14 kDa) and high affinities against antigens (K_D ~ nM) [239]. An α-synuclein-binding single-domain camelid antibody, NbSyn2, was identified by phage display and ^{1}H–^{15}N HSQC was used to map the epitope of NbSyn2 on α-synuclein by observing chemical shift perturbations of the backbone amide resonances. Titration of unlabelled NbSyn2 into ^{15}N-labeled α-synuclein resulted in both broadening and shifts of specific resonances in the HSQC spectrum of the latter [240, 241].

Small molecules are being developed to replicate the mode of action of antibodies by sequestering Aβ monomers from solution. Solution-state NMR has been used to identify sites of interaction of one such pharmaceutical lead compound, 10074-G5, which sequesters monomeric Aβ42 [242]. A challenge for NMR studies of Aβ42

is that the monomeric peptide is highly disordered in solution at physiological pH and temperature. Consequently, the solvent-exposed amide groups undergo hydrogen exchange, which causes extensive line broadening across the 2D ^{1}H – ^{15}N correlation spectra. ^{13}CO – ^{15}N (CON) experiments that utilise ^{13}C detection can reduce the impact of these exchange broadening effects, but they suffer from poor sensitivity. The 2D $H^{N-BEST}CON$ experiment was therefore developed to reduce line broadening and increase sensitivity by exploiting the larger ^{1}H (instead of ^{13}C) polarization as the starting point of the coherence transfer pathways [243]. 2D $H^{N-BEST}CON$ NMR experiments on uniformly ^{13}C, ^{15}N-labeled monomeric Aβ42 detected minimal perturbations of chemical shifts in the presence of one- and twofold concentrations of 10074-G5. However, it is known that chemical shift perturbations can be difficult to detect for disordered proteins. The inclusion of water presaturation in the pulse sequence caused many resonances to diminish in intensity as a result of saturation transfer, with the exception of those of C-terminal hydrophobic residues that are protected from solvent exchange. The presence of 10074-G5 was accompanied by the loss of resonances from the protected C-terminal residues, suggesting that binding of the small molecule is accompanied by conformational changes in Aβ42 that enhance solvent exposure. This work illustrates that, for disordered proteins, it is worthwhile to seek alternatives to chemical shift perturbations to detect interactions with small molecules that would otherwise go undiscovered.

3.6. Interactions with diagnostic agents

3.6.1. *In vivo* tracer ligands

Positron emission tomography (PET) is a clinical imaging modality that detects radioactive nuclei, principally ^{11}C and ^{18}F, of radiotracer ligands introduced into living subjects. As they undergo β-decay, the radioisotopes emit positrons that rapidly lose kinetic energy and interact with electrons to produce γ photons. The γ photons are detected to report the spatial distribution of the radioligand in tissue and the bloodstream. PET radioligands are produced using a cyclotron, and the short half-lives of the radioisotopes (~20 min for ^{11}C and ~110 min for ^{18}F) restrict how far the site of production can be physically located from the patient and scanner. PET is well-established in clinical oncology for detecting the enhanced uptake of radioligands such as ^{18}F-deoxyfluoroglucose by cancerous cells, which is exploited to locate malignant tumours.

More recently, PET has been used for Alzheimer's diagnosis, spearheaded by the design of small radioligands containing ^{11}C, such as Pittsburgh compound B (PiB), and ^{18}F, such as fluβpir and flutemetamol, that bind to fibrillar amyloid plaques in the brain. As this emerging application develops further, there is motivation to develop radioligands with higher affinity and selectivity for amyloid associated with specific diseases. In support of this goal, solid-state NMR has recently been demonstrated to detect and characterize the amyloid interactions of radioligand analogues in which the radioactive nuclei are replaced with the corresponding stable, spin-half NMR isotopes, ^{13}C and ^{19}F. It should be noted that the 'traditional' laboratory synthesis of ^{13}C- and ^{19}F-labelled ligands for NMR is rather different from the cyclotron chemistry used to produce the ^{11}C and ^{18}F counterparts for imaging. The latter chemistry must be rapid and usually involves proton bombardment of chemical precursors containing ^{14}N (to obtain ^{11}C) or ^{18}O (for ^{18}F).

MAS solid-state NMR spectroscopy has been used to characterize complexes of Aβ40 fibrils with a ^{13}C-methylated PiB derivative and with an unlabelled novel tracer compound, DABTA [244]. In common with other Alzheimer's PET ligands, these ligands are poorly water-soluble and, to avoid the use of organic solutions that may disrupt fibrils, the compounds were titrated into the fibril suspension in a bovine serum albumin carrier. Ligand binding can be readily visualised from the change in the colour of the sedimented fibrils. 2D ^{13}C – ^{13}C chemical shift mapping of [U-^{13}C,^{15}N]Aβ40 fibrils titrated with ligands revealed small chemical shift perturbations consistent with a minimal impact of the ligand on the fibrillar architecture. By contrast, selective chemical shift perturbations seen in proton ^{1}H-^{15}N correlation spectra are more sensitive to local effects of ligand binding, and suggest interactions of the ligands around the loop region connecting the two β-strands (involving residues Gly25-Lys28), and with residues Ile32 and Gly33 that are located in the strand β2. For the latter experiments, fibrils were also deuterated and amide protons back-substituted to minimise ^{1}H – ^{1}H dipolar broadening [244]. Unfortunately, proton-detected ^{1}H – ^{13}C correlation experiments were unable to detect the signals from the bound labelled ligand. The authors speculate that high-speed MAS (> 52 kHz) may be necessary to observe the ligand, because of the high proton density.

Binding of ^{19}F-labelled flutemetamol (**Fig. 19a**) to Aβ40 fibrils has been characterized by MAS solid-state NMR methods [245] 2D ^{13}C – ^{13}C and ^{13}C – ^{15}N correlation spectra of flutemetamol-bound fibrils show similar chemical shifts and intensity distributions to those for the apo peptide, indicating that the PET tracer does not cause observable conformational changes to the fibrils. The advantage of the stable isotope-labelled flutemetamol is that ^{19}F can be observed unambiguously when bound to the fibrils, with no overlap from background signals, and the large CSA of ^{19}F permits chemical shift tensor analysis of the bound ligand from spinning sideband pattern. Ligand binding to hydrated fibrils did not change the isotropic chemical shift or the sideband intensity envelope in the spectrum obtained with cross-polarization, indicating that the bound flutemetamol is similarly immobilized as in the solid powder. With the use of direct polarization (DP) and longer recycle delays favouring long-T_1 species, a second spectral component emerged with narrower

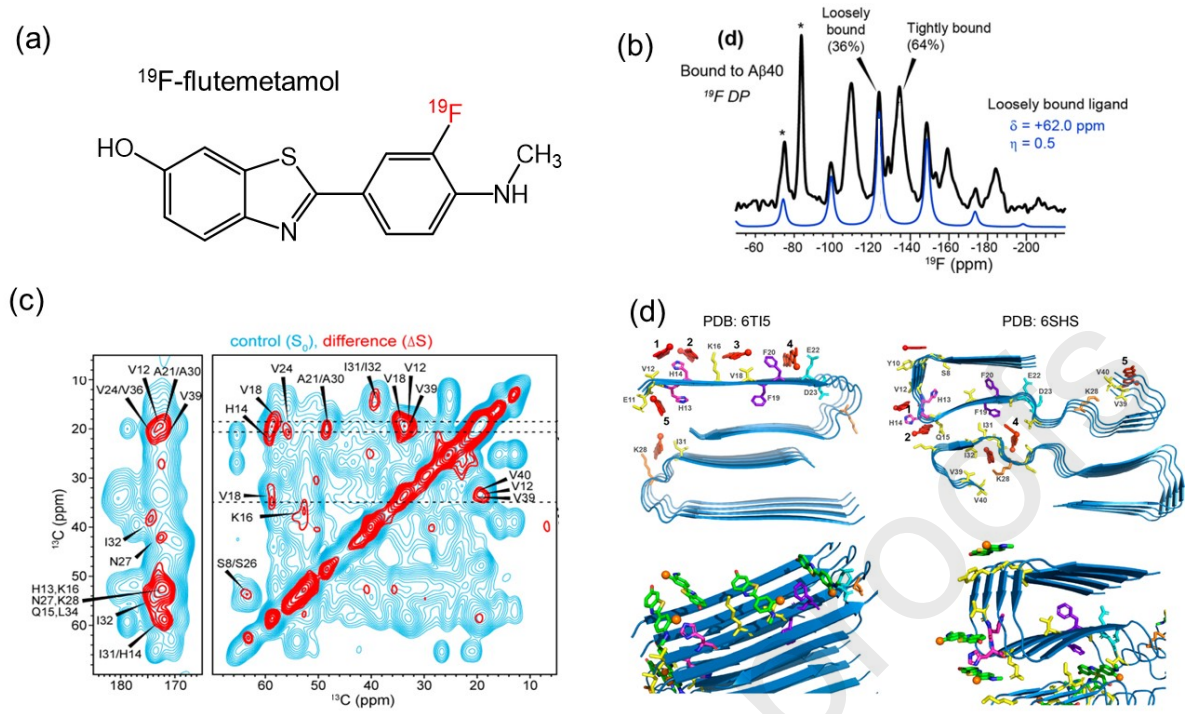

Fig. 19. Binding sites of PET imaging agent flutemetamol within Aβ40 fibrils, studied using ^{19}F solid-state NMR. (a) Chemical structure of the PET ligand. The ^{18}F radioisotope is replaced with ^{19}F for NMR analysis. (b) DP ^{19}F NMR spectrum (black) of flutemetamol bound to Aβ40 fibrils at 14.1 T reveals loosely bound and tightly bound ligand sites in the fibrils. The simulated lineshape for the loosely-bound component (blue) was obtained with the values of δ and asymmetry parameter, η, shown. (c) 2D ^{13}C – ^{13}C resolved dipolar correlation spectrum of [U-^{13}C]Aβ40 fibrils obtained with and without initial ^{1}H-^{19}F REDOR dephasing identifies resonances from protein sites (red) close to ^{19}F of the ligand. (d) Docking models of flutemetamol with an *in vitro* fibril structure (PDB 6TI5) and Alzheimer's brain fibril structure (PDB 6SHS), constrained by the experimental NMR data. Adapted with permission from [245]. Copyright 2022 American Chemical Society.

linewidths and smaller CSA than the main component, consistent with a second population of loosely bound ligand undergoing small amplitude motions. A further advantage of ^{19}F is that the proximity of the ligand to specific protein residues can be detected by exploiting REDOR dipolar dephasing of protein signals by the ligand. Signal dephasing may be observed for internuclear distances r_{IS} of up to 6.5 Å for ^{13}C – ^{19}F and 10.5 Å for ^{1}H – ^{19}F. 2D-resolved REDOR spectra of the flutemetamol-fibril complex indicated that three clusters of residues, V12 and H13/H14, V18 and F19/F20, A21, or A30, and V39/V40, are in close proximity to the ligand fluorine and constitute at least two binding pockets for flutemetamol (**Fig 9c**). Together, these two examples demonstrate that PET ligand-amyloid complexes can be observed by solid-state NMR and supply useful experimental restraints on computational docking simulations (**Fig 9d**). Future attention will likely focus on fluorinated PET ligands because of the logistical clinical benefit of ^{18}F having a relatively long radioactive half-life, coupled with the favourable NMR properties of ^{19}F. SSNMR comparisons of

different, and novel, fluorine-containing PET ligands are anticipated to be useful for identifying higher-affinity compounds with greater selectivity for specific amyloid types.

3.6.2. Amyloid-responsive dyes

The benzothiazole salt thioflavin T (ThT) and the azo dye Congo red (CR) are planar aromatic compounds that are used routinely as chemical stains to monitor the formation of amyloid *in vitro* and to detect the presence of amyloid in tissue. When ThT binds to the β-sheet-rich motifs of amyloid aggregates, the rotational planes of the benzothiazole and dimethylaniline rings become restricted, giving rise to markedly enhanced fluorescence and a characteristic red shift of its emission maximum to around 482 nm. Histological staining of amyloid by CR is characterized by apple-green birefringence under polarized light. NMR in the solution and solid states offers insights into the interactions of ThT and CR with monomeric and fibrillar amyloid proteins, their effects on protein aggregation state, and competition with other amyloid-binding molecules. Insights into the intriguing optical and diagnostic properties of ThT and CR have been gained from NMR spectroscopic investigations of their interactions with amyloid.

Interactions between ThT and amyloid species can be screened using solution-state 1D ^{1}H NMR spectroscopy to observe the dye [246]. Chemical shift perturbations and/or peak broadening for the signature peaks of the dye indicate its binding to monomeric or aggregated protein. Such measurements benefit from deuterium exchange to eliminate the protein amide proton signals, to avoid signal overlap with the observed aromatic proton resonances from the ligand. The ^{1}H NMR resonances of ThT in the presence of an excess of hIAPP fibrils (ThT:IAPP 1:8) were shown to undergo small changes in the peak frequencies and widths, consistent with a weak interaction [246], but when ThT was added to hIAPP oligomers the aromatic peaks were broadened beyond detection. The basic ^{1}H NMR experiments must be followed up with further experiments to confirm the origins of peak broadening. For example, peak broadening was observed for the hydrophobic residues of monomeric Aβ40 in the presence of CR. By obtaining spectra at different temperatures, and by pulsed field gradient NMR diffusion measurements, it was possible to attribute the peak broadening to chemical exchange processes (e.g., protein conformational exchange or ligand exchange) on the intermediate chemical shift timescale, and not to a significant increase in the size of the CR-Aβ complex [247]. CR has also been shown to inhibit or disrupt amyloid formation, possibly by interfering in the interactions between the β-sheet lamina that stabilize the fibrillar assemblies. Titration of Aβ40 with CR gives rise to peak broadening at low CR concentrations followed by the appearance of new signals at higher CR concentrations, consistent with a two-step binding process [247].

STD NMR has been used to confirm interaction of ThT with α-synuclein fibrils. Saturation transfer signals observed for the ThT aromatic protons suggest that the dye interacts closely with the fibrils [248]. STD NMR has also been used to demonstrate that ThT and two polyphenols, EGCG and its smaller metabolic product EGC, compete for the same binding site of α-synuclein fibrils. ThT fluorescence enhancement is often used to identify amyloid inhibitors, such as polyphenols, which prevent or decrease the rate of protein aggregation, but interpretation of the data can be problematic because polyphenols can displace ThT from its amyloid binding site(s). Displacement

of ThT from amyloid fibrils by polyphenols can diminish fluorescence intensity in much the same way as inhibition of amyloid formation would do, and so it is important to distinguish between these two quite different mechanisms.

The optical properties of CR and ThT in the presence of amyloid originate from changes in the conformational properties of the dyes' aromatic groups when bound to β-sheets. Solid-state NMR has been used to report the conformation of the dyes when bound to amyloid fibrils, with the aid of isotope labelling to enhance the signals from the dye. A 2D chemical shift tensor-correlation experiment was applied to [1,1'-$^{13}C_2$]CR (**Fig. 20a**) when bound to fibrils of the prion protein, HET-s(218-289) [249]. The experiment and labelling pattern enable determination of the torsional angle β, defining the relative orientations of the aromatic rings in the central biphenyl linkage of CR (**Fig. 20b**). Rotor-synchronized MAS sidebands along the diagonal and off-diagonal arise from intramolecular ^{13}C1–^{13}C1′ proton-driven spin-diffusion polarization transfer. The side-band intensities are sensitive to the relative orientations of the two ^{13}C chemical shift tensors, and report a small out-of-plane deviation of the two aromatic rings (**Fig 20c**). Computational docking analysis was performed using the HADDOCK software [250], in which the long axis of CR was assumed to coincide approximately with the fibrillar long axis (**Fig. 20d**). However, MAS solid-state NMR measurements (e.g., chemical shift perturbations and dipolar couplings) cannot easily verify this orientation of the molecule.

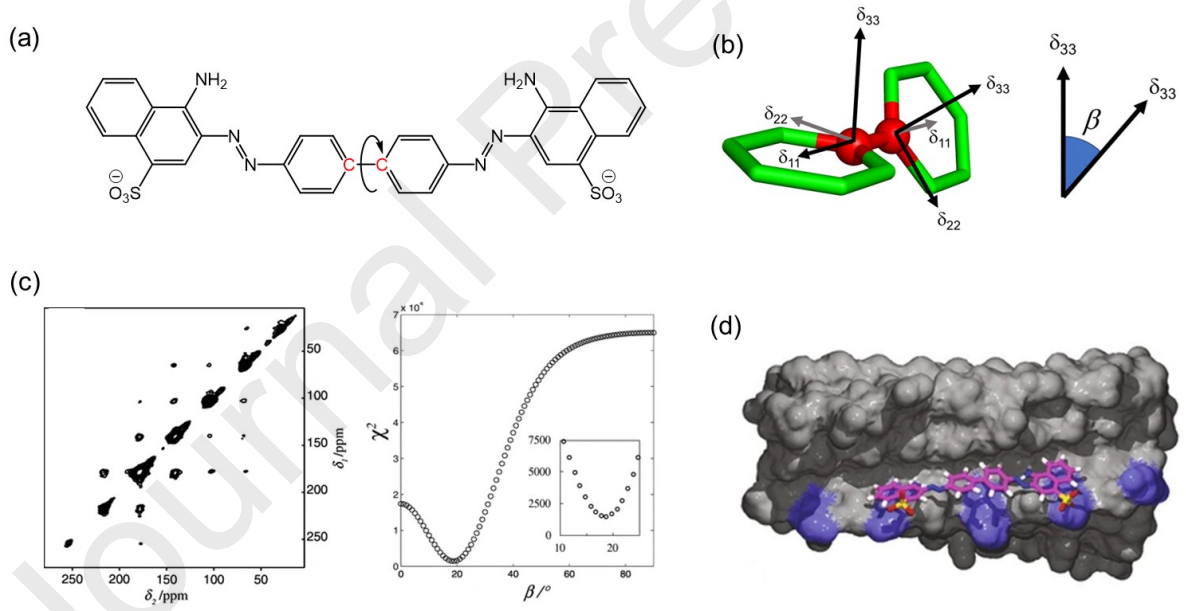

Fig. 20. Solid-state MAS NMR measurement of aromatic ^{13}C chemical shift tensor orientations in Congo red (CR) bound to prion protein fibrils. (a) Structure of CR denoting the two sites of ^{13}C incorporation (red). (b) The orientation of the chemical shift tensor elements, δ_{33}, of the two ^{13}C sites reports on the angle β between the planes of the aromatic rings. Spinning sideband intensities in an NMR ^{13}C – ^{13}C tensor-correlation spectrum recorded at 20.0 T are analysed to determine angle β. (d) Docking model of CR on fibrils. Note that the experiment does not report on the orientation of the ligand relative to the fibril axis. Adapted from [249] with permission.

4. The orientation question

The previous sections highlight the power and versatility of NMR in the solution and solid states for monitoring interactions between amyloid species and a diversity of ions, peptides, lipids, polysaccharides and small molecules. In favourable cases, NMR is capable of resolving the sites of interaction of accessory ions and molecules with monomeric and fibrillar amyloid proteins. As seen, binding sites within fibrillar assemblies may be mapped with the aid of MAS solid-state NMR detection of chemical shift perturbations and measurements of dipolar couplings of uniformly or strategically isotope-labelled fibril-ligand complexes. Such methods do not give a complete picture of the amyloid-ligand geometry, however. An important, yet often missing, feature of the molecular complex is the orientation of the ligand molecule in relation to the ubiquitous cross-β motif of amyloid fibrils. For instance, a ligand may align along the direction of inter-peptide hydrogen-bonding defining the fibrillar long axis (e.g., as assumed in Fig 20d); thus, it may be concluded that ligand binding requires a repeating array of appropriate amino acid functionalities present only in the assembly. Alternatively, the principal axis of the ligand molecule may be aligned perpendicular to the fibril axis, in which case all the appropriate binding residues may be present within a single protein monomer unit. NMR methods have been developed to provide insights into ligand orientations when bound to amyloid fibrils in solution and in the solid-state.

One solution NMR approach relies on measurements of transferred nuclear Overhauser effects (trNOEs) and ^{1}H – ^{13}C and ^{1}H – ^{15}N transferred residual dipole couplings (trRDCs) for weakly binding ligands as they undergo exchange between fibril-bound and free states. This method exploits the propensity of amyloid fibrils to align spontaneously in a magnetic field, with the fibril axis parallel to B_0, owing to the anisotropy of the diamagnetic susceptibility of the peptide bonds. Consequently, interacting ligands retain a weak alignment after dissociating from fibrils [251]. The structure and orientation of a designed inhibitor peptide iAβ5 (sequence LPFFD) interacting with fibrils of an Aβ peptide fragment were determined in this manner [252]. The bound conformation of the peptide was determined from trNOE data and orientational constraints were obtained from an order matrix derived from trRDCs, which described the orientation of the ligand principal alignment tensor relative to a fixed fibril coordinate system.

In the solid state, NMR methods have been developed that exploit the ability of amyloid fibrils to adopt a preferred orientation when deposited on planar surfaces, such as microscope cover slips. The fibrils align with their long axes, on average, parallel with the plane of the surface. A static NMR probehead with a flat coil, wound with rectangular geometry, is used to retain stacks of cover slips such that the B_0 direction is normal to the plane of the slides and at approximately 90° to the fibril long axes. The anisotropy of nuclear spin interactions (chemical shielding, dipolar, quadrupolar) of specific isotope labels reports the orientation of the fibrils relative to the magnetic field, and the orientation of bound ligands with respect to the fibril geometry. The oriented sample solid-state NMR approach has been used for many years to obtain orientational information for peptide bonds in lipid bilayer-embedded proteins.

The large chemical shift anisotropy of ^{19}F has been exploited using oriented sample solid-state NMR to determine the orientation of a fluorescent amyloid-diagnostic dye, FSB (**Fig. 21**), bound to Aβ40 fibrils oriented on a planar surface. A fibril coordinate system may be defined in which the *z*-axis is parallel with the fibril long axis (parallel with the surface) and the *y*-axis parallel with B_0 (**Fig. 21b**). The orientation of the ligand ^{19}F chemical shift tensor in this fibril frame is given by angles α_{CF}, β_{CF} and γ_{CF}. Angle α_{CF} takes all values from 0° to 360°, to reflect the cylindrical distribution on the planar surface of fibrils about their long axes, and unique values of angles β_{CF} and γ_{CF} define a particular orientation of the ligand relative to the fibril axis. The ^{19}F chemical shift tensor of the bound ligand therefore assumes a restricted distribution of orientations relative to B_0, which are defined by angles θ_{CM} and ϕ_{CM}. These angles, which may be considered to be a subset of the angles describing a powder distribution, are given by equations 14, 15a, and 15b:

$$\theta_{CM} = \cos^{-1}[\sin(\alpha_{CF})\sin(\beta_{CF})] \quad [14]$$

and

$$\phi_{CM} = \cos^{-1}\left[\frac{\sin(\alpha_{CF})\cos(\beta_{CF})\cos(\gamma_{CF}) + }{-\sin(\theta_{CM}}\right. \quad [15a]$$

if $\cos(\alpha_{CF})\cos(\gamma_{CF}) \geq \sin(\alpha_{CF})\cos(\beta_{CF})\sin(\gamma_{CF})$, or

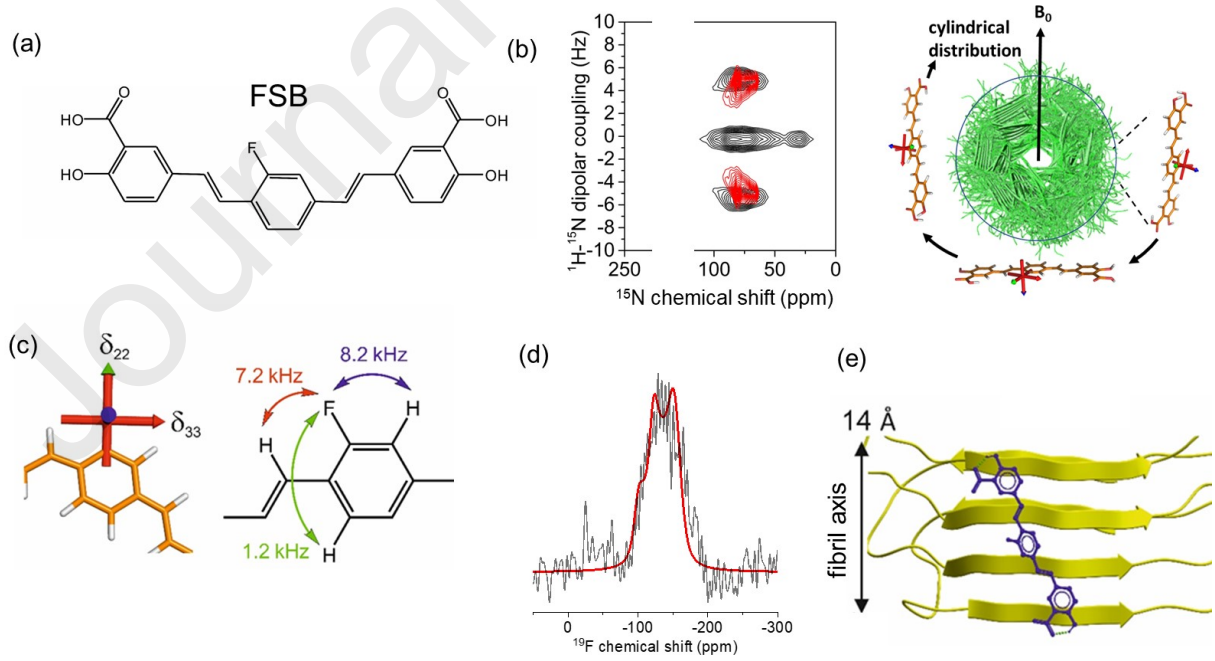

Fig. 21. Determination of ligand orientation when bound to an amyloid fibril using oriented sample ^{19}F NMR. (a) Structure of the fluorescent probe, FSB. Fluorescence

is enhanced when it binds to Aβ40 fibrils. (b) Aβ40 fibrils are prepared aligned on a planar surface with the fibril long axis perpendicular to B_0, as confirmed by PISEMA NMR of [U-^{15}N]Aβ40 fibrils. Bound FSB is distributed cylindrically around the oriented fibrils. (c) The predicted ^{19}F NMR lineshape for FSB depends on the orientations of the chemical shift tensor, δ, and ^{19}F – ^{1}H dipolar vectors relative to the fibril axis. (d) The NMR line shape is consistent with the long axis of FSB being tilted by ~40°with respect to the fibril axis. Spectra were recorded at 9.39 T. Adapted from [253] with permission. Copyright 2018 American Chemical Society.

$$\phi_{CM} = 2\pi - \cos^{-1}\left[\frac{\sin(\alpha_{CF})\cos(\beta_{CF})\cos(\gamma}{-\sin}\right. \quad \text{[15b]}$$

otherwise.

It is straightforward to calculate the ^{19}F NMR line shape for any given ligand orientation bound to an oriented fibril if the chemical shift tensor principal components are known or can be predicted by DFT calculations (**Fig. 21, c, d**). All that is required is a restricted crystallite file that can be generated using the equations above, which can be used in the SIMPSON simulation environment, for example. In the case of a fluorine-substituted aromatic ligand, the *z*-component of the chemical shift tensor is oriented in-plane with the benzene ring and the *x*-component along the C – F bond [253]. Simulated pure chemical shift line shapes for this arrangement can readily distinguish between the cases of the ligand bound to fibrils with the C – F bond parallel or perpendicular to the fibril axis. The observed NMR line shape (**Fig. 21d**) is compared with simulated spectra to find the closest fit by least-squares analysis. In practice, to observe a pure chemical shift line shape it is necessary to decouple protons during signal acquisition. Whilst this is readily achievable for ^{13}C and ^{15}N in commercial double-resonance flat-coil NMR probeheads, decoupling of protons from ^{19}F requires a more specialised probe design and high-power filters capable of discriminating between the similar Larmor frequencies of ^{1}H and ^{19}F. Consequently, ^{1}H – ^{19}F and ^{1}H – ^{1}H dipolar interactions need to be factored into the analysis when proton decoupling is unavailable [253]. Elimination of ^{19}F background signal using the DEPTH method, for example, may also be necessary if the probehead coil platform is constructed from fluorinated polymeric material. This approach was used to confirm that FSB binds to the fibrils with the long molecular axis of the ligand tilted by approximately 40° with respect to the fibril axis (**Fig. 21e**).

5. Conclusion and outlook

NMR spectroscopy underpinned much of the early pioneering research into the structures and assembly mechanisms of amyloid fibrils and oligomers. Solid-state NMR, in particular, was for many years unrivalled in its ability to provide atomic-level models of amyloid fibril architecture, most notably for Aβ. Likewise, solution-state NMR has provided valuable insights into the nature of early protein assemblies preceding the deposition of insoluble fibrils. Virtually all the NMR-derived structural models of amyloid species in the PDB have been obtained from recombinant proteins isolated from the numerous ions, molecules and surfaces that influence fibril formation *in vivo*. It is also now clear that amyloid fibrils are polymorphic entities and adopt structures that are highly dependent upon the assembly conditions and environment. Indeed,

the structures of amyloid fibrils propagated from *ex vivo* fibrils are now being shown to be quite different from the structures of fibrils formed in isolation. From a structural perspective, the future of amyloid research requires a much more detailed understanding of the complex interactions between the various components of amyloid – proteins, metal ions, accessory molecules and membranes – that have long been known to accumulate in plaques *in vivo*. NMR is beginning to fulfil this new and unique role, as cryo-EM continues apace as the method of choice for fibril structure determination. It is envisaged that the two complementary techniques will increasingly work hand in hand to gain a holistic picture of amyloid structure and interactions in the future [254].

Declaration of competing interest

The author declares that he has no known competing financial interests or personal relationships that could have appeared to influence the work reported in this paper.

Data availability

No data was used for the research described in the article.

References

[1] T.P.J. Knowles, M. Vendruscolo, C.M. Dobson, The amyloid state and its association with protein misfolding diseases, Nature Reviews Molecular Cell Biology, 15 (6) (2014) pp 384-396, DOI: 10.1038/nrm3810.

[2] T. Ikenoue, Y.H. Lee, J. Kardos, H. Yagi, T. Ikegami, H. Naiki, Y. Goto, Heat of supersaturation-limited amyloid burst directly monitored by isothermal titration calorimetry, Proc. Natl. Acad. Sci. U. S. A., 111 (18) (2014) pp 6654-6659, DOI: 10.1073/pnas.1322602111.

[3] H.A. Davies, J. Madine, D.A. Middleton, Comparisons with Amyloid-β Reveal an Aspartate Residue That Stabilizes Fibrils of the Aortic Amyloid Peptide Medin, J. Biol. Chem., 290 (12) (2015) pp 7791-7803, DOI: 10.1074/jbc.M114.602177.

[4] J. Madine, E. Jack, P.G. Stockley, S.E. Radford, L.C. Serpell, D.A. Middleton, Structural Insights into the Polymorphism of Amyloid-Like Fibrils Formed by Region 20-29 of Amylin Revealed by Solid-State NMR and X-ray Fiber Diffraction, J. Am. Chem. Soc., 130 (45) (2008) pp 14990-15001, DOI: 10.1021/ja802483d.

[5] A.I.P. Taylor, R.A. Staniforth, General Principles Underpinning Amyloid Structure, Front. Neurosci., 16 (2022) pp, DOI: 10.3389/fnins.2022.878869.

[6] D.M. Fowler, A.V. Koulov, W.E. Balch, J.W. Kelly, Functional amyloid - from bacteria to humans, Trends in Biochemical Sciences, 32 (5) (2007) pp 217-224, DOI: 10.1016/j.tibs.2007.03.003.

[7] R. Nelson, M.R. Sawaya, M. Balbirnie, A.O. Madsen, C. Riekel, R. Grothe, D. Eisenberg, Structure of the cross-β spine of amyloid-like fibrils, Nature, 435 (7043) (2005) pp 773-778, DOI: 10.1038/nature03680.

[8] M.R. Sawaya, S. Sambashivan, R. Nelson, M.I. Ivanova, S.A. Sievers, M.I. Apostol, M.J. Thompson, M. Balbirnie, J.J.W. Wiltzius, H.T. McFarlane, A.O. Madsen, C. Riekel, D. Eisenberg, Atomic structures of amyloid cross-β spines reveal varied steric zippers, Nature, 447 (7143) (2007) pp 453-457, DOI: 10.1038/nature05695.

[9] R. Kayed, E. Head, J.L. Thompson, T.M. McIntire, S.C. Milton, C.W. Cotman, C.G. Glabe, Common structure of soluble amyloid oligomers implies common mechanism of pathogenesis, Science, 300 (5618) (2003) pp 486-489, DOI: 10.1126/science.1079469.

[10] J. Zurdo, J.I. Guijarro, J.L. Jimenez, H.R. Saibil, C.M. Dobson, Dependence on solution conditions of aggregation and amyloid formation by an SH3 domain, J. Mol. Biol., 311 (2) (2001) pp 325-340, DOI: 10.1006/jmbi.2001.4858.

[11] J.I. Guijarro, M. Sunde, J.A. Jones, I.D. Campbell, C.M. Dobson, Amyloid fibril formation by an SH3 domain, Proc. Natl. Acad. Sci. U. S. A., 95 (8) (1998) pp 4224-4228, DOI: 10.1073/pnas.95.8.4224.

[12] M.D. Mukrasch, S. Bibow, J. Korukottu, S. Jeganathan, J. Biernat, C. Griesinger, E. Mandelkow, M. Zweckstetter, Structural Polymorphism of 441-Residue Tau at

Single Residue Resolution, PLoS Biol., 7 (2) (2009) pp 399-414, DOI: 10.1371/journal.pbio.1000034.

[13] A.T. Petkova, Y. Ishii, J.J. Balbach, O.N. Antzutkin, R.D. Leapman, F. Delaglio, R. Tycko, A structural model for Alzheimer's β-amyloid fibrils based on experimental constraints from solid state NMR, Proc. Natl. Acad. Sci. U. S. A., 99 (26) (2002) pp 16742-16747, DOI: 10.1073/pnas.262663499.

[14] A.T. Petkova, W.M. Yau, R. Tycko, Experimental constraints on quaternary structure in Alzheimer's β-amyloid fibrils, Biochemistry, 45 (2) (2006) pp 498-512, DOI: 10.1021/bi051952q.

[15] V. Daebel, S. Chinnathambi, J. Biernat, M. Schwalbe, B. Habenstein, A. Loquet, E. Akoury, K. Tepper, H. Muller, M. Baldus, C. Griesinger, M. Zweckstetter, E. Mandelkow, V. Vijayan, A. Lange, β-Sheet Core of Tau Paired Helical Filaments Revealed by Solid-State NMR, J. Am. Chem. Soc., 134 (34) (2012) pp 13982-13989, DOI: 10.1021/ja305470p.

[16] C.P. Jaroniec, C.E. MacPhee, V.S. Bajaj, M.T. McMahon, C.M. Dobson, R.G. Griffin, High-resolution molecular structure of a peptide in an amyloid fibril determined by magic angle spinning NMR spectroscopy, Proc. Natl. Acad. Sci. U. S. A., 101 (3) (2004) pp 711-716, DOI: 10.1073/pnas.0304849101.

[17] C. Seuring, J. Verasdonck, J. Gath, D. Ghosh, N. Nespovitaya, M.A. Walti, S.K. Maji, R. Cadalbert, P. Guntert, B.H. Meier, R. Riek, The three-dimensional structure of human β-endorphin amyloid fibrils, Nat. Struct. Mol. Biol., 27 (12) (2020) pp 1178-1184, DOI: 10.1038/s41594-020-00515-z.

[18] A. Wickramasinghe, Y.L. Xiao, N. Kobayashi, S.L. Wang, K.P. Scherpelz, T. Yamazaki, S.C. Meredith, Y. Ishii, Sensitivity-Enhanced Solid-State NMR Detection of Structural Differences and Unique Polymorphs in Pico- to Nanomolar Amounts of Brain-Derived and Synthetic 42-Residue Amyloid-β Fibrils, J. Am. Chem. Soc., 143 (30) (2021) pp 11462-11472, DOI: 10.1021/jacs.1c03346.

[19] D.T. Murray, M. Kato, Y. Lin, K.R. Thurber, I. Hung, S.L. McKnight, R. Tycko, Structure of FUS Protein Fibrils and Its Relevance to Self-Assembly and Phase Separation of Low-Complexity Domains, Cell, 171 (3) (2017) pp 615-627, DOI: 10.1016/j.cell.2017.08.048.

[20] A.B. Siemer, C. Ritter, M. Ernst, R. Riek, B.H. Meier, High-resolution solid-state NMR spectroscopy of the prion protein HET-s in its amyloid conformation, Angew. Chem. Int. Ed., 44 (16) (2005) pp 2441-2444, DOI: 10.1002/anie.200462952.

[21] C.J. Maynard, A.I. Bush, C.L. Masters, R. Cappai, Q.X. Li, Metals and amyloid-β in Alzheimer's disease, Int. J. Exp. Pathol., 86 (3) (2005) pp 147-159, DOI: 10.1111/j.0959-9673.2005.00434.x.

[22] M.A. Lovell, J.D. Robertson, W.J. Teesdale, J.L. Campbell, W.R. Markesbery, Copper, iron and zinc in Alzheimer's disease senile plaques, J. Neurol. Sci., 158 (1) (1998) pp 47-52, DOI: 10.1016/s0022-510x(98)00092-6.

[23] B.E. Stopschinski, B.B. Holmes, G.M. Miller, V.A. Manon, J. Vaquer-Alicea, W.L. Prueitt, L.C. Hsieh-Wilson, M.I. Diamond, Specific glycosaminoglycan chain length and sulfation patterns are required for cell uptake of tau versus α-synuclein and β-amyloid aggregates, J. Biol. Chem., 293 (27) (2018) pp 10826-10840, DOI: 10.1074/jbc.RA117.000378.

[24] H. Wang, P. Cao, D.P. Raleigh, Amyloid Formation in Heterogeneous Environments: Islet Amyloid Polypeptide Glycosaminoglycan Interactions, J. Mol. Biol., 425 (3) (2013) pp 492-505, DOI: 10.1016/j.jmb.2012.11.003.

[25] J. Di Domizio, S. Dorta-Estremera, M. Gagea, D. Ganguly, S. Meller, P. Li, B.H. Zhao, F.K. Tan, L.Q. Bi, M. Gilliet, W. Cao, Nucleic acid-containing amyloid fibrils potently induce type I interferon and stimulate systemic autoimmunity, Proc. Natl. Acad. Sci. U. S. A., 109 (36) (2012) pp 14550-14555, DOI: 10.1073/pnas.1206923109.

[26] Y. Fichou, Y.X. Lin, J.N. Rauch, M. Vigers, Z.K. Zeng, M. Srivastava, T.J. Keller, J.H. Freed, K.S. Kosik, S.I. Han, Cofactors are essential constituents of stable and seeding-active tau fibrils, Proc. Natl. Acad. Sci. U. S. A., 115 (52) (2018) pp 13234-13239, DOI: 10.1073/pnas.1810058115.

[27] T. Kampers, P. Friedhoff, J. Biernat, E.M. Mandelkow, RNA stimulates aggregation of microtubule-associated protein tau into Alzheimer-like paired helical filaments, FEBS Lett., 399 (3) (1996) pp 344-349, DOI: 10.1016/s0014-5793(96)01386-5.

[28] S.D. Ginsberg, P.B. Crino, V.M.Y. Lee, J.H. Eberwine, J.Q. Trojanowski, Sequestration of RNA in Alzheimer's disease neurofibrillary tangles and senile plaques, Ann. Neurol., 41 (2) (1997) pp 200-209, DOI: 10.1002/ana.410410211.

[29] J. Kiskis, H. Fink, L. Nyberg, J. Thyr, J.Y. Li, A. Enejder, Plaque-associated lipids in Alzheimer's diseased brain tissue visualized by nonlinear microscopy, Sci. Rep., 5 (2015) pp, DOI: 10.1038/srep13489.

[30] K.L. Stewart, S.E. Radford, Amyloid plaques beyond Aβ: a survey of the diverse modulators of amyloid aggregation, Biophys. Rev., 9 (2017) pp 405-419.

[31] J. Gsponer, M. Vendruscolo, Theoretical approaches to protein aggregation, Protein and Peptide Letters, 13 (3) (2006) pp 287-293, DOI: 10.2174/092986606775338407.

[32] W. Hwang, S.G. Zhang, R.D. Kamm, M. Karplus, Kinetic control of dimer structure formation in amyloid fibrillogenesis, Proc. Natl. Acad. Sci. U. S. A., 101 (35) (2004) pp 12916-12921, DOI: 10.1073/pnas.0402634101.

[33] Q. Ma, J.Y. Hu, J. Chen, Y. Liang, The Role of Crowded Physiological Environments in Prion and Prion-like Protein Aggregation, Int. J. Mol. Sci., 14 (11) (2013) pp 21339-21352, DOI: 10.3390/ijms141121339.

[34] Q.C. Zheng, M.T. Kebede, M.M. Kemeh, S. Islam, B. Lee, S.D. Bleck, L.A. Wurfl, N.D. Lazo, Inhibition of the Self-Assembly of Aβ and of Tau by Polyphenols: Mechanistic Studies, Molecules, 24 (12) (2019) pp, DOI: 10.3390/ijms22041859.

[35] V.N. Uversky, Unusual biophysics of intrinsically disordered proteins, Biochimica Et Biophysica Acta-Proteins and Proteomics, 1834 (5) (2013) pp 932-951, DOI: 10.1016/j.bbapap.2012.12.008.

[36] D. Eliezer, E. Kutluay, R. Bussell, G. Browne, Conformational properties of α-synuclein in its free and lipid-associated states, J. Mol. Biol., 307 (4) (2001) pp 1061-1073, DOI: 10.1006/jmbi.2001.4538.

[37] J.A. Williamson, A.D. Miranker, Direct detection of transient α-helical states in islet amyloid polypeptide, Protein Sci., 16 (1) (2007) pp 110-117, DOI: 10.1110/ps.062486907.

[38] B. Winner, R. Jappelli, S.K. Maji, P.A. Desplats, L. Boyer, S. Aigner, C. Hetzer, T. Loher, M. Vilar, S. Campioni, C. Tzitzilonis, A. Soragni, S. Jessberger, H. Mira, A. Consiglio, E. Pham, E. Masliah, F.H. Gage, R. Riek, In vivo demonstration that α-synuclein oligomers are toxic, Proc. Natl. Acad. Sci. U. S. A., 108 (10) (2011) pp 4194-4199, DOI: 10.1073/pnas.1100976108.

[39] G. Fusco, S.W. Chen, P.T.F. Williamson, R. Cascella, M. Perni, J.A. Jarvis, C. Cecchi, M. Vendruscolo, F. Chiti, N. Cremades, L.M. Ying, C.M. Dobson, A. De Simone, Structural basis of membrane disruption and cellular toxicity by α-synuclein oligomers, Science, 358 (6369) (2017) pp 1440-1443, DOI: 10.1126/science.aan6160.

[40] L.P. Yu, R. Edalji, J.E. Harlan, T.F. Holzman, A.P. Lopez, B. Labkovsky, H. Hillen, S. Barghorn, U. Ebert, P.L. Richardson, L. Miesbauer, L. Solomon, D. Bartley, K. Walter, R.W. Johnson, P.J. Hajduk, E.T. Olejniczak, Structural Characterization of a Soluble Amyloid β-Peptide Oligomer, Biochemistry, 48 (9) (2009) pp 1870-1877, DOI: 10.1021/bi802046n.

[41] N.L. Fawzi, J.F. Ying, D.A. Torchia, G.M. Clore, Kinetics of Amyloid-β Monomer-to-Oligomer Exchange by NMR Relaxation, J. Am. Chem. Soc., 132 (29) (2010) pp 9948-9951, DOI: 10.1021/ja1048253.

[42] D.M. Walsh, A. Lomakin, G.B. Benedek, M.M. Condron, D.B. Teplow, Amyloid β-protein fibrillogenesis - Detection of a protofibrillar intermediate, J. Biol. Chem., 272 (35) (1997) pp 22364-22372, DOI: 10.1074/jbc.272.35.22364.

[43] C. Lendel, M. Bjerring, A. Dubnovitsky, R.T. Kelly, A. Filippov, O.N. Antzutkin, N.C. Nielsen, T. Härd, A Hexameric Peptide Barrel as Building Block of Amyloid-β Protofibrils, Angew. Chem. Int. Ed., 53 (47) (2014) pp 12756-12760, DOI: 10.1002/anie.201406357.

[44] N.L. Fawzi, J.F. Ying, R. Ghirlando, D.A. Torchia, G.M. Clore, Atomic-resolution dynamics on the surface of amyloid-β protofibrils probed by solution NMR, Nature, 480 (7376) (2011) pp 268-272, DOI: 10.1038/nature10577.

[45] A. Dubnovitsky, A. Sandberg, M.M. Rahman, I. Benilova, C. Lendel, T. Härd, Amyloid-β Protofibrils: Size, Morphology and Synaptotoxicity of an Engineered Mimic, PLoS One, 8 (7) (2013) pp, DOI: 10.1371/journal.pone.0066101.

[46] K. Iwata, T. Fujiwara, Y. Matsuki, H. Akutsu, S. Takahashi, H. Naiki, Y. Goto, 3D structure of amyloid protofilaments of β_2-microglobulin fragment probed by solid-state NMR, Proc. Natl. Acad. Sci. U. S. A., 103 (48) (2006) pp 18119-18124, DOI: 10.1073/pnas.0607180103.

[47] N. Ferguson, J. Becker, H. Tidow, S. Tremmel, T.D. Sharpe, G. Krause, J. Flinders, M. Petrovich, J. Berriman, H. Oschkinat, A.R. Fersht, General structural motifs of amyloid protofilaments, Proc. Natl. Acad. Sci. U. S. A., 103 (44) (2006) pp 16248-16253, DOI: 10.1073/pnas.0607815103.

[48] T. Lührs, C. Ritter, M. Adrian, D. Riek-Loher, B. Bohrmann, H. Döeli, D. Schubert, R. Riek, 3D structure of Alzheimer's amyloid-β(1-42) fibrils, Proc. Natl. Acad. Sci. U. S. A., 102 (48) (2005) pp 17342-17347, DOI: 10.1073/pnas.0506723102.

[49] C. Wasmer, A. Lange, H. Van Melckebeke, A.B. Siemer, R. Riek, B.H. Meier, Amyloid fibrils of the HET-s(218-289) prion form a β solenoid with a triangular hydrophobic core, Science, 319 (5869) (2008) pp 1523-1526, DOI: 10.1126/science.1151839.

[50] M.D. Tuttle, G. Comellas, A.J. Nieuwkoop, D.J. Covell, D.A. Berthold, K.D. Kloepper, J.M. Courtney, J.K. Kim, A.M. Barclay, A. Kendall, W. Wan, G. Stubbs, C.D. Schwieters, V.M.Y. Lee, J.M. George, C.M. Rienstra, Solid-state NMR structure of a pathogenic fibril of full-length human α-synuclein, Nat. Struct. Mol. Biol., 23 (5) (2016) pp 409-415, DOI: 10.1038/nsmb.3194.

[51] S.S. Oakley, M.B. Maina, K.E. Marshall, Y.K. Al-Hilaly, C.R. Harrington, C.M. Wischik, L.C. Serpell, Tau Filament Self-Assembly and Structure: Tau as a Therapeutic Target, Front. Neurol., 11 (2020) pp, DOI: 10.3389/fneur.2020.590754.

[52] Y.K. Al-Hilaly, C. Hurt, J.E. Rickard, C.R. Harrington, J.M.D. Storey, C.M. Wischik, L.C. Serpell, A.B. Siemer, Solid-state NMR of paired helical filaments formed by the core tau fragment tau(297-391), Front. Neurosci., 16 (2022) pp, DOI: 10.3389/fnins.2022.988074.

[53] P. Friedhoff, A. Schneider, E.M. Mandelkow, E. Mandelkow, Rapid assembly of Alzheimer-like paired helical filaments from microtubule-associated protein tau monitored by fluorescence in solution, Biochemistry, 37 (28) (1998) pp 10223-10230, DOI: 10.1021/bi980537d.

[54] T. Miura, K. Suzuki, N. Kohata, H. Takeuchi, Metal binding modes of Alzheimer's amyloid β-peptide in insoluble aggregates and soluble complexes, Biochemistry, 39 (23) (2000) pp 7024-7031, DOI: 10.1021/bi0002479.

[55] L.Y. Lian, D.A. Middleton, Labelling approaches for protein structural studies by solution-state and solid-state NMR, Prog. Nucl. Magn. Reson. Spectrosc., 39 (3) (2001) pp 171-190, DOI: 10.1016/s0079-6565(01)00034-6.

[56] L.G. Jia, W.P. Zhao, W. Wei, X. Guo, W.J. Wang, Y. Wang, J.C. Sang, F.P. Lu, F.F. Liu, Expression and purification of amyloid β-protein, tau, and α-synuclein in Escherichia coli: a review, Crit. Rev. Biotechnol., 40 (4) (2020) pp 475-489, DOI: 10.1080/07388551.2020.1742646.

[57] V.A. Higman, Solid-state MAS NMR resonance assignment methods for proteins, Prog. Nucl. Magn. Reson. Spectrosc., 106 (2018) pp 37-65, DOI: 10.1016/j.pnmrs.2018.04.002.

[58] F. Castellani, B. van Rossum, A. Diehl, M. Schubert, K. Rehbein, H. Oschkinat, Structure of a protein determined by solid-state magic-angle-spinning NMR spectroscopy, Nature, 420 (6911) (2002) pp 98-102, DOI: 10.1038/nature01070.

[59] N.S. de Groot, R. Sabate, S. Ventura, Amyloids in bacterial inclusion bodies, Trends in Biochemical Sciences, 34 (8) (2009) pp 408-416, DOI: 10.1016/j.tibs.2009.03.009.

[60] S.M. Singh, A.K. Panda, Solubilization and refolding of bacterial inclusion body proteins, Journal of Bioscience and Bioengineering, 99 (4) (2005) pp 303-310, DOI: 10.1263/jbb.99.303.

[61] S.C. Jao, K. Ma, J. Talafous, R. Orlando, M.G. Zagorski, Trifluoroacetic acid pretreatment reproducibly disaggregates the amyloid β-peptide, Amyloid-Journal of Protein Folding Disorders, 4 (4) (1997) pp 240-252, DOI: 10.3109/13506129709003835.

[62] M.R. Nichols, M.A. Moss, D.K. Reed, S. Cratic-McDaniei, J.H. Hoh, T.L. Rosenberry, Amyloid-β protofibrils differ from Amyloid-β aggregates induced in dilute hexafluoroisopropanol in stability and morphology, J. Biol. Chem., 280 (4) (2005) pp 2471-2480, DOI: 10.1074/jbc.M410553200.

[63] A.J. Dear, T.C.T. Michaels, G. Meisl, D. Klenerman, S. Wu, S. Perrett, S. Linse, C.M. Dobson, T.P.J. Knowles, Kinetic diversity of amyloid oligomers, Proc. Natl. Acad. Sci. U. S. A., 117 (22) (2020) pp 12087-12094, DOI: 10.1073/pnas.1922267117.

[64] Y.L. Xiao, I. Matsuda, M. Inoue, T. Sasahara, M. Hoshi, Y. Ishii, NMR-based site-resolved profiling of β-amyloid misfolding reveals structural transitions from pathologically relevant spherical oligomer to fibril, J. Biol. Chem., 295 (2) (2020) pp 458-467, DOI: 10.1074/jbc.RA119.008522.

[65] S. Morin, A practical guide to protein dynamics from ^{15}N spin relaxation in solution, Prog. Nucl. Magn. Reson. Spectrosc., 59 (3) (2011) pp 245-262, DOI: 10.1016/j.pnmrs.2010.12.003.

[66] G. Lipari, A. Szabo, Model-Free Approach to the Interpretation of Nuclear Magnetic Resonance Relaxation in Macromolecules. 1. Theory and Range of Validity., J. Am. Chem. Soc., 104 (17) (1982) pp 4546-4559, DOI: 10.1021/ja00381a009.

[67] M.M. Tirado, C.L. Martinez, J.G. Delatorre, Comparison of Theories for the Translational and Rotational Diffusion Coefficients of Rod-Like Macromolecules - Application to Short DNA Fragments, J. Chem. Phys., 81 (4) (1984) pp 2047-2052, DOI: 10.1063/1.447827.

[68] N. Tjandra, S.E. Feller, R.W. Pastor, A. Bax, Rotational diffusion anisotropy of human ubiquitin from ^{15}N NMR relaxation, J. Am. Chem. Soc., 117 (50) (1995) pp 12562-12566, DOI: 10.1021/ja00155a020.

[69] P. Schanda, B. Brutscher, Very fast two-dimensional NMR spectroscopy for real-time investigation of dynamic events in proteins on the time scale of seconds, J. Am. Chem. Soc., 127 (22) (2005) pp 8014-8015, DOI: 10.1021/ja051306e.

[70] M. Kaur, C.M. Lewis, A. Chronister, G.S. Phun, L.J. Mueller, Non-Uniform Sampling in NMR Spectroscopy and the Preservation of Spectral Knowledge in the Time and Frequency Domains, J. Phys. Chem. A, 124 (26) (2020) pp 5474-5486, DOI: 10.1021/acs.jpca.0c02930.

[71] T.K. Karamanos, M.P. Jackson, A.N. Calabrese, S.C. Goodchild, E.E. Cawood, G.S.T. Section, A.P. Kalverda, E.W. Hewitt, S.E. Radford, Structural mapping of oligomeric intermediates in an amyloid assembly pathway, Elife, 8 (2019) pp, DOI: 10.7554/eLife.46574.

[72] A.J. Baldwin, S.J. Anthony-Cahill, T.P.J. Knowles, G. Lippens, J. Christodoulou, P.D. Barker, C.M. Dobson, Measurement of amyloid fibril length distributions by inclusion of rotational motion in solution NMR diffusion measurements, Angew. Chem. Int. Ed., 47 (18) (2008) pp 3385-3387, DOI: 10.1002/anie.200703915.

[73] Y. Yoshimura, K. Sakurai, Y.H. Lee, T. Ikegami, E. Chatani, H. Naiki, Y. Goto, Direct observation of minimum-sized amyloid fibrils using solution NMR spectroscopy, Protein Sci., 19 (12) (2010) pp 2347-2355, DOI: 10.1002/pro.515.

[74] T. Yamaguchi, K. Matsuzaki, M. Hoshino, Transient formation of intermediate conformational states of amyloid-β peptide revealed by heteronuclear magnetic resonance spectroscopy, FEBS Lett., 585 (7) (2011) pp 1097-1102, DOI: 10.1016/j.febslet.2011.03.014.

[75] K.S. Jensen, S. Linse, M. Nilsson, M. Akke, A. Malmendal, Revealing Well-Defined Soluble States during Amyloid Fibril Formation by Multilinear Analysis of NMR Diffusion Data, J. Am. Chem. Soc., 141 (47) (2019) pp 18649-18652, DOI: 10.1021/jacs.9b07952.

[76] B.B. Kharkov, I.S. Podkorytov, S.A. Bondarev, M.V. Belousov, V.A. Salikov, G.A. Zhouravleva, N.R. Skrynnikov, The Role of Rotational Motion in Diffusion NMR Experiments on Supramolecular Assemblies: Application to Sup35NM Fibrils, Angew. Chem. Int. Ed., 60 (28) (2021) pp 15445-15451, DOI: 10.1002/anie.202102408.

[77] Y. Suzuki, J.R. Brender, M.T. Soper, J. Krishnamoorthy, Y.L. Zhou, B.T. Ruotolo, N.A. Kotov, A. Ramamoorthy, E.N.G. Marsh, Resolution of Oligomeric Species during the Aggregation of Aβ(1-40) Using ^{19}F NMR, Biochemistry, 52 (11) (2013) pp 1903-1912, DOI: 10.1021/bi400027y.

[78] X. Sun, J.A. Ferguson, H.J. Dyson, P.E. Wright, A transthyretin monomer intermediate undergoes local unfolding and transient interaction with oligomers in a kinetically concerted aggregation pathway, J. Biol. Chem., 298 (8) (2022) pp, DOI: 10.1016/j.jbc.2022.102162.

[79] A.T. Alexandrescu, Amyloid accomplices and enforcers, Protein Sci., 14 (1) (2005) pp 1-12.

[80] J. Adamcik, R. Mezzenga, Amyloid Polymorphism in the Protein Folding and Aggregation Energy Landscape, Angew. Chem. Int. Ed., 57 (28) (2018) pp 8370-8382, DOI: 10.1002/anie.201713416.

[81] W. Close, M. Neumann, A. Schmidt, M. Hora, K. Annamalai, M. Schmidt, B. Reif, V. Schmidt, N. Grigorieff, M. Fandrich, Physical basis of amyloid fibril polymorphism, Nature Communications, 9 (2018) pp, DOI: 10.1038/s41467-018-03164-5.

[82] A.T. Petkova, R.D. Leapman, Z.H. Guo, W.M. Yau, M.P. Mattson, R. Tycko, Self-propagating, molecular-level polymorphism in Alzheimer's β-amyloid fibrils, Science, 307 (5707) (2005) pp 262-265, DOI: 10.1126/science.1105850.

[83] W. Qiang, W.M. Yau, R. Tycko, Structural Evolution of Iowa Mutant β-Amyloid Fibrils from Polymorphic to Homogeneous States under Repeated Seeded Growth, J. Am. Chem. Soc., 133 (11) (2011) pp 4018-4029, DOI: 10.1021/ja109679q.

[84] U. Ghosh, K.R. Thurber, W.M. Yau, R. Tycko, Molecular structure of a prevalent amyloid-β fibril polymorph from Alzheimer's disease brain tissue, Proc. Natl. Acad. Sci. U. S. A., 118 (4) (2021) pp, DOI: 10.1073/pnas.2023089118.

[85] U. Ghosh, W.M. Yau, J. Collinge, R. Tycko, Structural differences in amyloid-β fibrils from brains of nondemented elderly individuals and Alzheimer's disease patients, Proc. Natl. Acad. Sci. U. S. A., 118 (45) (2021) pp, DOI: 10.1073/pnas.2111863118.

[86] A.K. Paravastu, I. Qahwash, R.D. Leapman, S.C. Meredith, R. Tycko, Seeded growth of β-amyloid fibrils from Alzheimer's brain-derived fibrils produces a distinct fibril structure, Proc. Natl. Acad. Sci. U.S.A., 106 (18) (2009) pp 7443-7448, DOI: 10.1073/pnas.0812033106.

[87] Y. Li, D.A. Berthold, H.L. Frericks, R.B. Gennis, C.M. Rienstra, Partial ^{13}C and ^{15}N chemical-shift assignments of the disulfide-bond-forming enzyme DsbB by 3D magic-angle spinning NMR spectroscopy, ChemBioChem, 8 (4) (2007) pp 434-442, DOI: 10.1002/cbic.200600484.

[88] J. Pauli, M. Baldus, B. van Rossum, H. de Groot, H. Oschkinat, Backbone and side-chain ^{13}C and ^{15}N signal assignments of the α-spectrin SH3 domain by magic angle spinning solid-state NMR at 17.6 tesla, Chembiochem, 2 (4) (2001) pp 272-281, DOI: 10.1002/1439-7633(20010401)2:4<272::Aid-cbic272>3.0.Co;2-2.

[89] M. Baldus, A.T. Petkova, J. Herzfeld, R.G. Griffin, Cross polarization in the tilted frame: assignment and spectral simplification in heteronuclear spin systems, Mol. Phys., 95 (6) (1998) pp 1197-1207, DOI: 10.1080/002689798166215.

[90] J.R. Lewandowski, G. De Paepe, R.G. Griffin, Proton assisted insensitive nuclei cross polarization, J. Am. Chem. Soc., 129 (4) (2007) pp 728-729, DOI: 10.1021/ja0650394.

[91] Y. Nishiyama, G.J. Hou, V. Agarwal, Y.C. Su, A. Ramamoorthy, Ultrafast Magic Angle Spinning Solid-State NMR Spectroscopy: Advances in Methodology and

Applications, Chem. Rev., 123 (3) (2022) pp 918-988, DOI: 10.1021/acs.chemrev.2c00197.

[92] J. Stanek, L.B. Andreas, K. Jaudzems, D. Cala, D. Lalli, A. Bertarello, T. Schubeis, I. Akopjana, S. Kotelovica, K. Tars, A. Pica, S. Leone, D. Picone, Z.Q. Xu, N.E. Dixon, D. Martinez, M. Berbon, N. El Mammeri, A. Noubhani, S. Saupe, B. Habenstein, A. Loquet, G. Pintacuda, NMR Spectroscopic Assignment of Backbone and Side-Chain Protons in Fully Protonated Proteins: Microcrystals, Sedimented Assemblies, and Amyloid Fibrils, Angew. Chem. Int. Ed., 55 (50) (2016) pp 15503-15509, DOI: 10.1002/anie.201607084.

[93] D.H. Zhou, G. Shah, M. Cormos, C. Mullen, D. Sandoz, C.M. Rienstra, Proton-detected solid-state NMR Spectroscopy of fully protonated proteins at 40 kHz magic-angle spinning, J. Am. Chem. Soc., 129 (38) (2007) pp 11791-11801, DOI: 10.1021/ja073462m.

[94] L.B. Andreas, T. Le Marchand, K. Jaudzems, G. Pintacuda, High-resolution proton-detected NMR of proteins at very fast MAS, J. Magn. Reson., 253 (2015) pp 36-49, DOI: 10.1016/j.jmr.2015.01.003.

[95] E. Barbet-Massin, A.J. Pell, J.S. Retel, L.B. Andreas, K. Jaudzems, W.T. Franks, A.J. Nieuwkoop, M. Hiller, V. Higman, P. Guerry, A. Bertarello, M.J. Knight, M. Felletti, T. Le Marchand, S. Kotelovica, I. Akopjana, K. Tars, M. Stoppini, V. Bellotti, M. Bolognesi, S. Ricagno, J.J. Chou, R.G. Griffin, H. Oschkinat, A. Lesage, L. Emsley, T. Herrmann, G. Pintacuda, Rapid Proton-Detected NMR Assignment for Proteins with Fast Magic Angle Spinning, J. Am. Chem. Soc., 136 (35) (2014) pp 12489-12497, DOI: 10.1021/ja507382j.

[96] Y. Shen, F. Delaglio, G. Cornilescu, A. Bax, TALOS plus : a hybrid method for predicting protein backbone torsion angles from NMR chemical shifts, J. Biomol. NMR, 44 (4) (2009) pp 213-223, DOI: 10.1007/s10858-009-9333-z.

[97] S.G. Zech, A.J. Wand, A.E. McDermott, Protein structure determination by high-resolution solid-state NMR spectroscopy: Application to microcrystalline ubiquitin, J. Am. Chem. Soc., 127 (24) (2005) pp 8618-8626, DOI: 10.1021/ja0503128.

[98] J. Jeon, W.M. Yau, R. Tycko, Early events in amyloid-β self-assembly probed by time-resolved solid state NMR and light scattering, Nature Communications, 14 (1) (2023) pp, DOI: 10.1038/s41467-023-38494-6.

[99] K. Thurber, R. Tycko, Low-temperature dynamic nuclear polarization with helium-cooled samples and nitrogen-driven magic-angle spinning, J. Magn. Reson., 264 (2016) pp 99-106, DOI: 10.1016/j.jmr.2016.01.011.

[100] V.H. Pomin, X. Wang, Glycosaminoglycan-Protein Interactions by Nuclear Magnetic Resonance (NMR) Spectroscopy, Molecules, 23 (9) (2018) pp, DOI: 10.3390/molecules23092314.

[101] J.A. Cohlberg, J. Li, V.N. Uversky, A.L. Fink, Heparin and other glycosaminoglycans stimulate the formation of amyloid fibrils from α-synuclein in vitro, Biochemistry, 41 (5) (2002) pp 1502-1511, DOI: 10.1021/bi011711s|ISSN 0006-2960.

[102] J. Diaz-Nido, F. Wandosell, J. Avila, Glycosaminoglycans and β-amyloid, prion and tau peptides in neurodegenerative diseases, Peptides, 23 (7) (2002) pp 1323-1332.

[103] B. Klajnert, M. Cortijo-Arellano, M. Bryszewska, J. Cladera, Influence of heparin and dendrimers on the aggregation of two amyloid peptides related to Alzheimer's and prion diseases, Biochemical and Biophysical Research Communications, 339 (2) (2006) pp 577-582, DOI: 10.1016/j.bbrc.2005.11.053|ISSN 0006-291X.

[104] R. Kisilevsky, W.A. Szarek, Novel glycosaminoglycan precursors as anti-amyloid agents part II, J. Mol. Neurosci., 19 (1-2) (2002) pp 45-50, DOI: 10.1007/s12031-002-0009-3.

[105] D. Townsend, N.J. Fullwood, E.A. Yates, D.A. Middleton, Aggregation Kinetics and Filament Structure of a Tau Fragment Are Influenced by the Sulfation Pattern of the Cofactor Heparin, Biochemistry, 59 (41) (2020) pp 4003-4014, DOI: 10.1021/acs.biochem.0c00443.

[106] D. Townsend, E. Hughes, R. Hussain, G. Siligardi, S. Baldock, J. Madine, D.A. Middleton, Heparin and Methionine Oxidation Promote the Formation of Apolipoprotein A-I Amyloid Comprising α-Helical and β-Sheet Structures, Biochemistry, 56 (11) (2017) pp 1632-1644, DOI: 10.1021/acs.biochem.6b01120.

[107] S. Jha, S.M. Patil, J. Gibson, C.E. Nelson, N.N. Alder, A.T. Alexandrescu, Mechanism of Amylin Fibrillization Enhancement by Heparin, Journal of Biological Chemistry, 286 (26) (2011) pp 22894-22904, DOI: 10.1074/jbc.M110.215814.

[108] X. Zhou, Y.Y. Wang, W. Zheng, G.X. Deng, F.Y. Wang, L. Jin, Characterizing Heparin Tetrasaccharides Binding to Amyloid-β Peptide, Frontiers in Molecular Biosciences, 9 (2022) pp, DOI: 10.3389/fmolb.2022.824146.

[109] K. Nguyen, D.L. Rabenstein, Interaction of the Heparin-Binding Consensus Sequence of β-Amyloid Peptides with Heparin and Heparin-Derived Oligosaccharides, Journal of Physical Chemistry B, 120 (9) (2016) pp 2187-2197, DOI: 10.1021/acs.jpcb.5b12235.

[110] M.D. Mukrasch, J. Biernat, M. von Bergen, C. Griesinger, E. Mandelkow, M. Zweckstetter, Sites of tau important for aggregation populate β-structure and bind to microtubules and polyanions, Journal of Biological Chemistry, 280 (26) (2005) pp 24978-24986, DOI: 10.1074/jbc.M501565200.

[111] N. Sibille, A. Sillen, A. Leroy, J.M. Wieruszeski, B. Mulloy, I. Landrieu, G. Lippens, Structural impact of heparin binding to full-length Tau as studied by NMR spectroscopy, Biochemistry, 45 (41) (2006) pp 12560-12572, DOI: 10.1021/bi060964o.

[112] T.R. Rudd, M.A. Skidmore, S.E. Guimond, C. Cosentino, G. Torri, D.G. Fernig, R.M. Lauder, M. Guerrini, E.A. Yates, Glycosaminoglycan origin and structure revealed by multivariate analysis of NMR and CD spectra, Glycobiology, 19 (1) (2009) pp 52-67, DOI: 10.1093/glycob/cwn103.

[113] G.M. Castillo, W. Lukito, T.N. Wight, A.D. Snow, The sulfate moieties of glycosaminoglycans are critical for the enhancement of β-amyloid protein fibril formation, Journal of Neurochemistry, 72 (4) (1999) pp 1681-1687.

[114] J. Madine, M.J. Pandya, M.R. Hicks, A. Rodger, E.A. Yates, S.E. Radford, D.A. Middleton, Site-Specific Identification of an Aβ Fibril-Heparin Interaction Site by Using Solid-State NMR Spectroscopy, Angewandte Chemie-International Edition, 51 (52) (2012) pp 13140-13143, DOI: 10.1002/anie.201204459.

[115] K.L. Stewart, E. Hughes, E.A. Yates, G.R. Akien, T.Y. Huang, M.A. Lima, T.R. Rudd, M. Guerrini, S.C. Hung, S.E. Radford, D.A. Middleton, Atomic Details of the Interactions of Glycosaminoglycans with Amyloid-β Fibrils, Journal of the American Chemical Society, 138 (27) (2016) pp 8328-8331, DOI: 10.1021/jacs.6b02816.

[116] K.L. Stewart, E. Hughes, E.A. Yates, D.A. Middleton, S.E. Radford, Molecular Origins of the Compatibility between Glycosaminoglycans and Aβ40 Amyloid Fibrils, J. Mol. Biol., 429 (16) (2017) pp 2449-2462, DOI: 10.1016/j.jmb.2017.07.003.

[117] J. Madine, J.C. Clayton, E.A. Yates, D.A. Middleton, Exploiting a ^{13}C-labelled heparin analogue for in situ solid-state NMR investigations of peptide-glycan interactions within amyloid fibrils, Organic & Biomolecular Chemistry, 7 (11) (2009) pp 2414-2420, DOI: 10.1039/b820808e.

[118] A.K. Paravastu, R.D. Leapman, W.M. Yau, R. Tycko, Molecular structural basis for polymorphism in Alzheimer's β-amyloid fibrils, Proceedings of the National Academy of Sciences of the United States of America, 105 (47) (2008) pp 18349-18354, DOI: 10.1073/pnas.0806270105.

[119] K.G. Malmos, M. Bjerring, C.M. Jessen, E.H.T. Nielsen, E.T. Poulsen, G. Christiansen, T. Vosegaard, T. Skrydstrup, J.J. Enghild, J.S. Pedersen, D.E. Otzen, How Glycosaminoglycans Promote Fibrillation of Salmon Calcitonin, Journal of Biological Chemistry, 291 (32) (2016) pp 16849-16862, DOI: 10.1074/jbc.M116.715466.

[120] N. Nespovitaya, J. Gath, K. Barylyuk, C. Seuring, B.H. Meier, R. Riek, Dynamic Assembly and Disassembly of Functional beta-Endorphin Amyloid Fibrils, J. Am. Chem. Soc., 138 (3) (2016) pp 846-856, DOI: 10.1021/jacs.5b08694.

[121] M.W. Risor, D.W. Juhl, M. Bjerring, J. Mathiesen, J.J. Enghild, N.C. Nielsen, D.E. Otzen, Critical Influence of Cosolutes and Surfaces on the Assembly of Serpin-Derived Amyloid Fibrils, Biophysical Journal, 113 (3) (2017) pp 580-596, DOI: 10.1016/j.bpj.2017.06.030.

[122] T. Wiegand, A.A. Malar, R. Cadalbert, M. Ernst, A. Bockmann, B.H. Meier, Asparagine and Glutamine Side-Chains and Ladders in HET-s(218-289) Amyloid Fibrils Studied by Fast Magic-Angle Spinning NMR, Frontiers in Molecular Biosciences, 7 (2020) pp, DOI: 10.3389/fmolb.2020.582033.

[123] M. Schledorn, A.A. Malar, A. Torosyan, S. Penzel, D. Klose, A. Oss, M.L. Org, S.S. Wang, L. Lecoq, R. Cadalbert, A. Samoson, A. Bockmann, B.H. Meier, Protein NMR Spectroscopy at 150 kHz Magic-Angle Spinning Continues To Improve

Resolution and Mass Sensitivity, ChemBioChem, 21 (17) (2020) pp 2540-2548, DOI: 10.1002/cbic.202000341.

[124] Z.Q. Zhang, S.A. McCallum, J. Xie, L. Nieto, F. Corzana, J. Jimenez-Barbero, M. Chen, J. Liu, R.J. Linhardtt, Solution structures of chemoenzymatically synthesized heparin and its precursors, Journal of the American Chemical Society, 130 (39) (2008) pp 12998-13007, DOI: 10.1021/ja8026345.

[125] M. Serra-Batiste, M. Ninot-Pedrosa, M. Bayoumi, M. Gairi, G. Maglia, N. Carulla, Aβ42 assembles into specific β-barrel pore-forming oligomers in membrane-mimicking environments, Proc. Natl. Acad. Sci. U. S. A., 113 (39) (2016) pp 10866-10871, DOI: 10.1073/pnas.1605104113.

[126] K.J. Korshavn, A. Bhunia, M.H. Lim, A. Ramamoorthy, Amyloid-beta adopts a conserved, partially folded structure upon binding to zwitterionic lipid bilayers prior to amyloid formation, Chem. Commun., 52 (5) (2016) pp 882-885, DOI: 10.1039/c5cc08634e.

[127] G.P. Gorbenko, P.K.J. Kinnunen, The role of lipid-protein interactions in amyloid-type protein fibril formation, Chemistry and Physics of Lipids, 141 (1-2) (2006) pp 72-82, DOI: 10.1016/j.chemphyslip.2006.02.006.

[128] S.A. Kotler, P. Walsh, J.R. Brender, A. Ramamoorthy, Differences between amyloid-beta aggregation in solution and on the membrane: insights into elucidation of the mechanistic details of Alzheimer's disease, Chem. Soc. Rev., 43 (19) (2014) pp 6692-6700, DOI: 10.1039/c3cs60431d.

[129] B. Falcon, J. Zivanov, W.J. Zhang, A.G. Murzin, H.J. Garringer, R. Vidal, R.A. Crowther, K.L. Newell, B. Ghetti, M. Goedert, S.H.W. Scheres, Novel tau filament fold in chronic traumatic encephalopathy encloses hydrophobic molecules, Nature, 568 (7752) (2019) pp 420-423, DOI: 10.1038/s41586-019-1026-5.

[130] A. Kakio, S. Nishimoto, K. Yanagisawa, Y. Kozutsumi, K. Matsuzaki, Cholesterol-dependent formation of GM1 ganglioside-bound amyloid β-protein, an endogenous seed for Alzheimer amyloid, J. Biol. Chem., 276 (27) (2001) pp 24985-24990, DOI: 10.1074/jbc.M100252200.

[131] Q. Cheng, Z.W. Hu, K.E. Doherty, Y.J. Tobin-Miyaji, W. Qiang, The on-fibrillation-pathway membrane content leakage and off-fibrillation pathway lipid mixing induced by 40-residue β-amyloid peptides in biologically relevant model liposomes, Biochimica Et Biophysica Acta-Biomembranes, 1860 (9) (2018) pp 1670-1680, DOI: 10.1016/j.bbamem.2018.03.008.

[132] M.F.M. Sciacca, C. Tempra, F. Scollo, D. Milardi, C. La Rosa, Amyloid growth and membrane damage: Current themes and emerging perspectives from theory and experiments on Aβ and hIAPP, Biochimica Et Biophysica Acta-Biomembranes, 1860 (9) (2018) pp 1625-1638, DOI: 10.1016/j.bbamem.2018.02.022.

[133] S.M. Butterfield, H.A. Lashuel, Amyloidogenic Protein Membrane Interactions: Mechanistic Insight from Model Systems, Angew. Chem. Int. Ed., 49 (33) (2010) pp 5628-5654, DOI: 10.1002/anie.200906670.

[134] M. Jakubec, E. Barias, S. Furse, M.L. Govasli, V. George, D. Turcu, I.A. Iashchishyn, L.A. Morozova-Roche, O. Halskau, Cholesterol-containing lipid nanodiscs promote an α–synuclein binding mode that accelerates oligomerization, FEBS J., 288 (6) (2021) pp 1887-1905, DOI: 10.1111/febs.15551.

[135] M.S. Terakawa, Y.X. Lin, M. Kinoshita, S. Kanemura, D. Itoh, T. Sugiki, M. Okumura, A. Ramamoorthy, Y.H. Lee, Impact of membrane curvature on amyloid aggregation, Biochimica Et Biophysica Acta-Biomembranes, 1860 (9) (2018) pp 1741-1764, DOI: 10.1016/j.bbamem.2018.04.012.

[136] K. Hiruma-Shimizu, H. Shimizu, G.S. Thompson, A.P. Kalverda, S.G. Patching, Deuterated detergents for structural and functional studies of membrane proteins: Properties, chemical synthesis and applications, Mol. Membr. Biol., 32 (5-8) (2015) pp 139-155, DOI: 10.3109/09687688.2015.1125536.

[137] D. Eliezer, E. Kutluay, R. Bussell, G. Browne, Conformational properties of α-synuclein in its free and lipid-associated states, J. Mol. Biol., 307 (4) (2001) pp 1061-1073, DOI: 10.1006/jmbi.2001.4538.

[138] J.A. Loureiro, S. Andrade, L. Goderis, R. Gomez-Gutierrez, C. Soto, R. Morales, M.C. Pereira, (De)stabilization of α-Synuclein Fibrillary Aggregation by Charged and Uncharged Surfactants, Int. J. Mol. Sci., 22 (22) (2021) pp, DOI: 10.3390/ijms222212509.

[139] S. Zhang, S. Yoo, D.T. Snyder, B.B. Katz, A. Henrickson, B. Demeler, V.H. Wysocki, A.G. Kreutzer, J.S. Nowick, A Disulfide-Stabilized Aβ that Forms Dimers but Does Not Form Fibrils, Biochemistry, 61 (4) (2022) pp 252-264, DOI: 10.1021/acs.biochem.1c00739.

[140] K. Dahse, M. Garvey, M. Kovermann, A. Vogel, J. Balbach, M. Fandrich, A. Fahr, DHPC Strongly Affects the Structure and Oligomerization Propensity of Alzheimer's Aβ(1-40) Peptide, J. Mol. Biol., 403 (4) (2010) pp 643-659, DOI: 10.1016/j.jmb.2010.09.021.

[141] T.G. Fletcher, D.A. Keire, The interaction of β-amyloid protein fragment (12-28) with lipid environments, Protein Sci., 6 (3) (1997) pp 666-675.

[142] R.P.R. Nanga, J.R. Brender, S. Vivekanandan, A. Ramamoorthy, Structure and membrane orientation of IAPP in its natively amidated form at physiological pH in a membrane environment, Biochimica Et Biophysica Acta-Biomembranes, 1808 (10) (2011) pp 2337-2342, DOI: 10.1016/j.bbamem.2011.06.012.

[143] S.M. Patil, S.H. Xu, S.R. Sheftic, A.T. Alexandrescu, Dynamic α-Helix Structure of Micelle-bound Human Amylin, J. Biol. Chem., 284 (18) (2009) pp 11982-11991, DOI: 10.1074/jbc.M809085200.

[144] M. Yagi-Utsumi, T. Kameda, Y. Yamaguchi, K. Kato, NMR characterization of the interactions between lyso-GM1 aqueous micelles and amyloid-β, FEBS Lett., 584 (4) (2010) pp 831-836, DOI: 10.1016/j.febslet.2010.01.005.

[145] M.P. Williamson, Y. Suzuki, N.T. Bourne, T. Asakura, Binding of amyloid β-peptide to ganglioside micelles is dependent on histidine-13, Biochemical Journal, 397 (2006) pp 483-490, DOI: 10.1042/bj20060293.

[146] D. Huster, X.L. Yao, M. Hong, Membrane protein topology probed by ^{1}H spin diffusion from lipids using solid-state NMR spectroscopy, J. Am. Chem. Soc., 124 (5) (2002) pp 874-883, DOI: 10.1021/ja017001r.

[147] G. Comellas, L.R. Lemkau, D.H.H. Zhou, J.M. George, C.M. Rienstra, Structural Intermediates during α-Synuclein Fibrillogenesis on Phospholipid Vesicles, J. Am. Chem. Soc., 134 (11) (2012) pp 5090-5099, DOI: 10.1021/ja209019s.

[148] L. Antonschmidt, R. Dervisoglu, V. Sant, K.T. Movellan, I. Mey, D. Riedel, C. Steinem, S. Becker, L.B. Andreas, C. Griesinger, Insights into the molecular mechanism of amyloid filament formation: Segmental folding of α-synuclein on lipid membranes, Science Advances, 7 (20) (2021) pp, DOI: 10.1126/sciadv.abg2174.

[149] R.D. Akinlolu, M. Nam, W. Qiang, Competition between Fibrillation and Induction of Vesicle Fusion for the Membrane-Associated 40-Residue β-Amyloid Peptides, Biochemistry, 54 (22) (2015) pp 3416-3419, DOI: 10.1021/acs.biochem.5b00321.

[150] T. Le Marchand, T. Schubeis, M. Bonaccorsi, P. Paluch, D. Lalli, A.J. Pell, L.B. Andreas, K. Jaudzems, J. Stanek, G. Pintacuda, ^{1}H-Detected Biomolecular NMR under Fast Magic-Angle Spinning, Chem. Rev., 122 (10) (2022) pp 9943-10018, DOI: 10.1021/acs.chemrev.1c00918.

[151] T. Deo, Q.H. Cheng, S. Paul, W. Qiang, A. Potapov, Application of DNP-enhanced solid-state NMR to studies of amyloid-β peptide interaction with lipid membranes, Chemistry and Physics of Lipids, 236 (2021) pp, DOI: 10.1016/j.chemphyslip.2021.105071.

[152] Z. Niu, W.J. Zhao, Z.F. Zhang, F.S. Xiao, X.Q. Tang, J. Yang, The Molecular Structure of Alzheimer β-Amyloid Fibrils Formed in the Presence of Phospholipid Vesicles, Angew. Chem. Int. Ed., 53 (35) (2014) pp 9294-9297, DOI: 10.1002/anie.201311106.

[153] J. Seelig, Deuterium Magnetic Resonance - Theory and Application to Lipid Membranes, Q. Rev. Biophys., 10 (3) (1977) pp 353-418, DOI: 10.1017/s0033583500002948.

[154] A.V. Filippov, A.M. Khakimov, B.V. Munavirov, ^{31}P NMR Studies of Phospholipids, in: Annual Reports on NMR Spectroscopy, Vol 85, 2015, pp. 27-92.

[155] E. Terzi, G. Holzemann, J. Seelig, Interaction of Alzheimer β-amyloid peptide(1-40) with lipid membranes, Biochemistry, 36 (48) (1997) pp 14845-14852, DOI: 10.1021/bi971843e.

[156] Y. Nakazawa, Y. Suzuki, M.P. Williamson, H. Saito, T. Asakura, The interaction of amyloid Aβ(1-40) with lipid bilayers and ganglioside as studied by ^{31}P solid-state NMR, Chemistry and Physics of Lipids, 158 (1) (2009) pp 54-60, DOI: 10.1016/j.chemphyslip.2008.12.001.

[157] M. Bokvist, F. Lindstrom, A. Watts, G. Grobner, Two types of Alzheimer's β-amyloid (1-40) peptide membrane interactions: Aggregation preventing transmembrane anchoring Versus accelerated surface fibril formation, J. Mol. Biol., 335 (4) (2004) pp 1039-1049, DOI: 10.1016/j.jmb.2003.11.046.

[158] A.H.M. Emwas, Z.A. Al-Talla, X.R. Guo, S. Al-Ghamdi, H.T. Al-Masri, Utilizing NMR and EPR spectroscopy to probe the role of copper in prion diseases, Magn. Reson. Chem., 51 (5) (2013) pp 255-268, DOI: 10.1002/mrc.3936.

[159] D. Aucoin, Y.J. Xia, T. Theint, P.S. Nadaud, K. Surewicz, W.K. Surewicz, C.P. Jaroniec, Protein-solvent interfaces in human Y145Stop prion protein amyloid fibrils probed by paramagnetic solid-state NMR spectroscopy, J. Struct. Biol., 206 (1) (2019) pp 36-42, DOI: 10.1016/j.jsb.2018.04.002.

[160] T. Theint, Y.J. Xia, P.S. Nadaud, D. Mukhopadhyay, C.D. Schwieters, K. Surewicz, W.K. Surewicz, C.P. Jaroniec, Structural Studies of Amyloid Fibrils by Paramagnetic Solid-State Nuclear Magnetic Resonance Spectroscopy, J. Am. Chem. Soc., 140 (41) (2018) pp 13161-13166, DOI: 10.1021/jacs.8b06758.

[161] C.P. Jaroniec, Solid-state nuclear magnetic resonance structural studies of proteins using paramagnetic probes, Solid State Nucl. Magn. Reson., 43-44 (2012) pp 1-13, DOI: 10.1016/j.ssnmr.2012.02.007.

[162] C.P. Jaroniec, Structural studies of proteins by paramagnetic solid-state NMR spectroscopy, J. Magn. Reson., 253 (2015) pp 50-59, DOI: 10.1016/j.jmr.2014.12.017.

[163] C. Sanchez-Lopez, R. Cortes-Mejia, M.C. Miotto, A. Binolfi, C.O. Fernandez, J.M. del Campo, L. Quintanar, Copper Coordination Features of Human Islet Amyloid Polypeptide: The Type 2 Diabetes Peptide, Inorganic Chemistry, 55 (20) (2016) pp 10727-10740, DOI: 10.1021/acs.inorgchem.6b01963.

[164] C. Hureau, Y. Coppel, P. Dorlet, P.L. Solari, S. Sayen, E. Guillon, L. Sabater, P. Faller, Deprotonation of the Asp1-Ala2 Peptide Bond Induces Modification of the Dynamic Copper(II) Environment in the Amyloid-β Peptide near Physiological pH, Angew. Chem. Int. Ed., 48 (50) (2009) pp 9522-9525, DOI: 10.1002/anie.200904512.

[165] A. Abelein, S. Ciofi-Baffoni, C. Morman, R. Kumar, A. Giachetti, M. Piccioli, H. Biverstal, Molecular Structure of Cu(II)-Bound Amyloid-beta Monomer Implicated in Inhibition of Peptide Self-Assembly in Alzheimer's Disease, Jacs Au, 2 (11) (2022) pp 2571-2584, DOI: 10.1021/jacsau.2c00438.

[166] S. Ciofi-Baffoni, A. Gallo, R. Muzzioli, M. Piccioli, The IR-^{15}N-HSQC-AP experiment: a new tool for NMR spectroscopy of paramagnetic molecules, J. Biomol. NMR, 58 (2) (2014) pp 123-128, DOI: 10.1007/s10858-013-9810-2.

[167] I. Bertini, R. Pierattelli, Copper(II) proteins are amenable for NMR investigations, Pure and Applied Chemistry, 76 (2) (2004) pp 321-333, DOI: 10.1351/pac200476020321.

[168] M.G.M. Weibull, S. Simonsen, C.R. Oksbjerg, M.K. Tiwari, L. Hemmingsen, Effects of Cu(II) on the aggregation of amyloid-β, J. Biol. Inorg. Chem., 24 (8) (2019) pp 1197-1215, DOI: 10.1007/s00775-019-01727-5.

[169] F. Bousejra-ElGarah, C. Bijani, Y. Coppel, P. Faller, C. Hureau, Iron(II) Binding to Amyloid-β, the Alzheimer's Peptide, Inorganic Chemistry, 50 (18) (2011) pp 9024-9030, DOI: 10.1021/ic201233b.

[170] L. Ghalebani, A. Wahlstrom, J. Danielsson, S. Warmlander, A. Graslund, pH-dependence of the specific binding of Cu(II) and Zn(II) ions to the amyloid-β peptide, Biochemical and Biophysical Research Communications, 421 (3) (2012) pp 554-560, DOI: 10.1016/j.bbrc.2012.04.043.

[171] L.M. Hou, M.G. Zagorski, NMR reveals anomalous copper(II) binding to the amyloid Aβ peptide of Alzheimer's disease, J. Am. Chem. Soc., 128 (29) (2006) pp 9260-9261, DOI: 10.1021/ja046032u.

[172] C. Hureau, V. Balland, Y. Coppel, P.L. Solari, E. Fonda, P. Faller, Importance of dynamical processes in the coordination chemistry and redox conversion of copper amyloid-β complexes, J. Biol. Inorg. Chem., 14 (7) (2009) pp 995-1000, DOI: 10.1007/s00775-009-0570-0.

[173] A. Abelein, S. Ciofi-Baffoni, C. Mörman, R. Kumar, A. Giachetti, M. Piccioli, H. Biverstål, Molecular Structure of Cu(II)-Bound Amyloid-β Monomer Implicated in Inhibition of Peptide Self-Assembly in Alzheimer's Disease, Jacs Au, 2 (11) (2022) pp 2571-2584, DOI: 10.1021/jacsau.2c00438.

[174] H. Eury, C. Bijani, P. Faller, C. Hureau, Copper(II) Coordination to Amyloid β: Murine versus Human Peptide, Angew. Chem. Int. Ed., 50 (4) (2011) pp 901-905, DOI: 10.1002/anie.201005838.

[175] C.D. Syme, R.C. Nadal, S.E.J. Rigby, J.H. Viles, Copper binding to the amyloid-β (Aβ) peptide associated with Alzheimer's disease - Folding, coordination geometry, pH dependence, stoichiometry, and affinity of Aβ-(1-28): Insights from a range of complementary spectroscopic techniques, J. Biol. Chem., 279 (18) (2004) pp 18169-18177, DOI: 10.1074/jbc.M313572200.

[176] E. Gaggelli, Z. Grzonka, H. Kozlowski, C. Migliorini, E. Molteni, D. Valensin, G. Valensin, Structural features of the Cu(II) complex with the rat Aβ(1-28) fragment, Chem. Commun., (3) (2008) pp 341-343, DOI: 10.1039/b713453c.

[177] S. Ahmadi, S.L. Zhu, R. Sharma, B. Wu, R. Soong, R.D. Majumdar, D.I. Wilson, A.J. Simpson, H.B. Kraatz, Aggregation of Microtubule Binding Repeats of Tau Protein is Promoted by Cu2+, Acs Omega, 4 (3) (2019) pp 5356-5366, DOI: 10.1021/acsomega.8b03595.

[178] A. Soragni, B. Zambelli, M.D. Mukrasch, J. Biemat, S. Jeganathan, C. Griesinger, S. Ciurli, E. Mandelkow, M. Zweckstetter, Structural characterization of binding of Cu(II) to Tau protein, Biochemistry, 47 (41) (2008) pp 10841-10851, DOI: 10.1021/bi8008856.

[179] A. Binolfi, R.M. Rasia, C.W. Bertoncini, M. Ceolin, M. Zweckstetter, C. Griesinger, T.M. Jovin, C.O. Fernandez, Interaction of α-synuclein with divalent metal ions reveals key differences: A link between structure, binding specificity and fibrillation enhancement, J. Am. Chem. Soc., 128 (30) (2006) pp 9893-9901, DOI: 10.1021/ja0618649.

[180] R.M. Rasia, C.W. Bertoncini, D. Marsh, W. Hoyer, D. Cherny, M. Zweckstetter, C. Griesinger, T.M. Jovin, C.O. Fernandez, Structural characterization of copper(II) binding to α-synuclein: Insights into the bioinorganic chemistry of Parkinson's disease, Proc. Natl. Acad. Sci. U. S. A., 102 (12) (2005) pp 4294-4299, DOI: 10.1073/pnas.0407881102.

[181] P. Ranjan, D. Ghosh, D.S. Yarramala, S. Das, S.K. Maji, A. Kumar, Differential copper binding to α-synuclein and its disease-associated mutants affect the aggregation and amyloid formation, Biochimica Et Biophysica Acta-General Subjects, 1861 (2) (2017) pp 365-374, DOI: 10.1016/j.bbagen.2016.11.043.

[182] Y.H. Sung, C. Rospigliosi, D. Eliezer, NMR mapping of copper binding sites in α-synuclein, Biochimica Et Biophysica Acta-Proteins and Proteomics, 1764 (1) (2006) pp 5-12, DOI: 10.1016/j.bbapap.2005.11.003.

[183] A. Binolfi, A.A. Valiente-Gabioud, R. Duran, M. Zweckstetter, C. Griesinger, C.O. Fernandez, Exploring the Structural Details of Cu(I) Binding to α-Synuclein by NMR Spectroscopy, J. Am. Chem. Soc., 133 (2) (2011) pp 194-196, DOI: 10.1021/ja107842f.

[184] S. Parthasarathy, F. Long, Y. Miller, Y.L. Xiao, D. McElheny, K. Thurber, B.Y. Ma, R. Nussinov, Y. Ishii, Molecular-Level Examination of Cu^{2+} Binding Structure for Amyloid Fibrils of 40-Residue Alzheimer's β by Solid-State NMR Spectroscopy, J. Am. Chem. Soc., 133 (10) (2011) pp 3390-3400, DOI: 10.1021/ja1072178.

[185] S. Parthasarathy, B. Yoo, D. McElheny, W. Tay, Y. Ishii, Capturing a Reactive State of Amyloid Aggregates, J. Biol. Chem., 289 (14) (2014) pp 9998-10010, DOI: 10.1074/jbc.M113.511345.

[186] D. Valensin, C. Migliorini, G. Valensin, E. Gaggelli, G. La Penna, H. Kozlowski, C. Gabbiani, L. Messori, Exploring the Reactions of β-Amyloid (Aβ) Peptide 1-28 with Al-III and Fe-III Ions, Inorganic Chemistry, 50 (15) (2011) pp 6865-6867, DOI: 10.1021/ic201069v.

[187] Q.Y. Zhao, Y.Q. Tao, K. Zhao, Y.Y. Ma, Q.H. Xu, C. Liu, S.N. Zhang, D. Li, Structural Insights of Fe^{3+}-Induced α-synuclein Fibrillation in Parkinson's Disease, J. Mol. Biol., 435 (1) (2023) pp, DOI: 10.1016/j.jmb.2022.167680.

[188] G. De Gregorio, F. Biasotto, A. Hecel, M. Luczkowski, H. Kozlowski, D. Valensin, Structural analysis of copper(I) interaction with amyloid β peptide, J. Inorg. Biochem., 195 (2019) pp 31-38, DOI: 10.1016/j.jinorgbio.2019.03.006.

[189] C.D. Syme, J.H. Viles, Solution ^{1}H NMR investigation of Zn^{2+} and Cd^{2+} binding to amyloid-β peptide (Aβ) of Alzheimer's disease, Biochimica Et Biophysica Acta-

Proteins and Proteomics, 1764 (2) (2006) pp 246-256, DOI: 10.1016/j.bbapap.2005.09.012.

[190] J. Danielsson, R. Pierattelli, L. Banci, A. Graslund, High-resolution NMR studies of the zinc-binding site of the Alzheimer's amyloid β-peptide, FEBS J., 274 (1) (2007) pp 46-59, DOI: 10.1111/j.1742-4658.2006.05563.x.

[191] E. Gaggelli, A. Janicka-Klos, E. Jankowska, H. Kozlowski, C. Migliorini, E. Molteni, D. Valensin, G. Valensin, E. Wieczerzak, NMR studies of the Zn^{2+} interactions with rat and human β-amyloid (1-28) peptides in water-micelle environment, J. Phys. Chem. B, 112 (1) (2008) pp 100-109, DOI: 10.1021/jp075168m.

[192] J.R. Brender, K. Hartman, R.P.R. Nanga, N. Popovych, R.D. Bea, S. Vivekanandan, E.N.G. Marsh, A. Ramamoorthy, Role of Zinc in Human Islet Amyloid Polypeptide Aggregation, J. Am. Chem. Soc., 132 (26) (2010) pp 8973-8983, DOI: 10.1021/ja1007867.

[193] V.S. Mithu, B. Sarkar, D. Bhowmik, M. Chandrakesan, S. Maiti, P.K. Madhu, Zn^{2+} Binding Disrupts the Asp(23)-Lys(28) Salt Bridge without Altering the Hairpin-Shaped Cross-beta Structure of Aβ(42) Amyloid Aggregates, Biophys. J., 101 (11) (2011) pp 2825-2832, DOI: 10.1016/j.bpj.2011.10.023.

[194] A.K. Buell, E.K. Esbjorner, P.J. Riss, D.A. White, F.I. Aigbirhio, G. Toth, M.E. Welland, C.M. Dobson, T.P.J. Knowles, Probing small molecule binding to amyloid fibrils, Physical Chemistry Chemical Physics, 13 (45) (2011) pp 20044-20052, DOI: 10.1039/c1cp22283j.

[195] R. Perneczky, F. Jessen, T. Grimmer, J. Levin, A. Floel, O. Peters, L. Froelich, Anti-amyloid antibody therapies in Alzheimer's disease, Brain, 146 (3) (2023) pp 842-849, DOI: 10.1093/brain/awad005.

[196] R. Mishra, B. Bulic, D. Sellin, S. Jha, H. Waldmann, R. Winter, Small-molecule inhibitors of islet amyloid polypeptide fibril formation, Angew. Chem. Int. Ed., 47 (25) (2008) pp 4679-4682, DOI: 10.1002/anie.200705372.

[197] K. Pagano, S. Tomaselli, H. Molinari, L. Ragona, Natural Compounds as Inhibitors of Aβ Peptide Aggregation: Chemical Requirements and Molecular Mechanisms, Front. Neurosci., 14 (2020) pp, DOI: 10.3389/fnins.2020.619667.

[198] M. Mayer, B. Meyer, Characterization of ligand binding by saturation transfer difference NMR spectroscopy, Angew. Chem. Int. Ed., 38 (12) (1999) pp 1784-1788, DOI: 10.1002/(sici)1521-3773(19990614)38:12<1784::Aid-anie1784>3.3.Co;2-h.

[199] R. Ahmed, B. VanSchouwen, N. Jafari, X.D. Ni, J. Ortega, G. Melacini, Molecular Mechanism for the (-)-Epigallocatechin Gallate-Induced Toxic to Nontoxic Remodeling of Aβ Oligomers, J. Am. Chem. Soc., 139 (39) (2017) pp 13720-13734, DOI: 10.1021/jacs.7b05012.

[200] R. Ahmed, G. Melacini, A solution NMR toolset to probe the molecular mechanisms of amyloid inhibitors, Chem. Commun., 54 (37) (2018) pp 4644-4652, DOI: 10.1039/c8cc01380b.

[201] G.R. Lamberto, A. Binolfi, M.L. Orcellet, C.W. Bertoncini, M. Zweckstetter, C. Griesinger, C.O. Fernandez, Structural and mechanistic basis behind the inhibitory interaction of PcTS on α-synuclein amyloid fibril formation, Proc. Natl. Acad. Sci. U. S. A., 106 (50) (2009) pp 21057-21062, DOI: 10.1073/pnas.0902603106.

[202] J.N. Rao, V. Dua, T.S. Ulmer, Characterization of α-synuclein interactions with selected aggregation-inhibiting small molecules, Biochemistry, 47 (16) (2008) pp 4651-4656, DOI: 10.1021/bi8002378.

[203] C. Dalvit, G. Fogliatto, A. Stewart, M. Veronesi, B. Stockman, WaterLOGSY as a method for primary NMR screening: Practical aspects and range of applicability, J. Biomol. NMR, 21 (4) (2001) pp 349-359, DOI: 10.1023/a:1013302231549.

[204] J. Asencio-Hernandez, B. Kieffer, M.A. Delsuc, NMR WaterLOGSY Reveals Weak Binding of Bisphenol A with Amyloid Fibers of a Conserved 11 Residue Peptide from Androgen Receptor, PLoS One, 11 (9) (2016) pp, DOI: 10.1371/journal.pone.0161948.

[205] C. Dalvit, S. Santi, R. Neier, A Ligand-Based NMR Screening Approach for the Identification and Characterization of Inhibitors and Promoters of Amyloid Peptide Aggregation, Chemmedchem, 12 (17) (2017) pp 1458-1463, DOI: 10.1002/cmdc.201700319.

[206] S. Pushpakom, F. Iorio, P.A. Eyers, K.J. Escott, S. Hopper, A. Wells, A. Doig, T. Guilliams, J. Latimer, C. McNamee, A. Norris, P. Sanseau, D. Cavalla, M. Pirmohamed, Drug repurposing: progress, challenges and recommendations, Nature Reviews Drug Discovery, 18 (1) (2019) pp 41-58, DOI: 10.1038/nrd.2018.168.

[207] G. Tin, T. Mohamed, A. Shakeri, A.T. Pham, P.P.N. Rao, Interactions of Selective Serotonin Reuptake Inhibitors with β-Amyloid, ACS Chem. Neurosci., 10 (1) (2019) pp 226-234, DOI: 10.1021/acschemneuro.8b00160.

[208] S.T. Ngo, M.S. Li, Curcumin Binds to Aβ(1-40) Peptides and Fibrils Stronger Than Ibuprofen and Naproxen, J. Phys. Chem. B, 116 (34) (2012) pp 10165-10175, DOI: 10.1021/jp302506a.

[209] H. Nedaei, N. Rezaei-Ghaleh, K. Giller, S. Becker, L. Karami, A.A. Moosavi-Movahedi, C. Griesinger, A.A. Saboury, The calcium-free form of atorvastatin inhibits amyloid-β(1-42) aggregation in vitro, J. Biol. Chem., 298 (3) (2022) pp, DOI: 10.1016/j.jbc.2022.101662.

[210] E. Prade, H.J. Bittner, R. Sarkar, J.M.L. del Amo, G. Althoff-Ospelt, G. Multhaup, P.W. Hildebrand, B. Reif, Structural Mechanism of the Interaction of Alzheimer Disease Aβ Fibrils with the Non-steroidal Anti-inflammatory Drug (NSAID) Sulindac Sulfide, J. Biol. Chem., 290 (48) (2015) pp 28737-28745, DOI: 10.1074/jbc.M115.675215.

[211] C.Q. Liang, Y.M. Li, Peptides for disrupting and degrading amyloids, Curr. Opin. Chem. Biol., 64 (2021) pp 124-130, DOI: 10.1016/j.cbpa.2021.05.011.

[212] B. Dorgeret, L. Khemtemourian, I. Correia, J.L. Soulier, O. Lequin, S. Ongeri, Sugar-based peptidomimetics inhibit amyloid β-peptide aggregation, Eur. J. Med. Chem., 46 (12) (2011) pp 5959-5969, DOI: 10.1016/j.ejmech.2011.10.008.

[213] R.K. Kar, Z. Gazova, Z. Bednarikova, K.H. Mroue, A. Ghosh, R.Y. Zhang, K. Ulicna, H.C. Siebert, N.E. Nifantiev, A. Bhunia, Evidence for Inhibition of Lysozyme Amyloid Fibrillization by Peptide Fragments from Human Lysozyme: A Combined Spectroscopy, Microscopy, and Docking Study, Biomacromolecules, 17 (6) (2016) pp 1998-2009, DOI: 10.1021/acs.biomac.6b00165.

[214] N. Ghosh, L.M. Kundu, Breaker peptides against amyloid-β aggregation: a potential therapeutic strategy for Alzheimer's disease, Future Med. Chem., 13 (20) (2021) pp 1767-1794, DOI: 10.4155/fmc-2021-0184.

[215] Z. Niu, E. Prade, E. Malideli, K. Hille, A. Jussupow, Y.G. Mideksa, L.M. Yan, C. Qian, M. Fleisch, A.C. Messias, R. Sarkar, M. Sattler, D.C. Lamb, M.J. Feige, C. Camilloni, A. Kapurniotu, B. Reif, Structural Insight into IAPP-Derived Amyloid Inhibitors and Their Mechanism of Action, Angew. Chem. Int. Ed., 59 (14) (2020) pp 5771-5781, DOI: 10.1002/anie.201914559.

[216] J. Madine, A.J. Doig, D.A. Middleton, Design of an N-methylated peptide inhibitor of alpha-synuclein aggregation guided by solid-state NMR, J. Am. Chem. Soc., 130 (25) (2008) pp 7873-7881, DOI: 10.1021/ja075356q.

[217] S.N. Zhang, J. Li, Q.H. Xu, W.C. Xia, Y.Q. Tao, C.W. Shi, D. Li, S.Q. Xiang, C. Liu, Conformational Dynamics of an α-Synuclein Fibril upon Receptor Binding Revealed by Insensitive Nuclei Enhanced by Polarization Transfer-Based Solid-State Nuclear Magnetic Resonance and Cryo-Electron Microscopy, J. Am. Chem. Soc., (2023) pp, DOI: 10.1021/jacs.2c10854.

[218] R. Roy, S. Paul, Illustrating the Effect of Small Molecules Derived from Natural Resources on Amyloid Peptides, J. Phys. Chem. B, 127 (3) (2023) pp 600-615, DOI: 10.1021/acs.jpcb.2c07607600J.

[219] C.B. Andersen, Y. Yoshimura, J. Nielsen, D.E. Otzen, F.A.A. Mulder, How epigallocatechin gallate binds and assembles oligomeric forms of human alpha-synuclein, J. Biol. Chem., 296 (2021) pp, DOI: 10.1016/j.jbc.2021.100788.

[220] Y. Suzuki, J.R. Brender, K. Hartman, A. Ramamoorthy, E.N.G. Marsh, Alternative Pathways of Human Islet Amyloid Polypeptide Aggregation Distinguished by ^{19}F Nuclear Magnetic Resonance-Detected Kinetics of Monomer Consumption, Biochemistry, 51 (41) (2012) pp 8154-8162, DOI: 10.1021/bi3012548.

[221] Z.X. Xu, G.L. Ma, Q. Zhang, C.H. Chen, Y.M. He, L.H. Xu, G.R. Zhou, Z.H. Li, H.J. Yang, P. Zhou, Inhibitory Mechanism of Epigallocatechin Gallate on Fibrillation and Aggregation of Amidated Human Islet Amyloid Polypeptide, Chemphyschem, 18 (12) (2017) pp 1611-1619, DOI: 10.1002/cphc.201700057.

[222] D. Townsend, E. Hughes, G. Akien, K.L. Stewart, S.E. Radford, D. Rochester, D.A. Middleton, Epigallocatechin-3-gallate remodels apolipoprotein A-I amyloid fibrils

into soluble oligomers in the presence of heparin, J. Biol. Chem., 293 (33) (2018) pp 12877-12893, DOI: 10.1074/jbc.RA118.002038.

[223] R. Huang, S. Vivekanandan, J.R. Brender, Y. Abe, A. Naito, A. Ramamoorthy, NMR Characterization of Monomeric and Oligomeric Conformations of Human Calcitonin and Its Interaction with EGCG, J. Mol. Biol., 416 (1) (2012) pp 108-120, DOI: 10.1016/j.jmb.2011.12.023.

[224] S.H. Son, J.M. Do, J.N. Yoo, H.W. Lee, N.K. Kim, H.S. Yoo, M.S. Gee, J.H. Kim, J.H. Seong, K.S. Inn, M.D. Seo, J.K. Lee, N.J. Kim, Identification of ortho catechol-containing isoflavone as a privileged scaffold that directly prevents the aggregation of both amyloid-β plaques and tau-mediated neurofibrillary tangles and its in vivo evaluation, Bioorg. Chem., 113 (2021) pp, DOI: 10.1016/j.bioorg.2021.105022.

[225] J.M. Lopez del Amo, U. Fink, M. Dasari, G. Grelle, E.E. Wanker, J. Bieschke, B. Reif, Structural Properties of EGCG-Induced, Nontoxic Alzheimer's Disease A beta Oligomers, J. Mol. Biol., 421 (4-5) (2012) pp 517-524, DOI: 10.1016/j.jmb.2012.01.013.

[226] S. Sinha, Z.M. Du, P. Maiti, F.G. Klarner, T. Schrader, C.Y. Wang, G. Bitan, Comparison of Three Amyloid Assembly Inhibitors: The Sugar scyllo-Inositol, the Polyphenol Epigallocatechin Gallate, and the Molecular Tweezer CLR01, ACS Chem. Neurosci., 3 (6) (2012) pp 451-458, DOI: 10.1021/cn200133x.

[227] M. Mayer, B. Meyer, Group epitope mapping by saturation transfer difference NMR to identify segments of a ligand in direct contact with a protein receptor, J. Am. Chem. Soc., 123 (25) (2001) pp 6108-6117, DOI: 10.1021/ja0100120.

[228] P.K. Singh, V. Kotia, D. Ghosh, G.M. Mohite, A. Kumar, S.K. Maji, Curcumin Modulates α-Synuclein Aggregation and Toxicity, ACS Chem. Neurosci., 4 (3) (2013) pp 393-407, DOI: 10.1021/cn3001203.

[229] N. Iwaya, N. Goda, M. Matsuzaki, A. Narita, Y. Shigemitsu, T. Tenno, Y. Abe, M. Hoshi, H. Hiroaki, Principal component analysis of data from NMR titration experiment of uniformly ^{15}N labeled amyloid-β (1-42) peptide with osmolytes and phenolic compounds, Archives of Biochemistry and Biophysics, 690 (2020) pp, DOI: 10.1016/j.abb.2020.108446.

[230] A.S. Pithadia, A. Bhunia, R. Sribalan, V. Padmini, C.A. Fierke, A. Ramamoorthy, Influence of a curcumin derivative on hIAPP aggregation in the absence and presence of lipid membranes, Chem. Commun., 52 (5) (2016) pp 942-945, DOI: 10.1039/c5cc07792c.

[231] V.S. Mithu, B. Sarkar, D. Bhowmik, A.K. Das, M. Chandrakesan, S. Maiti, P.K. Madhu, Curcumin Alters the Salt Bridge-containing Turn Region in Amyloid-β (1-42) Aggregates, J. Biol. Chem., 289 (16) (2014) pp 11122-11131, DOI: 10.1074/jbc.M113.519447.

[232] Y.L. Xiao, B.Y. Ma, D. McElheny, S. Parthasarathy, F. Long, M. Hoshi, R. Nussinov, Y. Ishii, Aβ(1-42) fibril structure illuminates self-recognition and replication

of amyloid in Alzheimer's disease, Nat. Struct. Mol. Biol., 22 (6) (2015) pp 499-U497, DOI: 10.1038/nsmb.2991.

[233] Y. Masuda, M. Fukuchi, T. Yatagawa, M. Tada, K. Takeda, K. Irie, K. Akagi, Y. Monobe, T. Imazawa, K. Takegoshi, Solid-state NMR analysis of interaction sites of curcumin and 42-residue amyloid β-protein fibrils, Biorg. Med. Chem., 19 (20) (2011) pp 5967-5974, DOI: 10.1016/j.bmc.2011.08.052.

[234] R. Brüschweiler, F.L. Zhang, Covariance nuclear magnetic resonance spectroscopy, J. Chem. Phys., 120 (11) (2004) pp 5253-5260, DOI: 10.1063/1.1647054.

[235] I. Morgado, K. Wieligmann, M. Bereza, R. Ronicke, K. Meinhardt, K. Annamalai, M. Baumann, J. Wacker, P. Hortschansky, M. Malesevic, C. Parthier, C. Mawrin, C. Schiene-Fischer, K.G. Reymann, M.T. Stubbs, J. Balbach, M. Gorlach, U. Horn, M. Fandrich, Molecular basis of β-amyloid oligomer recognition with a conformational antibody fragment, Proc. Natl. Acad. Sci. U. S. A., 109 (31) (2012) pp 12503-12508, DOI: 10.1073/pnas.1206433109.

[236] A.S. Konig, N.S. Rosener, L. Gremer, M. Tusche, D. Flender, E. Reinartz, W. Hoyer, P. Neudecker, D. Willbold, H. Heise, Structural details of amyloid-β oligomers in complex with human prion protein as revealed by solid-state MAS NMR spectroscopy, J. Biol. Chem., 296 (2021) pp, DOI: 10.1016/j.jbc.2021.100499.

[237] W. Hoyer, C. Gronwall, A. Jonsson, S. Stahl, T. Hard, Stabilization of a β-hairpin in monomeric Alzheimer's amyloid-β peptide inhibits amyloid formation, Proc. Natl. Acad. Sci. U. S. A., 105 (13) (2008) pp 5099-5104, DOI: 10.1073/pnas.0711731105.

[238] W. Hoyer, T. Hard, Interaction of Alzheimer's Aβ peptide with an engineered binding protein - Thermodynamics and kinetics of coupled folding-binding, J. Mol. Biol., 378 (2) (2008) pp 398-411, DOI: 10.1016/j.jmb.2008.02.040.

[239] E. De Genst, P.H. Chan, E. Pardon, S.T.D. Hsu, J.R. Kumita, J. Christodoulou, L. Menzer, D.Y. Chirgadze, C.V. Robinson, S. Muyldermans, A. Matagne, L. Wyns, C.M. Dobson, M. Dumoulin, A Nanobody Binding to Non-Amyloidogenic Regions of the Protein Human Lysozyme Enhances Partial Unfolding but Inhibits Amyloid Fibril Formation, J. Phys. Chem. B, 117 (42) (2013) pp 13245-13258, DOI: 10.1021/jp403425z.

[240] E.J. De Genst, T. Guilliams, J. Wellens, E.M. O'Day, C.A. Waudby, S. Meehan, M. Dumoulin, S.T.D. Hsu, N. Cremades, K.H.G. Verschueren, E. Pardon, L. Wyns, J. Steyaert, J. Christodoulou, C.M. Dobson, Structure and Properties of a Complex of α-Synuclein and a Single-Domain Camelid Antibody, J. Mol. Biol., 402 (2) (2010) pp 326-343, DOI: 10.1016/j.jmb.2010.07.001.

[241] A. Vuchelen, E. O'Day, E. De Genst, E. Pardon, L. Wyns, M. Dumoulin, C.M. Dobson, J. Christodoulou, S.T.D. Hsu, ^{1}H, ^{13}C and ^{15}N assignments of a camelid nanobody directed against human α-synuclein, Biomolecular Nmr Assignments, 3 (2) (2009) pp 231-233, DOI: 10.1007/s12104-009-9182-4.

[242] G.T. Heller, F.A. Aprile, T.C.T. Michaels, R. Limbocker, M. Perni, F.S. Ruggeri, B. Mannini, T. Lohr, M. Bonomi, C. Camilloni, A. De Simone, I.C. Felli, R. Pierattelli, T.P.J. Knowles, C.M. Dobson, M. Vendruscolo, Small-molecule sequestration of amyloid-β as a drug discovery strategy for Alzheimer's disease, Science Advances, 6 (45) (2020) pp, DOI: 10.1126/sciadv.abb5924.

[243] S. Gil, T. Hosek, Z. Solyom, R. Kummerle, B. Brutscher, R. Pierattelli, I.C. Felli, NMR Spectroscopic Studies of Intrinsically Disordered Proteins at Near-Physiological Conditions, Angew. Chem. Int. Ed., 52 (45) (2013) pp 11808-11812, DOI: 10.1002/anie.201304272.

[244] Z. Niu, R. Sarkar, M. Aichler, H.J. Wester, B.H. Yousefi, B. Reif, Mapping the Binding Interface of PET Tracer Molecules and Alzheimer Disease Aβ Fibrils by Using MAS Solid-State NMR Spectroscopy, ChemBioChem, 21 (17) (2020) pp 2495-2502, DOI: 10.1002/cbic.202000143.

[245] P. Duan, K.J. Chen, G. Wijegunawardena, A.J. Dregni, H.K. Wang, H.F. Wu, M. Hong, Binding Sites of a Positron Emission Tomography Imaging Agent in Alzheimer's β-Amyloid Fibrils Studied Using ^{19}F Solid-State NMR, J. Am. Chem. Soc., 144 (3) (2022) pp 1416-1430, DOI: 10.1021/jacs.1c12056.

[246] K.J. Robbins, G. Liu, G.X. Lin, N.D. Lazo, Detection of Strongly Bound Thioflavin T Species in Amyloid Fibrils by Ligand-Detected H-1 NMR, J. Phys. Chem. Lett., 2 (7) (2011) pp 735-740, DOI: 10.1021/jz200066b.

[247] M.O. Pedersen, K. Mikkelsen, M.A. Behrens, J.S. Pedersen, J.J. Enghild, T. Skrydstrup, A. Malmendal, N.C. Nielsen, NMR Reveals Two-Step Association of Congo Red to Amyloid-β in Low-Molecular-Weight Aggregates, J. Phys. Chem. B, 114 (48) (2010) pp 16003-16010, DOI: 10.1021/jp108035y.

[248] D. Roy, D. Bhattacharyya, A. Bhunia, Do Catechins (ECG and EGCG) Bind to the Same Site as Thioflavin T (ThT) in Amyloid Fibril? Answer From Saturation Transfer Difference NMR, Nat. Prod. Commun., 14 (5) (2019) pp, DOI: 10.1177/1934578x19849791.

[249] C. Gowda, G. Zandomeneghi, H. Zimmermann, A.K. Schutz, A. Bockmann, M. Ernst, B.H. Meier, The conformation of the Congo-red ligand bound to amyloid fibrils HET-s(218-289): a solid-state NMR study, J. Biomol. NMR, 69 (4) (2017) pp 207-213, DOI: 10.1007/s10858-017-0148-z.

[250] G.C.P. van Zundert, J. Rodrigues, M. Trellet, C. Schmitz, P.L. Kastritis, E. Karaca, A.S.J. Melquiond, M. van Dijk, S.J. de Vries, A. Bonvin, The HADDOCK2.2 Web Server: User-Friendly Integrative Modeling of Biomolecular Complexes, J. Mol. Biol., 428 (4) (2016) pp 720-725.

[251] Z.J. Chen, B. Reif, Measurements of residual dipolar couplings in peptide inhibitors weakly aligned by transient binding to peptide amyloid fibrils, J. Biomol. NMR, 29 (4) (2004) pp 525-530, DOI: 10.1023/B:JNMR.0000034353.98902.4f.

[252] Z.J. Chen, G. Krause, B. Reif, Structure and orientation of peptide inhibitors bound to β-amyloid fibrils, J. Mol. Biol., 354 (4) (2005) pp 760-776, DOI: 10.1016/j.jmb.2005.09.055.

[253] D. Townsend, E. Hughes, K.L. Stewart, J.M. Griffin, S.E. Radford, D.A. Middleton, Orientation of a Diagnostic Ligand Bound to Macroscopically Aligned Amyloid-β Fibrils Determined by Solid-State NMR, J. Phys. Chem. Lett., 9 (22) (2018) pp 6611-6615, DOI: 10.1021/acs.jpclett.8b02448.

[254] M.G. Iadanza, R. Silvers, J. Boardman, H.I. Smith, T.K. Karamanos, G.T. Debelouchina, Y.C. Su, R.G. Griffin, N.A. Ranson, S.E. Radford, The structure of a β_2-microglobulin fibril suggests a molecular basis for its amyloid polymorphism, Nature Communications, 9 (2018) pp, DOI: 10.1038/s41467-018-06761-6.

Glossary

AD

Alzheimer's disease

CP

Cross-polarization

CR

Congo red

CSA

Chemical shift (or shielding) anisotropy

DARR

Dipolar-assisted rotational resonance

EGCG

(-)-Epigallocatechin-3-gallate

HFIP

Hexafluoroisopropanol

hIAPP

Human islet amyloid polypeptide

HSQC

Heteronuclear single-quantum coherence

L(H)MWH

Low (High) molecular weight heparin

MAS

Magic-angle spinning

NOESY

Nuclear Overhauser effect spectroscopy

PDSD

Proton-driven spin-diffusion

PET

Positron emission tomography

PFG

Pulsed field gradient

PRE

Paramagnetic relaxation enhancement

REDOR

Rotational-echo double-resonance

ROESY

Rotating frame NOE enhancement spectroscopy

SRE

Self-recognition element

STD

Saturation transfer difference

TEM

Transmission electron microscopy

TFE

Trifluoroethanol

ThT

Thioflavin T

trRDC

Transferred residual dipolar coupling

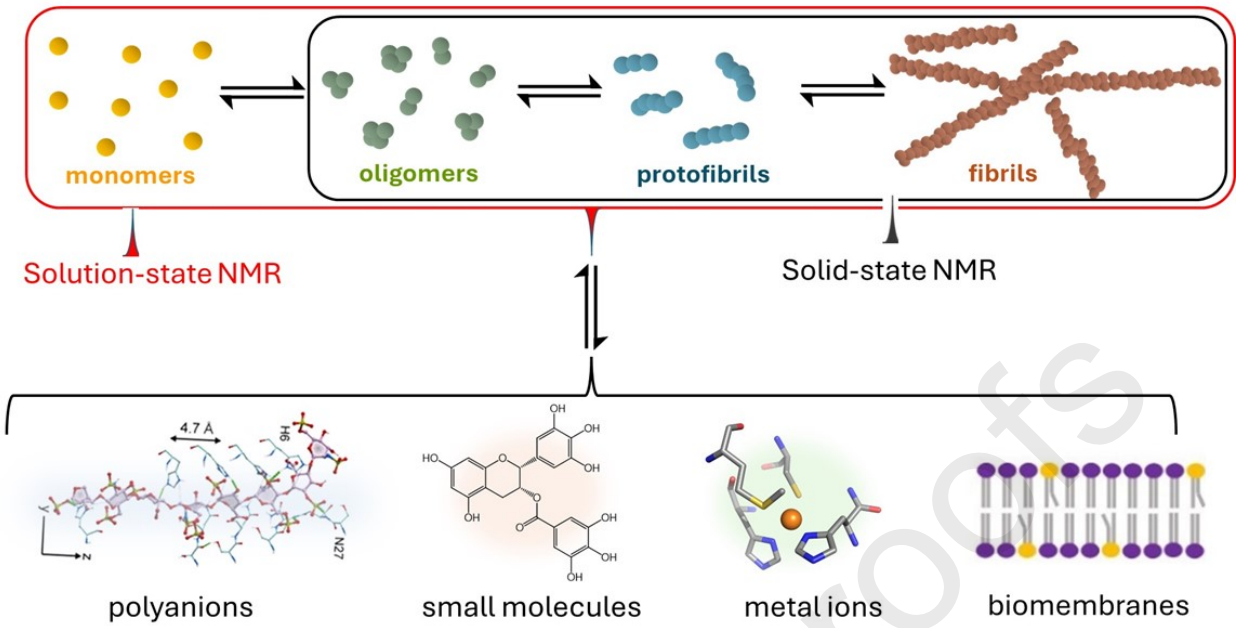

Highlights

- Amyloid proteins associated with human diseases interact with various accessory molecules and metal ions, and with cell membranes
- NMR provides unique atomic insights into interactions of amyloid species with physiological interaction partners.
- Solution NMR is ideal for characterizing interactions involving small, soluble amyloid species
- Solid state NMR methods report interactions with insoluble amyloid fibrils
- Information is obtained from the perspective of the protein and/or interaction partner.
- Also provides information on amyloid diagnostic and therapeutic molecules

Declaration of interests

☒ The authors declare that they have no known competing financial interests or personal relationships that could have appeared to influence the work reported in this paper.

☐ The authors declare the following financial interests/personal relationships which may be considered as potential competing interests: